

Supplementary Text

Materials and Methods

Strain construction

All the strains used in this study were described in Table S2. Unless stated otherwise, all the strains used were derived from the *E. coli* prototrophic strain NCM3722^{1,2}.

Gene Deletion: To construct a *ptsHI-crr* operon deletion strain NQ721, a kanamycin resistance (*km*) gene from pKD4³ was PCR amplified and integrated into *E. coli* NCM3722 chromosome to replace the entire *ptsHI-crr* operon (from the *ptsH* start codon to the *crr* stop codon) by using the λ Red system³. The *km* gene in NQ721 was then flipped out by using pCP20 plasmid⁴ resulting in strain NQ748. For brevity, we refer to this strain as Δ *pts*.

fryA, *ptsA*, *ptsP*, *dhaM* are four known genes homologous to *ptsI*, encoding EI enzymes in PTS system⁵. Deletion alleles of Δ *fryA*, Δ *ptsA*, Δ *ptsP*, Δ *dhaM* were purchased from Keio deletion collection⁶. Each of these alleles was transferred into strain NQ748 by phage P1^{vir} mediated transduction and then transformed with pCP20 plasmid to flip out *km* gene subsequently, resulting in strain NQ506 harboring Δ *ptsHI-crr*, Δ *fryA*, Δ *ptsA*, Δ *ptsP* and Δ *dhaM* finally after four steps of P1 transduction and *km* gene flipping out. For brevity, we refer to strain NQ506 as Δ 5EI Δ *pts*.

A Δ *cyaA* deletion allele⁷, a Δ *glpR* deletion allele⁸ and a Δ *gltD* deletion allele obtained from the Keio deletion collection were transferred into NCM3722 strain by phage P1^{vir} mediated transduction respectively, resulting into strains NQ93, NQ372 and FG1195. The Δ *glpR* deletion allele was also transferred into NQ474 (see construction below), resulting into strain NQ489. A Δ *cpdA* deletion allele obtained from the Keio deletion collection was similarly transferred into strain NCM3722, NQ748 and NQ506 respectively, yielding strains NQ385, NQ976 and NQ977.

Chromosomal P*glpF-lacZ*, P*fucP-lacZ*, P*lacUV5-lacZ*, P*lac- Δ _{Crp}-lacZ*, P*glnA-lacZ*, P*thrA-lacZ*, P*lysC-lacZ*, P*pcysJ-lacZ*, P*lac-gfp* and P_{L_{tet}-O1}-*lacZ* fusions: The *glpFK* promoter (P*glpF*) region (-273 bp to -1 bp relative to *glpF* translational start point), the *fucPIK* promoter (P*fucP*) region (-400 bp to -1 bp relative to *fucP* translational start point), the *glnALG* promoter (P*glnA*) region (-379 bp to -1 bp relative to *glnA* translational start point), the *thrLABC* promoter (P*thrA*) region (-331 bp to +48 bp relative to *thrA* translational start point), the *lysC* promoter (P*lysC*) region (-579 bp to -1 bp relative to *glnA* translational start point) and the *cysJIH* promoter (P*pcysJ*) region (-291 bp to -1 bp relative to *cysJ* translational start point), were amplified from genomic DNA of NCM3722. The *lacUV5* promoter (P*lacUV5*) region (-232 bp to -1 bp relative to *lacZ* translational start point) were amplified from genomic DNA of CA8224.1⁹. To construct a *Plac* promoter without cAMP-Crp binding site, the NCM3722 *lacZYA* promoter (P*lac*) region (-232 bp to -1 bp relative to *lacZ* translational start point) was first amplified, then its Crp-cAMP binding site (TGTGAGTTA GCTCACT) centered at -61.5 was replaced by a random sequence (CAGACGTTAGCTCACT) using fusion PCR. To be simple, we called this modified *Plac* promoter with above scrambled cAMP-Crp binding site as P*lac- Δ O_{Crp}*. These DNA fragments were then inserted into the *XhoI* and *BamHI* sites of plasmid pKDT¹⁰ (modified from pKD13³ by

adding a *rrnB* terminator sequence (*rrnBT*) downstream of the *km* gene), yielding plasmids pKDTglpF, pKDTglnH, pKDTfucP, pKDTglnA, pKDTthrA, pKDTlysC, pKDTcysJ, pKDTUV5 and pKDTlacM, respectively. The DNA regions containing the *km* gene, *rrnBT* and one of these promoters were PCR amplified from above plasmids and subsequently integrated into the chromosome of *E. coli* strain NQ309 to replace part of *lacI* and the entire *PlacZ* (from +134 bp after *lacI* translational start codon to *lacZ* translational start codon), individually³. Then each of the promoter-*lacZ* fusions was transferred to different genetic backgrounds by phage P1_{vir} mediated transduction. The *PfucP-lacZ*, *PlacUV5-lacZ*, *Plac-Δ_{Crp}-lacZ*, *PglnA-lacZ*, *PthrA-lacZ*, *PlysC-lacZ* and *PcysJ-lacZ* fusions were transferred into strain NCM3722 respectively, resulting in strains NQ554, NQ1053, NQ367, NQ158, NQ481, NQ980 and NQ979. *PglpF-lacZ* fusion was transferred into a *ΔglpR* strain NQ372, resulting in strain NQ373. *PglnA-lacZ* fusion was also transferred into a *ΔcyaA* strain, a *glnL302* (NtrB^{con})^{11,12} strain and a *gltD*-null and titratable *gdhA* strain NQ474 (see construction below), resulting in strains NQ780, NQ315 and NQ477 respectively. The *PfucP-lacZ*, *PthrA-lacZ*, *PlysC-lacZ*, *PcysJ-lacZ*, *Plac-Δ_{Crp}-lacZ* and *PlacUV5-lacZ* fusions were also transferred into strain NQ474, resulting into strains NQ1180, NQ482, NQ983, NQ982, NQ475 and NQ1054 respectively. *PglpF-lacZ* fusion was transferred into a *ΔglpR* strain NQ489, resulting into strain NQ490.

To construct *PlacZ-gfp* fusion, the *lacZYA* promoter (*PlacZ*) regions (-278 bp to -7 bp relative to *lacZ* translational start point) were amplified from genomic DNA of NCM3722, then substituted for *PglnK* in plasmid pKDT_ *PglnK-gfp*¹³, resulting into plasmid pKDT_ *PlacZ-gfp*. The DNA region containing the *km-rrnBT-PlacZ-gfp* from this plasmid was then PCR amplified and integrated into the chromosome of *E. coli* strain NQ309 at *intS* region.

The *intS::km-rrnBT-PlacZ-gfp* allele was transferred into a *ΔmotA* strain EQ54¹³, resulting into strain EQ123 after flipping out its *km* gene by using pCP20 plasmid. A *ΔamtB-glnK* allele¹³ was then transferred into strain EQ123, resulting into strain EQ129.

To construct *P_{Ltet-O1}-lacZ* fusion, *P_{Ltet-O1}-lacZ* allele from strain EQ37¹⁰ was transferred into strain NCM3722 and NQ102 (see construction below) respectively, resulting into strains NQ122 and NQ124.

Chromosomal *Pu-lacY* and *Pu-glpFK* fusions: DNA fragment containing the *Pu* promoter (-1 bp to -178 bp relative to the transcriptional start site) was amplified by PCR from a *Pu* promoter containing plasmid pEZ9¹⁴, then inserted into the *SalI* and *BamHI* sites of plasmid pKD13, producing plasmid pKDPu. Using this plasmid as a template, the region containing the *km* gene and *Pu* promoter was PCR amplified and integrated into the chromosome of *E. coli* strain NQ351 between the *lacZ* and *lacY* (from *lacZ* stop codon to *lacY* start codon), and in front of *glpF* (-1 bp to -252 bp relative to the translational start point of *glpF*) respectively, by using the λ Red system³. Because the activation of *Pu* promoter needs the XylR protein, we constructed a strain NQ386 in which a synthetic *lacZ* promoter *P_{Llac-O1}*¹⁵ (a promoter that is repressed by LacI but does not need Crp-cAMP for activation) driving *xylR* (*xylR* gene was cloned from pEZ6¹⁴) was inserted at the *attB* site. The *km-Pu-lacY* and *km-Pu-glpFK* constructs in NQ351 were transferred into strain NQ386 containing *P_{Llac-O1}-xylR* by P1 transduction, resulting in strains NQ381 and NQ399, respectively. Alleles of *ΔptsHI-crr* deletion (*Δpts*) and *ΔptsHI-crr* deletion combined with *ΔfryA*, *ΔptsA*, *ΔptsP* and *ΔdhaM* (*Δ5EI Δpts*) were transferred into strain NQ381 after several rounds of P1 transduction and *km* gene flipping out respectively, resulting in strains

NQ773 and NQ567.

Construction of titratable *gdhA* strain: The $P_{Ltet-O1}$ promoter¹⁵ was amplified by PCR and inserted into the *Sall* and *Bam*HI sites of plasmid pKD13, producing plasmid pKD13ptet. Using this plasmid as template, the region containing the *km* gene and the $P_{Ltet-O1}$ promoter was PCR amplified and integrated into the chromosome of *E. coli* strain NQ309 to replace *gdhA* promoter (-350 bp to -1 bp relative to the translational start point of *gdhA*). This *km*- $P_{Ltet-O1}$ driven *gdhA* was transferred into a Δ *gltD* strain FG1195, yielding strain NQ5. The *km* gene in NQ5 was flipped out by using pCP20 plasmid, resulting in strain NQ102. To titrate $P_{Ltet-O1}$ promoter by TetR, we used a strain that carried a $P_{Ltet-O1}$ promoter driven *tetR* at the *attB* site¹⁰. This *bla*- $P_{Ltet-O1}$ -*tetR* allele at the *attB* site was then transferred into strain NQ5, yielding strain NQ34. The *km* gene in NQ34 was flipped out by using pCP20 plasmid, resulting in strain NQ474.

α -ketoglutarate (akg) growth mutant selection: NCM3722 cannot utilize akg as a sole carbon source (Table S17 and Fig. S24). To select a NCM3722 mutant that can grow on akg, 10^8 NCM3722 cells from an overnight LB culture were washed by N⁻C⁻ minimal medium with 10 mM akg-Na and 20 mM NH₄Cl, then were plated on the same minimal medium agar plates. After incubation at 37°C for 48 hrs, 260 single colonies arose. Sequence analyses of six single colonies showed that the *kgtP* regulatory region of each akg-positive mutant harbored a C to T point substitution at the -10 element, thereby changing the -10 hexamer from “TATAAC” to “TATAAT”. One such mutant, named NQ738 (a *kgtP*^{up} mutation), was selected for further study and its growth on akg was further confirmed. *Plac*UV5-*lacZ*, *Plac*- Δ C_{TP}-*lacZ* and *PglnA*-*lacZ* fusions were then transferred into strain NQ738 by phage P1_{vir} mediated transduction, resulting in strain NQ1078, NQ739 and NQ747 respectively.

Growth of bacterial culture

Growth medium: Most of the cultures were grown based on the N⁻C⁻ minimal medium¹⁶, which contains K₂SO₄ (1 g), K₂HPO₄·3H₂O (17.7 g), KH₂PO₄ (4.7 g), MgSO₄·7H₂O (0.1 g), and NaCl (2.5 g) in one liter, and is supplemented with various carbon and nitrogen sources. For carbon-limited growth of wild-type cells, 20 mM NH₄Cl and each of carbon sources below were used: 10 mM glucose-phosphate +10 mM gluconate, 20 mM gluconate, 0.2% (w/v) lactose, 0.4% (w/v) glucose, 0.4% (v/v) glycerol, 20 mM maltose, 20 mM pyruvate, 20 mM fructose, 20 mM sorbitol, 60 mM acetate, 20 mM oxaloacetate (oaa), and 20 mM mannose. For carbon-limited growth with *Pu-lacY* strains, N⁻C⁻ minimal medium, 20 mM NH₄Cl, and 0.2% (w/v) lactose with various concentrations of 3MBA (0-0.5 mM) were used. For carbon-limited growth with *Pu-glpFK* strains, N⁻C⁻ minimal medium, 20 mM NH₄Cl, and 0.4 % (v/v) glycerol with various concentrations of 3MBA (0-0.5 mM) were used. For anabolic limited growth using titratable *gdhA* strains in NQ34 background, N⁻C⁻ minimal medium, 20 mM NH₄Cl, 0.2% (w/v) lactose or 0.4% (w/v) glucose or 0.4% (v/v) glycerol, and various amounts of cTc (10-100 ng/ml) were used. Five rich defined media used in this study are: 1) N⁻C⁻ minimal medium, 20 mM NH₄Cl, 0.4% (w/v) glucose supplemented with 7 amino acids (glycine, histidine, isoleucine, leucine, lysine, methionine, phenylalanine) which cannot be used as the sole carbon source; 2) N⁻C⁻ minimal medium, 20 mM NH₄Cl, 0.4% (w/v) glucose supplemented with 9 amino acids (proline, serine, tryptophan, glutamate, glutamine, aspartate, asparagine, alanine, arginine) each of which can be used as the sole carbon source; 3) N⁻C⁻ minimal medium, 20 mM NH₄Cl, 0.4% (w/v)

glucose supplemented with the above 7 and 9 amino acids together; the remaining four amino acids were not included due to either poor stability or solubility; 4) N⁻C⁻ minimal medium, 20 mM NH₄Cl, 0.4% (w/v) glucose, 0.2% (w/v) casamino acids; and 5) glucose rich defined medium¹⁷. For all but casamino acids, the concentration of each amino acid used is the same as that used in rich defined medium¹⁷. 1 mM IPTG was added to above media when necessary to fully induce the native *lacZ* operon or P_{Lac-O1} promoter driving XylR.

Batch culture growth: All batch culture growth was performed in a 37°C water bath shaker shaking at 250 rpm. The culture volume was either 5 ml in 20 mm × 150 mm test tubes (for steady state experiments) or 12 ml in 125 ml flasks (for transient repression experiments), with culture height of no more than 2 cm (test tube) or 1 cm (flask) to ensure aeration. Each experiment was carried out in three steps: seed culture in LB broth, pre-culture and experimental culture in identical N⁻C⁻ minimal medium. For seed culture, one colony from fresh LB agar plate was inoculated into liquid LB and cultured at 37°C with shaking. After 4-5 hrs, cells were centrifuged and washed once with desired N⁻C⁻ minimal medium. Then depending on the specific growth rate in each condition, cells in various cultures were diluted to different densities in identical N⁻C⁻ minimal medium, and cultured in 37°C water bath shaker overnight (pre-culture), so that the overnight culture was kept in exponential growth for 4-10 doublings. Cells from the overnight pre-culture was then washed with identical minimal medium (pre-warmed to 37°C), diluted to OD₆₀₀ = 0.005-0.025 in identical pre-warmed minimal medium, and cultured in 37°C water bath shaker (experimental culture). After three cell doublings, samples were collected for various measurements, mostly in the range of OD₆₀₀ = 0.1 to 0.5, covering two doublings during exponential growth. OD₆₀₀ was monitored periodically during the experimental culture growth. 200 µl cell culture was collected in a Sterna Sub-Micro Cuvette for OD₆₀₀ measurement using a Thermal Spectrophotometer every half doubling of growth. The time taken for each sample collection is < 30 sec and had no measureable effect on cell growth. Due to the small volume of cuvette used in this work, the total amount of samples removed was a small fraction of the culture volume therefore cell growth is not affected.

Nutrient-limited chemostat: The nitrogen-limited continuous culture fed with lactose or glucose as a sole carbon source was operated in an ATR Multifors chemostat system with a 500 ml culture vessel. The medium was N⁻C⁻-based, with 10 mM lactose or 0.2% (w/v) glucose and 2 mM NH₄Cl included in the reservoir medium as excess-carbon and limited-nitrogen sources, respectively. Chemostat parameters were: culture volume, 300 ml; temperature, 37 ± 0.2°C; pH, 7.1 ± 0.1; agitation, 800 ± 20 rpm; and aeration, 0.5 L/min. The bacterial growth rate, which is equivalent to the culture dilution rate, was set by a peristaltic pump controlling medium feeding rate. The feeding rate was checked and recorded after each sampling and calibrated immediately after each new dilution rate setting. Wild-type strain NCM3722 (using lactose as the sole carbon source) or NQ354 ($\Delta lacI$; using glucose as the sole carbon source) was first grown to late exponential phase in a batch culture. 25 ml of cells were centrifuged and washed twice with the nitrogen-limited medium and inoculated into the chemostat vessel. The initial dilution rate was set at the lowest at ~0.20 hr⁻¹. The first set of samples was taken after about 10 generations of cell growth in order to ensure establishment of a steady state. Subsequent equilibrations of the culture between each change of dilution rate and sampling were performed with at least 8 generations of cell growth. The dilution rate was increased 0.15 ± 0.02 hr⁻¹ after each sampling until a level that was higher than the maximum growth rate: a steady-state growth can no longer

be maintained as cells started to be washed out and nitrogen became not limited any more in the culture. The dilution rate was then reverted to the first lowest setting to ensure reproducibility within one chemostat experiment.

The sulfur-limited continuous culture was performed similarly, with the following differences. The medium was also N⁺C⁻-based, but with all sulfate salts replaced by proper amount of chloride salts in order to maintain the same medium osmolality. 0.2% (w/v) glycerol, 10 mM NH₄Cl, and 40 μM K₂SO₄ were included in the reservoir medium as excess-carbon, excess-nitrogen, and limited-sulfur sources, respectively. The strain used was NQ354 ($\Delta lacI$). The initial dilution rate was set at $\sim 0.16 \text{ hr}^{-1}$, and the step-wise rate increase was ~ 0.10 to 0.11 hr^{-1} .

Microfluidic chemostat: The detailed procedure for growing cells in a microfluidic chemostat was described in Ref.13. Briefly, cells grew overnight in the medium with saturating concentrations of lactose (50mM) and NH₄Cl (20mM). The next day, the culture was diluted and loaded into the microfluidic chemostat. The fresh growth medium with various concentrations of lactose and NH₄Cl was introduced into the microfluidic chemostat. The microfluidic chemostat was fixed onto a microscope stage in a fluorescent microscope (Nikon TI-U) that was housed in a 37°C microscope incubator (InVivo Scientific). After 2~3 generations of unperturbed growth in the microfluidic chemostat, phase contrast images and fluorescence images of growing cells were recorded with CCD camera (Clara, Andor) once or twice per doubling. The images were analyzed with a custom-built Matlab program. First, the program identified pixel positions occupied by cells with phase contrast images, obtained a size of a growing colony in time series and calculated the growth rate of the colony. In order to get fluorescence levels, fluorescence intensities over the cell-occupying area identified by phase contrast images were averaged.

Protein, RNA, and internal metabolite Measurements

Total protein quantification: The Biuret method was used for total protein quantification²⁰. Briefly, 1.8 ml of cell culture at a certain OD₆₀₀ during the exponential phase was collected by centrifugation. The cell pellet was washed with water and re-suspended in 0.2 ml water and fast frozen on dry ice. The cell pellet was then thawed in water bath at RT. 0.1 ml 3M NaOH was added to the cell pellet and samples were incubated at 100°C heat block for 5 min to hydrolyze proteins. Samples were then cooled in water bath at RT for 5 min. The biuret reactions are carried out by adding 0.1 ml 1.6% CuSO₄ to above samples with thorough mixing at RT for 5 min. Samples were then centrifuged and the absorbance at 555 nm was measured by a spectrophotometer. Same biuret reaction was also applied to a series of BSA standards to get a standard curve. Protein amounts in the above samples were determined by the BSA standard curve.

β-Galactosidase Assay: Samples (0.25 ml cell culture) were collected, fast frozen on dry ice and stored at -80°C prior to β-Galactosidase assay. For steady state study, four to five samples were collected for each culture during exponential growth (for OD₆₀₀ = 0.1~0.5). For transient repression study by various metabolites, five to seven samples were collected during exponential growth (for OD₆₀₀ = 0.06-0.5) before a metabolite (20 mM final concentration) was added. After addition, samples were taken every 4-5 min for the first 30 min, then every 10-15 min until an additional 1-2 cell doublings.

For each sample collected, β -Galactosidase activity was measured at 37°C by the traditional Miller method¹⁸. For steady state studies, the activities obtained (in unit of U/ml=OD₄₂₀/min/ml) were plotted against the respective OD₆₀₀, and the resulting slope from linear regression is taken to be the “LacZ expression level” (in unit of U/ml OD₆₀₀, or “Miller Unit”, or “MU” in short). For the transient repression study, β -Galactosidase activity was plotted against time (semi-log scale) to give a direct visual effect. To quantify the transient repression effect, β -Galactosidase activity was plotted against the corresponding OD₆₀₀. The LacZ expression level (in Miller Unit) before the addition of metabolite was determined by calculating the slope of β -Galactosidase activity vs OD₆₀₀ using all the data points obtained before the addition. The LacZ expression level during the transient repression period was obtained as the average of the instantaneous LacZ expression level, with the latter defined as the local slope of the plot of β -Galactosidase activity vs OD₆₀₀ between two consecutive points (taken ~every 5 min).

Absolute LacZ level determination: For the absolute quantitation of the LacZ expression level, the activity of purified β -Galactosidase (Sigma) was measured by the above Miller assay and the activity of 1 μ g of the purified enzyme was found to be equivalent to 1848 U. Thus, one unit activity corresponds to $1/1848 = 5.4 \times 10^{-4}$ μ g β -Galactosidase. Total protein assay (see method below) found the total protein per OD₆₀₀ to be ~ 314 μ g/ml OD₆₀₀ independent of the growth conditions (Fig. S14). Therefore, 1 Miller Unit = 3.2×10^{-3} U/ μ g total protein, and the fraction of β -Galactosidase in total protein giving rise to one Miller Unit is $\sim 1.7 \times 10^{-6}$ μ g β -Galactosidase / μ g total protein. Alternatively, 10,000 Miller Units corresponds to 1.7% of the proteome being β -Galactosidase.

Total RNA quantification: The RNA quantification method is based on the method used by Benthin *et al*¹⁹ with modifications. Briefly, 1.5 ml of cell culture at exponential phase was collected by centrifugation and the cell pellet was fast frozen on dry ice. The cell pellet was thawed and washed twice with 0.6 ml cold 0.1 M HClO₄, then digested with 0.3 ml 0.3 M KOH for 60 min at 37°C with constant shaking. The cell extracts were then neutralized with 0.1 ml 3 M HClO₄ and centrifuged at 13,000 rpm for 5 min. The supernatant was collected and the precipitate was washed twice with 0.55 ml 0.5 M HClO₄. A final volume of 1.5 ml of supernatant was then centrifuged and the supernatant was measured for its absorbance at 260 nm on a Bio-Rad spectrophotometer. The RNA concentration (μ g/ml/ OD₆₀₀) was given by $OD_{260} \times 31/OD_{600}$, where we have used the converting factor of 31 between the OD₂₆₀ and RNA concentration. The converting factor of 31 is based on the molar extinction coefficient is 10.5 mmole⁻¹cm⁻¹ and the average molecular weight of an *E. coli* RNA nucleotide residue is 324.

***kgtP* expression level analysis by quantitative Real-time PCR:** Strains NCM3722 (wt *kgtP*) and NQ738 (*kgtP*^{up}) were grown exponentially in N⁻C⁻ medium with 20 mM NH₄Cl, and one of the following carbon sources: 0.4% (v/v) glycerol, 0.4 (w/v) glucose or 0.2% (w/v) lactose. When OD₆₀₀ reached ~0.5, samples (0.6 ml cell cultures) were collected and treated by RNAprotect Bacteria Reagent (Qiagen) to inactivate RNase activities. Then total RNA for each sample was extracted using RNeasy Mini Kit (Qiagen) and followed by a further treatment with Turbo DNA-free DNase (Ambion) to remove any residual genomic DNA. Subsequent real-time PCR was performed using iScriptTM One-Step RT-PCR Kit with SYBR Green (Bio-Rad) and Bio-Rad iQ5 Multicolor Real-Time PCR Detection System. 100 ng and 1 ng total RNA was used

to detect *kgtP* and 16S rRNA (internal control) expression levels respectively. Primers *kgtP*-F (CGCTGTCCGATAAGATTGGT) and *kgtP*-R (CTCACTATCAGCAGGGCACA) were used for *kgtP* detection. Primers *rrsB*-F (GCTTGCTTCTTTGCTGACGAGT) and *rrsB*-R (TGAGCCGTTACCCACCTAC) were used for 16S rRNA (*rrsB*) detection. To analyze the data, the mRNA level of *kgtP* of NCM3722 strain grown in glycerol was normalized to 1 and all other *kgtP* mRNA levels were determined relative to this value.

Measurement of the intra-cellular glutamate and α -ketoglutarate concentrations: NQ5 cells were grown in minimal medium with 0.4% (v/v) glycerol and 3–20 mM NH_4Cl . At each of the growth conditions, metabolites were extracted and quantified. Internal glutamate was extracted by using a “no-harvest” protocol, and the fluorescent derivatives were quantified by a HPLC-based method as reported²⁴. Internal α -ketoglutarate was extracted by using a “harvest” protocol, and the fluorescent derivatives were quantified by HPLC as reported²⁵.

cAMP excretion assays

It is difficult to determine the intra-cellular cAMP concentrations reliably due to large amounts of cAMP excreted into the medium. The cAMP excretion rate is expected to be proportional to the internal cAMP level²¹. Therefore we used cAMP excretion rate defined as the external cAMP level per OD_{600} multiplied by the specific growth rate, as a proxy.

Sample collection: 1 ml cell culture collected at various OD_{600} levels during exponential growth was fast filtered through a 0.22- μm -pore-size nylon membrane and the filtrate was fast frozen on dry ice and stored at -80°C for further cAMP assay. For steady state study, four to five cAMP assay samples per cell culture were collected at $\text{OD}_{600} = 0.1\sim 0.6$. For transient repression study, five cAMP assay samples were collected for each culture before the addition of oaa. Then at $\text{OD}_{600}\sim 0.5$, 20 mM (final concentration) oaa was added to each cell culture and cAMP assay samples were taken every 4–5 min for ~ 30 min, then every 10–15 min until OD_{600} reached ~ 1.5 .

Measurement of cAMP: We adopted the chloroacetaldehyde derivatization technique for the ethenylation of cAMP as described previously²² with slight modification. 80 μl cAMP sample aliquot or 16 pmol cAMP standard was incubated for 30 min at 70°C in the presence of 1.2 M chloroacetaldehyde (Sigma), 25 mM Na_2HPO_4 [pH 4.0], and 5 mM EDTA in a final volume of 200 μl . The reaction mixture was transferred to ice, alkalized by adding one-third volume of 0.5 M NH_4HCO_3 , filtered through a 0.22- μm -pore-size nylon membrane, and analyzed by high performance liquid chromatography (HPLC) within the day. To quantify ethenylated cAMP, we adopted and modified ion-pair reversed phase HPLC originally developed for separation and quantification of ethenylated adenosine compounds²³. The HPLC system used was Shimadzu Prominence HPLC system composed of LC-20AB binary pump, SIL-10AF autosampler, and RF-10AxL fluorescence detector as main modules. Eluent flow-rate was 1.5 ml/min. The eluent used was a TBAS (Tetrabutylammoniumhydrogensulfate, Waters Corp) buffer (5.7 mM TBAS, 30.5 mM KH_2PO_4 adjusted to pH 5.8 with phosphoric acid) and an acetonitrile buffer (acetonitrile:TBAS buffer, 2:1). 70 μl sample aliquot was injected on XTerra MS C₁₈ column (3.0 x 50 mm, I.D. 3 mm, 5 μm particle size; Waters Corp.) equipped with its guard column and maintained at 40°C during separation. The elution was isocratic with 90% TBAS buffer (10% acetonitrile buffer) for 3 min after injection, decreased to 50% TBAS buffer in 3 sec, remaining

isocratic for 1.9 min, and re-equilibrated with 90% TBAS buffer for 2 min. The fluorescence signal was monitored at an excitation wavelength of 280 nm and an emission wavelength of 410 nm. Ethenylated cAMP typically eluted between 1.5 and 1.6 min. This peak was not observed in the filtrate of the Δ cytA strain-grown culture (Fig. S11a).

Analysis of transient cAMP excretion: To quantify the transient effect of oaa addition on cAMP excretion rate of a culture, we separately obtained the excretion rate before and during the transient repression period for the culture. The cAMP excretion rate before oaa addition was determined by calculating the slope of cAMP external concentration vs OD₆₀₀ plot using all the data points obtained before oaa addition, and multiplying the slope by the growth rate. The cAMP excretion rate during the transient repression period was represented by the averaged cAMP excretion rate. For the latter, we first calculated the local slope in the plot of cAMP external concentration vs OD₆₀₀ between consecutive time points (every ~5 min) after oaa addition, and then multiplying each slope by the specific growth rate to get the “instantaneous” cAMP excretion rate. These instantaneous excretion rates were averaged to obtain the average excretion rate shown in Fig. 3e.

***In vitro* adenylate cyclase activity assay**

Adenylate cyclase (AC) of *E. coli* is a membrane-bound protein. To the best of our knowledge, no one has succeeded in assaying the *in vitro* AC activity using reconstitute membrane vesicles with purified AC. In our study, we adopted a previous AC activity assay method²⁶ using permeabilized cells with slight modifications as described below. Because this is a whole cell assay, we deleted the cAMP phosphodiesterase (encoded by *cpdA*) in all the *E. coli* strains used in the analysis, in order to avoid the degradation of cAMP synthesized by AC. The *cpdA* deletion itself does not affect catabolite repression (the C-line) nor transient repression; see Fig. S33.

In our method, various *E. coli* strains were grown in minimal medium until mid-exponential phase. Cells were then collected by centrifugation at 4500 rpm for 10 min at 4°C and washed with cold 50 mM Tris, pH 7.5. Cell pellets were re-suspended and concentrated in the same Tris buffer to give a total OD₆₀₀ ~15, which contained ~5 mg total protein/ml. This concentrated cell suspension was then supplied with 1% (v/v, final concentration) toluene and was shaken at 70 rpm at RT for 10 min to permeabilize cells. Subsequently, 400 µl of the permeabilized cells containing ~2 mg total protein were added to 1.6 ml reaction buffer to give a 2 ml reaction system and the mixture was further incubated at 30°C water bath for 20 min. This 2 ml reaction system contains 50 mM Bicine buffer, pH 9.0, 1 mM ATP, 15 mM K₂HPO₄, 20 mM MgCl₂, 20 mM phosphocreatine di(tris) (Sigma) and 100 U/ml creatine phosphate kinase (Sigma). At various time intervals during this incubation period (0 - 20 min) at 30°C, reaction mixtures were taken out and heated at 100°C for 5 min to stop the reaction. The cAMP amount in each reaction mixture terminated at different time points was quantified by a cAMP assay kit (RPN225, GE Healthcare). The amount of cAMP generated at each time point per total protein was plotted and the slope from the linear regression analysis represents the AC activity. To study the repression effect of various metabolites (oaa, akg, pyr, succ) on AC activity, 0 or 10 mM final concentration of each metabolite was added to the above 1.6 ml reaction buffer first, then 400 µl toluene-treated cells were added to this mixture to start the assay as described above. To obtain the relative AC activity shown in Fig. 4d for each strain background, the AC activities obtained with

various metabolite additions were normalized by the AC activity obtained from the same strain but without any metabolite addition.

Supplementary Notes (Theoretical Analysis)

Supplementary Note 1: Proteome fractions and the proteome partition model.

As described in the main text and illustrated in Fig. S17, proteins exhibiting similar growth-rate dependences upon various modes of growth limitation are grouped into ‘sectors’. For example, the ribosomal proteins and other proteins affiliated with the translational process comprise the “R-sector”, whose total mass content as a fraction of the total proteome mass is denoted as ϕ_R . Similarly, we define a C-sector (of mass fraction ϕ_C), consisting of the catabolic and energy-generating proteins which are up-regulated specifically in response to C-limitation. In addition to the examples shown in Fig. S5, the broad membership of genes belonging to this sector is well documented in numerous transcriptomic and proteomic studies²⁷⁻³¹. We also introduce an A-sector (of mass fraction ϕ_A), consisting of proteins needed for the assimilation of ammonia and the biosynthesis of amino acids. We expect the expressions of these genes to behave similarly as *PglnA* (Fig. 1d, see also Fig. S13), as were reported anecdotally in previous studies³². The existence of other sectors of metabolism whose responses have not been specifically probed in this study (e.g., sulfur and nucleotide assimilation, nucleotide synthesis, anaerobic metabolism) are lumped together into an additional U-sector of mass fraction ϕ_U . Finally, there may exist a growth-rate independent sector (I) of mass fraction ϕ_I . The existence of such a sector, postulated to contain core, housekeeping proteins, is also supported by results from early proteomic study²⁹.

By their definitions, the above five proteome fractions are constrained by

$$\phi_R(\lambda) + \phi_C(\lambda) + \phi_A(\lambda) + \phi_U(\lambda) + \phi_I = 1 \quad [\text{S1}]$$

for any growth condition. Other than the I-sector which is growth-rate independent, the growth-rate dependences of these sectors are assumed to have the following characteristics: Each sector increases upon one mode of growth limitation (“specific response”) but decreases upon other modes of growth limitations (“general response”). Thus the C-sector increases upon C-limitation (solid red line in Fig. 1a) but decreases upon A-limitation (dashed red line in Fig. 1a) and translational limitation (Fig. S15b), while the A-sector increases upon A-limitation (dashed blue line in Fig. 1d) but decreases upon C-limitations (solid blue line in Fig. 1d) and translational limitation (Fig. S15c), and the R-sector increases upon translational limitation (dashed green lines in Fig. S15a) but decrease upon C- and A- limitation (green line in Fig. 1c). The U-sector, comprised of genes that do not respond specifically to C-, A-, or translational limitations, are expected to exhibit only general responses, i.e., decreasing with decreasing growth rate as exemplified in Fig. S16.

We denote the maximum proteome fraction of a sector j (*specific* response of the sector extrapolated to $\lambda = 0$) as $\phi_{j,\max}$, and the minimum proteome fraction of the sector (*general* response extrapolated to $\lambda = 0$) as $\phi_{j,0}$. It will be useful to interpret $\phi_{j,0}$ as the growth-rate independent part of sector j , and introduce the growth-rate dependent part as $\Delta\phi_j(\lambda) \equiv \phi_j(\lambda) - \phi_{j,0}$; see Fig. S17. The constraint [S1] can be rewritten as

$$\Delta\phi_R(\lambda) + \Delta\phi_C(\lambda) + \Delta\phi_A(\lambda) + \Delta\phi_U(\lambda) = \phi_{\max}, \quad [\text{S2}]$$

where

$$\phi_{\max} \equiv 1 - \phi_I - \phi_{R,0} - \phi_{C,0} - \phi_{A,0} - \phi_{U,0} \quad [\text{S3}]$$

can be viewed as a “cap” on how large the proteome fraction of a sector can be increased to under specific responses. As illustrated in Fig. S17, the growth-rate independent components in Eq. [S3] act as an effective sector (Q) of mass fraction $\phi_Q = \phi_I + \sum_j \phi_{j,0}$ as was introduced in Ref. 17, such that $\phi_{\max} = 1 - \phi_Q$. Note that in term of $\Delta\phi_j$, the maximal proteome fraction of specific response corresponds to $\Delta\phi_j(\lambda = 0) = \phi_{j,\max} - \phi_{j,0}$ and the minimal proteome fraction of general response corresponds to $\Delta\phi_j(\lambda = 0) = 0$. Eq. [2] then yields the important relation

$$\phi_{j,\max} - \phi_{j,0} = \phi_{\max} \quad [\text{S4}]$$

for *each* sector j .

In Fig. 1 of the main text, we see that the general response of each sector has a linear growth-rate dependence. We will write them as follows:

$$\phi_R(\lambda) - \phi_{R,0} = \Delta\phi_R(\lambda) = \lambda / \nu_R, \quad [\text{S5}]$$

$$\phi_C(\lambda) - \phi_{C,0} = \Delta\phi_C(\lambda) = \lambda / \nu_C, \quad [\text{S6}]$$

$$\phi_A(\lambda) - \phi_{A,0} = \Delta\phi_A(\lambda) = \lambda / \nu_A, \quad [\text{S7}]$$

$$\phi_U(\lambda) - \phi_{U,0} = \Delta\phi_U(\lambda) = \lambda / \nu_U, \quad [\text{S8}]$$

where the ν s are phenomenological parameters whose inverses give the slopes of the linear growth-rate dependences. As will be clear from their molecular interpretations (Supp Note 4), the values of these parameters are determined by the properties of the metabolic enzymes (ν_C , ν_A , ν_U) and the translational machineries (ν_R). Their numerical values can be deduced for various strains/medium studied (Supp Note 3) and are listed in Table S5, S14, and S15.

The central component of the proteome partition model is the simplifying assumption that Eqs.[S5]-[S8] describe not only the general responses (as observed), but also the *specific* responses. We shall show below that with this assumption, Eqs. [S5]-[S8] together with Eq. [S2] *quantitatively* account for all the specific responses. Moreover, we will explain in Supp Note 4 how Eqs.[S5]-[S8] may arise naturally from a single constraint, that the rate of protein synthesis is the bottleneck of cell growth. Finally in Supp Note 5, we will describe how cellular regulatory mechanisms ensure that Eqs.[S5]-[S8] are simultaneously satisfied during steady-state growth.

Under our assumption, the growth rate λ can be obtained by simply solving Eqs. [S5]-[S8] simultaneously with the constraint [S2], yielding the result

$$\lambda(\nu_R, \nu_C, \nu_A, \nu_U) = \phi_{\max} / (\nu_R^{-1} + \nu_C^{-1} + \nu_A^{-1} + \nu_U^{-1}). \quad [\text{S9}]$$

Thus in our model, the parameters ν s and ϕ_{\max} determine the growth rate of the cells. While the ν s are medium/condition dependent as described in Supp Notes 3 and 4, ϕ_{\max} is a fixed constant; its value (~43% of the proteome) can be deduced experimentally (Supp Note 2 and Fig. S18).

With the knowledge that the growth rate depends on all the ν s (state variables in the sense of thermodynamics), the opposing linear growth-rate dependences of the general and specific

responses shown in Figs. 1 and 2 can be seen to follow simply from Eqs. [S5]-[S8]. Consider for instance the C-sector (Eq. [S6]): If the growth rate is changed by varying any parameters other than ν_C , then ϕ_C is linear in λ , i.e., the general response decreases with decreasing growth rate. This behavior corresponds to the NC-lines for the C-sectors (dashed and dotted lines in Fig. 1a). We can thus identify the non-carbon (NC) modes of growth limitation with those that do not affect the value of ν_C . However, if growth is affected by changing the value of ν_C , then Eq. [S6] no longer implies a linear relation between ϕ_C and λ . In this case, the growth-rate dependence of ϕ_C can be obtained by substituting Eqs. [S5], [S7], [S8] in [S2], yielding

$$\phi_C(\lambda) = \phi_{C,\max} - \lambda \cdot (\nu_R^{-1} + \nu_A^{-1} + \nu_U^{-1}), \quad [\text{S10}]$$

with $\phi_{C,\max} = \phi_{\max} + \phi_{C,0}$. Eq. [S10] is exactly of the form of the C-line (Eq. [1] of the main text), with the intercept

$$\lambda_C = \phi_{C,\max} / (\nu_R^{-1} + \nu_A^{-1} + \nu_U^{-1}). \quad [\text{S11}]$$

Thus, C-limitation (varying carbon sources, or changing the rate of carbon uptake) corresponds to varying ν_C in the model, and the specific response (the response of the C-sector to C-limitation) is seen as the consequence of general responses by the other proteome fractions to C-limitation (Eqs. [S5], [S7], [S8]), together with the constraint [S2]. Note that by comparing Eqs. [S9] and [S11], we see that λ_C , the x-intercept of the C-line, is the growth rate corresponding to $\nu_C \rightarrow \infty$, i.e., the situation where carbon uptake is not growth limiting at all.

Similarly, the A-sector has the following growth-rate dependence upon varying ν_A ,

$$\phi_A(\lambda) = \phi_{A,\max} - \lambda \cdot (\nu_R^{-1} + \nu_C^{-1} + \nu_U^{-1}) \quad [\text{S12}]$$

with $\phi_{A,\max} = \phi_{\max} + \phi_{A,0}$. Eq. [S12] gives the A-line (Eq. [2] of the main text), with the intercept

$$\lambda_A = \phi_{A,\max} / (\nu_R^{-1} + \nu_C^{-1} + \nu_U^{-1}). \quad [\text{S13}]$$

We can thus associate A-limitation (e.g., the effect of GDH titration as depicted in Fig. S6) to varying ν_A in the model. The predictions [S11] and [S13] are quantitatively verified by the data shown in Figs. 1, 2, S19-S20, as described in detail in Supp Note 3; see also Fig. S21.

Supplementary Note 2: Unnecessary protein expression and the determination of ϕ_{\max} .

In this note, we discuss the parameter ϕ_{\max} in the proteome partition model described in Supp Note 1. This is an important global parameter whose value directly affects the growth rate (Eq. [S9]). Its value can be determined experimentally by considering the effect of the unnecessary expression of a protein, e.g., LacZ reporters in medium not containing lactose. Suppose this protein product comprises a fraction ϕ_{UE} of the proteome. Eq. [S2] is changed to

$$\Delta\phi_R + \Delta\phi_C + \Delta\phi_A + \Delta\phi_U + \phi_{UE} = \phi_{\max}. \quad [\text{S14}]$$

Using Eqs. [S5]-[S8] in Supp Note 1, we have

$$\lambda(\nu_R, \nu_C, \nu_A, \nu_U; \phi_{UE}) = \frac{\phi_{\max} - \phi_{UE}}{\nu_R^{-1} + \nu_C^{-1} + \nu_A^{-1} + \nu_U^{-1}}. \quad [\text{S15}]$$

If we compare the strains with/without unnecessary protein expression in otherwise identical background and grown in the same medium, then all the ν s are fixed. We have

$$\delta\lambda \equiv 1 - \frac{\lambda(\phi_{UE})}{\lambda(\phi_{UE} = 0)} = \frac{\phi_{UE}}{\phi_{\max}}. \quad [\text{S16}]$$

Thus, by quantifying $\delta\lambda$, the relative change in growth rate due to unnecessary protein, and the absolute amount of the protein expressed (ϕ_{UE}), we can obtain the scale ϕ_{\max} ; see Fig. S18. This result obtained ($\phi_{\max} \approx 43\%$) is similar to that estimated previously¹⁷ (with $\phi_{R,\max} \approx 51\%$ and $\phi_{R,0} \approx 7\%$ for growth in minimal medium) using explicit conversion factors. Note that the prediction [S16] does not depend on how the unnecessary expression is regulated. This result is verified in Fig. S18 whether LacZ expression driven by a catabolic promoter (*PlacZ*) and a synthetic constitutive promoter (P_{LtetO1}) are found to fall on the same line described by Eq. [S16].

Next we consider the effect when the unnecessary protein expressed is a reporter of the C-sector, as *PlacZ-LacZ* expression, used as the indicator of C-sector, was enough to cause detectable changes in the growth rate according to Fig. S18. Towards this end, we model the unnecessary protein expression to be proportional to the C-sector, i.e.,

$$\phi_{UE} = c \cdot \phi_C \quad [\text{S17}]$$

with a proportionality constant c . Using Eq. [S17] in Eq. [S14] along with Eqs. [S5], [S7], [S8] for C-limited growth (varying v_C), we obtain

$$\phi_{UE} = \frac{c}{1+c} \cdot \left[\phi_{C,\max} - \lambda \cdot (v_R^{-1} + v_A^{-1} + v_U^{-1}) \right]. \quad [\text{S18}]$$

Comparing to the growth-rate dependence of C-sector in the absence of reporter (Eq. [S10]), we see that the reporter expression changes only the overall scale in protein expression and does not affect the important quantity, i.e., the x-intercept λ_c . Under NC-limitation,

$$\phi_{UE} = c \cdot \left[\phi_{C,0} + \lambda / v_C \right] \quad [\text{S19}]$$

according to Eqs. [S17] and [S6].

Comparing Eqs. [S18] and [S19], we see that the overall scales differ by a factor of $1+c$. For strains expressing *PlacZ-lacZ* (either via IPTG induction or LacI deletion), we estimated the proportionality constant c to be $\sim 13\%$ ^a. This degree of discrepancy between the scales of Eqs. [S18] and [S19] is not noticeable given the uncertainties in the other parameters of the C-line.

Supplementary Note 3: Quantitative analysis based on the normalized proteome fractions.

The proteome partition model described in Supp. Note 1 cannot be directly confronted with data in quantitative terms, because the absolute values of the proteome fractions are not known other than the R-sector. Specifically, except for the R-sector for which the RNA-protein ratio can be directly converted to the fraction of ribosomal proteins through the known stoichiometry of the

^a For glucose minimal medium, $f_C \approx 25\%$ according to Fig. 2b. Thus $\phi_C \approx 11\%$ since $\phi_{\max} \approx 43\%$. The level of LacZ expression in glucose minimal medium is 8200 MU, which is about 1.4% of the proteome (see Supp Methods for the conversion). Thus $\phi_{UE} \approx 1.4\%$. The proportionality constant is then obtained as $c = \phi_{UE} / \phi_C \approx 13\%$.

ribosome¹⁷, the best we can hope to learn about the C- and A- sectors is that their proteome fractions ϕ_C and ϕ_A are proportional to the reporters, e.g., *PlacZ* and *PglnA* in Fig. 1.

However, the following observation makes quantitative analysis possible: By dividing both sides of the constraint [S2] by ϕ_{\max} and noting that the difference between the maximal specific response $\phi_{j,\max}$ and the minimal general response $\phi_{j,0}$ is just ϕ_{\max} (Eq.[S4]) for *each* sector j , Eq. [S2] can be written in a much-simplified form,

$$f_R(\lambda) + f_C(\lambda) + f_A(\lambda) + f_U(\lambda) = 1, \quad [\text{S20}]$$

where

$$f_j(\lambda) \equiv \frac{\phi_j(\lambda) - \phi_{j,0}}{\phi_{j,\max} - \phi_{j,0}} = \frac{\Delta\phi_j(\lambda)}{\phi_{\max}} \quad [\text{S21}]$$

is the “normalized proteome fraction” for the sector j . *A very convenient feature of the normalized fraction $f_j(\lambda)$ is that it can be obtained quantitatively from the reporter level for each sector.* E.g., if sector j has a reporter whose level (reporter amount per total protein) is Z_j , and if $\Delta Z_j(\lambda) \propto \Delta\phi_j(\lambda)$ where $\Delta Z_j(\lambda) \equiv Z_j(\lambda) - Z_{j,0}$ then the normalized fraction is obtained as

$$f_j(\lambda) = \frac{Z_j(\lambda) - Z_{j,0}}{Z_{j,\max} - Z_{j,0}}, \quad [\text{S22}]$$

where $Z_{j,\max}$ and $Z_{j,0}$ are respectively the maximum specific response and minimum general response of the reporter. In this way, we can convert the results of *PlacZ*, *PglnA* reporters (L and G in Fig. 1a and 1d) into normalized fractions f_C and f_A respectively (right axis of these plots). [Note that although reporter expressions are normalized to OD₆₀₀ (MU), the ratio of total protein amount to OD₆₀₀ is growth rate independent (Fig. S14).] Similarly, taking the RNA/protein ratio (r) as a reporter of the R-sector, we can obtain the normalized fraction f_R (right axis of Fig. 1c and S15a), without invoking the stoichiometry of the ribosome. Note that this approach does not even require the linear growth-rate dependence of the various sectors.

Next we analyze the cases where the proteome fractions do take on *linear* growth-rate dependences as observed in our experiments.

	specific response	general response
<i>PlacZ</i> expression (L)	$L = L_{\max} \cdot (1 - \lambda / \lambda_C)$	$L = L_0 + \alpha_C \cdot \lambda$
<i>PglnA</i> expression (G)	$G = G_{\max} \cdot (1 - \lambda / \lambda_A)$	$G = G_0 + \alpha_A \cdot \lambda$
RNA/protein (r)	$r = r_{\max} \cdot (1 - \lambda / \lambda_R)$	$r = r_0 + \alpha_R \cdot \lambda$

Table N1: Linear dependences of *PlacZ*, *PglnA* reporter levels, L and G respectively, as shown in Figs. 1a, 1d, and the RNA/protein ration r as shown in Fig. 1c and S15a, are sorted into two groups, specific and general response, and denoted by the expressions above. The values of the empirical parameters defined here are provided in Tables S5, S14-S15.

The empirical growth-rate dependences of the reporters of the various sectors are summarized in Table N1 above, with the values of the parameters given in Tables S5, S14-S15. These relations lead to the following expressions for the normalized fractions (using Eq. [S22]):

	normalized specific response	normalized general response
C-sector	$f_C = 1 - \lambda / \tilde{\lambda}_C; \tilde{\lambda}_C = \lambda_C \cdot (1 - L_0 / L_{\max})$	$f_C = \tilde{\alpha}_C \cdot \lambda; \tilde{\alpha}_C = \alpha_C / (L_{\max} - L_0)$
A-sector	$f_A = 1 - \lambda / \tilde{\lambda}_A; \tilde{\lambda}_A = \lambda_A \cdot (1 - G_0 / G_{\max})$	$f_A = \tilde{\alpha}_A \cdot \lambda; \tilde{\alpha}_A = \alpha_A / (G_{\max} - G_0)$
R-sector	$f_R = 1 - \lambda / \tilde{\lambda}_R; \tilde{\lambda}_R = \lambda_R \cdot (1 - r_0 / r_{\max})$	$f_R = \tilde{\alpha}_R \cdot \lambda; \tilde{\alpha}_R = \alpha_R / (r_{\max} - r_0)$

Table N2: Expressions and the definitions of the scaled parameters, $\tilde{\lambda}$ s for the normalized specific responses and $\tilde{\alpha}$ s for the normalized general responses. The values of these scaled parameters are provided at the bottom of Tables S5, S14-S15.

Comparing the expressions of the general response $f_j = \tilde{\alpha}_j \cdot \lambda$ for a sector j with Eqs. [S5]-[S8] (and remembering the definition [S21] for the normalized proteome fraction), we can obtain the phenomenological parameters of the proteome partition model (Supp Note 1) in terms of the parameters $\tilde{\alpha}$ s:

$$v_j^{-1} = \phi_{\max} \cdot \tilde{\alpha}_j. \tag{S23}$$

The values of the v s are given in Tables S5, S14-S15.

The normalized response of each sector under different modes of growth limitations is enumerated in the Table N3 below:

	C-limited	A-limited	R-limited
C-sector	$f_C = 1 - \lambda / \tilde{\lambda}_C$	$f_C = \tilde{\alpha}_C \cdot \lambda$	$f_C = \tilde{\alpha}_C \cdot \lambda$
A-sector	$f_A = \tilde{\alpha}_A \cdot \lambda$	$f_A = 1 - \lambda / \tilde{\lambda}_A$	$f_A = \tilde{\alpha}_A \cdot \lambda$
R-sector	$f_R = \tilde{\alpha}_R \cdot \lambda$	$f_R = \tilde{\alpha}_R \cdot \lambda$	$f_R = 1 - \lambda / \tilde{\lambda}_R$
U-sector	$f_U = \tilde{\alpha}_U \cdot \lambda$	$f_U = \tilde{\alpha}_U \cdot \lambda$	$f_U = \tilde{\alpha}_U \cdot \lambda$

Table N3: Normalized forms of specific and general responses to various modes of growth limitation. The parameters ($\tilde{\lambda}$ and $\tilde{\alpha}$ except for $\tilde{\alpha}_U$) are defined in Table N2; their values are given in Table S5, S14-S15.

Applying the constraint [S20] to each mode of growth limitation, we obtain the following constraints among the parameters $\tilde{\alpha}$ and $\tilde{\lambda}$:

$$\tilde{\alpha}_R + \tilde{\alpha}_U + \tilde{\alpha}_A = \tilde{\lambda}_C^{-1} \quad \text{under C-limitation,} \tag{S24}$$

$$\tilde{\alpha}_R + \tilde{\alpha}_U + \tilde{\alpha}_C = \tilde{\lambda}_A^{-1} \quad \text{under A-limitation,} \tag{S25}$$

$$\tilde{\alpha}_U + \tilde{\alpha}_C + \tilde{\alpha}_A = \tilde{\lambda}_R^{-1} \quad \text{under R-limitation.} \tag{S26}$$

Note that with the relation [S23], Eqs. [S24] and [S25] can be identified as the same as Eqs. [S11] and [S13] predicted in Supp Note 1 for the x-intercept of the C- and A- lines, λ_C and λ_A respectively.

Using Eq. [S24] and the values of the other scaled parameters ($\tilde{\lambda}_C, \tilde{\alpha}_A, \tilde{\alpha}_R$ as listed in Table S16) for wild-type cells under C-limited growth, we obtained $\tilde{\alpha}_U \approx 0.13 \pm 0.04 h$, which is the slope of the purple line drawn in Fig. 2b). This is $\sim 30\%$ of the value of $\tilde{\alpha}_R \approx 0.44 \pm 0.02 h$ (Table S14), suggesting that $f_U \approx 0.3 \cdot f_R$ for C-limited growth. Using these values of $\tilde{\alpha}_U$ and $\tilde{\alpha}_R$, together with the values of $\tilde{\alpha}_C$ for A-limited growth with glycerol and glucose as carbon sources (Table S5), Eq. [S25] predicts the values of $\tilde{\lambda}_A$ (bottom of Table S16, shown as the dashed black lines in Figs. 2c and S19 respectively). Similarly, Eq. [S24] is used to predict the value of $\tilde{\lambda}_C$ for C-limited growth under a fixed degree of GDH titration (black line in Fig. S20), and Eq. [S26] is used to predict the value of $\tilde{\lambda}_R$ for translational limitation with glucose as the carbon source (black line in Fig. S22). Also listed in Table S16 (last row) are the unscaled values of $\lambda_C, \lambda_A, \lambda_R$ for the different strains/medium. They compare well to the respective best-fit values; see Fig. S21.

The congruence between the predicted and observed results for these 3 unrelated modes of growth limitations (Figs. 2b, 2c, S19-S22) strongly support our key hypothesis that the observed linear relations are not independent but are results of the proteome-level constraint [S20].

Supplementary Note 4: The origin of the linear growth rate dependences.

We next investigate the molecular origin(s) of the linear growth-rate dependences observed in Figs. 1, 2, and summarized by Eqs. [S5]-[S8] of Supp Note 1. The ribosomal fraction ϕ_R is long known to exhibit a linear dependence on the growth rate λ upon nutrient limitation, with a slope whose inverse (ν_R) is set^b by the peptide elongation rate¹⁷. The linear dependence between ϕ_R and λ arises simply from observing that the rate of accumulation of total protein mass (M), $\lambda \cdot M$ for balanced exponential growth, is given by the number of ribosomes ($\phi_R \cdot M$) each translating at the maximal rate (ν_R), *if all ribosomes are engaged in translation*. Thus, it reflects the fact that protein synthesis by ribosome is the bottleneck of cell growth^{17,33}. [The offset $\phi_{R,0}$ reflects the existence of a fraction of ribosomes not engaged in translation, e.g., the “free” ribosomes ready to initiate translation; see Ref. 17].

The linear growth-rate dependence of the C-sector (Eq. [S6]) is characterized by a slope which varies inversely with the quality of the carbon source; see Fig. 1a (red dashed and dotted lines). The inverse of the slope, ν_C , reflects the efficiency of catabolism of this carbon source, since it can be defined as $\nu_C = \partial \lambda / \partial \phi_C$, i.e., the incremental increase in growth per investment of

^b The value obtained from Fig. 1D, $\nu_R \approx 5.3 h^{-1}$ (Table S14), is comparable to that obtained previously from Ref. 17 ($\kappa_i / \rho \approx 5.9 h^{-1}$ in their notation).

the proteome in the catabolic sector^c. Similarly, the linear growth-rate dependence of the A-sector is characterized by a slope whose inverse, ν_A can be defined similarly as the efficiency of amino acid synthesis, as $\nu_A = \partial\lambda / \partial\phi_A$, and the slope of the U-sector dependence on growth rate is characterized by the inverse of $\nu_U = \partial\lambda / \partial\phi_U$.

The meaning of the linear growth-rate dependences exhibited by Eqs. [S5]-[S8] can be appreciated by considering the metabolic fluxes processed by each sector. For instance, the carbon flux can be written as $J_C = \lambda / Y_C$, where Y_C is the carbon yield. Eq. [S6] then becomes

$$J_C = \nu_C \cdot \Delta\phi_C / Y_C. \quad [\text{S27}]$$

Since the proteome fraction is proportional to the enzyme concentration (since the total protein mass of a cell is proportional to the cell volume¹⁰), Eq. [S27] states that the carbon flux is proportional to the concentration of C-sector proteins up to a constant offset. This arises if carbon catabolism is operating in the enzyme-limited regime^d, with the offset possibly arising from carbon loss/excretion, or the same enzymes supplying non-carbon related fluxes. Similarly, the nitrogen (ammonium) flux can be written as $J_N = \lambda / Y_N$, where Y_N is the nitrogen yield. As the bulk of the cellular nitrogen is used in amino acid synthesis³⁶, we have

^c From Table S5, $\nu_C \approx 8.0 \text{ h}^{-1}$ for wild-type cells grown in glucose minimal medium. At the growth rate of $\sim 0.85 \text{ h}^{-1}$ (Table S1), this corresponds to an investment of $\phi_C \approx 11\%$ of the proteome for carbon catabolism. Note that ν_C of glucose is almost 3x that of glycerol (3.0 h^{-1}). However, the growth rate of the cell in glucose is only $\sim 40\%$ faster than in glycerol ($\sim 0.63 \text{ h}^{-1}$). Similarly, ν_C of lactose (20 h^{-1}) is 2.5x that of glucose, but growth in lactose is only 10% faster (Table S1). These results reflect the Michaelis dependence of the growth rate on the ν s (Eq. [S9]).

^d It is useful to compare Eq. [S27] to typical enzyme dominated reactions. Let us suppose that the C-sector involves N_C catabolic enzymes each with mass m_c and catalytic rate k_c . Then the total carbon flux, measured in the amount of sugar uptake per dry mass, is $J_C = k_c \cdot N_C / M_{\text{cell}}$ where M_{cell} is the dry mass of the cell. Let $\Delta\phi_C = N_C \cdot m_c / M$, where M is the total protein mass. Then Eq. [S27] becomes $\nu_C m_c = Y_C k_c \cdot (M / M_{\text{cell}})$. Taking $M = 0.66 \cdot M_{\text{cell}}$ for our strains, then for growth in lactose minimal medium where $\nu_C \approx 20 \text{ h}^{-1}$ (Table S5) and $Y_C \approx 150 \text{ g d.w./mol lac}$ (since 1mM lactose supports the growth of 0.3 OD₆₀₀, and 1 OD₆₀₀ is $\sim 0.15 \text{ g dry weight}$), we obtain $k_c \approx m_c \cdot 0.34 / \text{min}$, with m_c measured in number of amino acids. Of the two primary enzymes needed for the utilization of lactose, LacY and LacZ (denoted by Y and Z respectively), $m_Y \approx 400$, $m_Z \approx 4000$, $k_Y \approx 10 / \text{sec}$ (Ref. 34) and $k_Z \approx 480 / \text{sec}$ (Ref. 35); this amounts to a minimal total enzyme mass of $m_c \approx 23000$ to achieve a catalytic rate of : $480 / \text{sec}$. The formula above predicts $k_c \approx 130 / \text{sec}$ for $m_c \approx 23000$, giving $\sim 27\%$ of the reported rates. Thus the estimate gave the right order of magnitude. Discrepancies may lie in the other catabolic enzymes expressed, e.g., the *gal* operon needed to metabolize galactose derived from the degradation of lactose, the *fuc* operon which is induced without any apparent signals (Fig. S5); there are also uncertainties in the estimates of the catalytic rates which are done at different temperatures (see Ref. 34 and references therein.) Note that for cells grown at $\sim 1/\text{hr}$ in lactose minimal medium (Table S1), the size of the C-sector is $\Delta\phi_C \approx 5\%$ according to Eq. [S6] with $\nu_C \approx 20 \text{ h}^{-1}$. This is consistent with the measured LacZ expression level of 5800 MU (Table S1), corresponding to 1% of the proteome (see Supp. Method for conversion), which together with a possibly larger amount of LacY, comprise about half of the C-sector.

$$J_N = v_A \cdot \Delta\phi_A / Y_N, \quad [\text{S28}]$$

which occurs if amino acid synthesis is operating in the enzyme-limited regime. An analogous equation for the U-sector is,

$$J_U = v_U \cdot \Delta\phi_U / Y_U. \quad [\text{S29}]$$

Recent metabolomics studies³⁷ indeed found that the concentrations of many cellular metabolites are at levels significantly larger than the K_M values of the corresponding enzymes, supporting the notion suggested here by the enzyme-limited forms of the metabolic fluxes (Eqs. [S27]-[S29]). Moreover, operating metabolic reactions in the enzyme-limited regions is a very reasonable strategy if protein synthesis is indeed the bottleneck of growth. Thus Eqs. [S27]-[S29], which underlie Eqs. [S6]-[S8], can be seen as reflection of the cell's response to protein synthesis as the growth bottleneck, as Eq. [S5] was established long ago.

Supplementary Note 5: A coarse-grained theory of bacterial growth control.

In Supp Note 1 and 4, we showed that all of the linear growth-rate dependences characterized in Figs. 1 and 2 of the main text can be understood from several principles: (i) the bacterial growth law (Eq. [S5]), (ii) enzyme-limited metabolism (Eqs. [S27]-[S29]), (iii) the flux matching condition

$$Y_j J_j = \lambda \quad [\text{S30}]$$

for each component of the flux J_j , and (iv) the constraint [S2] among the proteome fractions.

Together they pose a constrained optimization problem: For cells to grow fast, it should increase its ribosomal fraction of the proteome as much as possible (as dictated by the growth law [S5]); it should also increase the various metabolic fractions of the proteome as much as possible to support increased metabolic fluxes (Eqs. [S27]-[S30]) demanded by faster growth. However, the sum of the proteome fractions is constrained by [S2]. The cell is apparently able to allocate the appropriate proteome fractions to satisfy the metabolic and proteome constraints simultaneously, since simultaneous algebraic solution of these equations (i.e, Eqs. [S2], and [S5]-[S8]), which is equivalent to Eqs. [S2], [S5], [S27]-[S30]), describes the data well (see Supp Note 3).

How does the cell “solve” these coupled algebraic equations simultaneously? At the molecular level, the expression of cellular proteins is of course dictated by the regulatory mechanisms. We will show in a coarse-grained model below that this can be accomplished by the integral feedback scheme of metabolic control depicted in Fig. 3a of the main text.

We shall first focus on the coordination of the C- and A- fluxes. The expressions of the C- and A- sector proteins are controlled by the precursor K in the feedback model of Fig. 3a, denoted by $\Delta\phi_C(K)$ and $\Delta\phi_A(K)$. These proteome fractions in turn lead to K -dependent fluxes $J_C(K)$ and $J_N(K)$. The crux of the feedback scheme is that these two fluxes affect the changes in the level of K itself (hence the name “integral feedback”). Converting to a common flux currency using Eq. [S29], we have

$$\frac{dK}{dt} \propto Y_C J_C(K) - Y_N J_N(K). \quad [\text{S31}]$$

From the dependence of the fluxes on the proteome fractions (Eqs. [S27],[S28]), the steady-state condition for Eq. [S31], i.e., $dK / dt = 0$ leads to

$$v_C \cdot \Delta\phi_C(K^*) = v_A \cdot \Delta\phi_A(K^*), \quad [\text{S32}]$$

where K^* is the steady-state value of K . [The direction of the regulation ensures that K^* is a stable solution; see Fig. S36]. Eq. [S32] is a statement of *metabolome-proteome coordination*, and illustrates how the cell simultaneously “solves” Eq. [S27] and [S28]. It implicitly defines the solution $K^*(v_C, v_A)$ which depends on the medium and genetic parameters (v_C, v_A) , as long as the solution exists for suitable forms of $\Delta\phi_C(K)$ and $\Delta\phi_A(K)$ (to be discussed below). The forms of $\Delta\phi_C(K^*)$ and $\Delta\phi_A(K^*)$ together with $K^*(v_C, v_A)$ then specifies the values of the proteome fractions ϕ_C , and ϕ_A in different medium (specified by v_C and v_A), as well as $\lambda(K^*)$ through Eqs. [S6] and [S7]. The growth-rate dependences of these proteome fractions are implicitly determined by the functions $\Delta\phi_C(K^*)$, $\Delta\phi_A(K^*)$ and $\lambda(K^*)$.

The same feedback strategy can be used to set the R-sector. As depicted in Fig. 3a, the feedback agent here is the level of the amino acid. J_N , which supplies the amino acids, must be balanced by J_R , which is the flux by which the amino acids are consumed by the ribosomes. The latter is given by

$$J_R = v_R \cdot \Delta\phi_R / Y_R \quad [S33]$$

where Y_R captures the amino acid content of the biomass. Ribosomal synthesis is repressed by the shortage of amino acids via ppGpp³⁸. In a coarse-grained model, we represent this regulation simply as $\Delta\phi_R(a)$ where a describes the generic amino acid level. Then the amino acid removal flux is a -dependent, denoted by $J_R(a)$, and the integral feedback scheme is described by the equation

$$\frac{da}{dt} \propto Y_N J_N(K) - Y_R J_R(a). \quad [S34]$$

The steady-state condition of Eq. [S34] then leads to the coordination of the A- and R-sectors via Eqs. [S33] and [S28]:

$$v_A \cdot \Delta\phi_A(K^*) = v_R \cdot \Delta\phi_R(a^*) \quad [S35]$$

where a^* is the steady-state value of a . Similar feedback schemes can be used to bring the other sectors of metabolism (sulfate, phosphate assimilation, nucleotide synthesis, etc., lumped together as sector-U in this work) into coordination with each other.

The key to the above analysis is the existence of solutions to the steady-state conditions, [S32] and [S35]. Discussion of this issue requires the explicit forms of gene regulation. We will do so for the C-A coordination by K (Eq. [S32]). Since we are comparing gene expression across conditions with different growth rates, some care is required in defining gene regulation¹⁰. We introduce here the concept of a reference gene which is not under any specific regulation, at the transcriptional, translational, or post-translational level; this could be a native gene or a synthetic gene inserted into the chromosome, expressed at a low level so that it does not affect the behavior of the cell. Let the proteome fraction of this reference gene product be ϕ_0 . Then the regulation functions for the C- and A-sectors, g_C and g_A respectively, can be defined from the protein ratios. We define

$$g_C(K) \equiv \Delta\phi_C(K) / \phi_0, \quad [S36]$$

$$g_A(K) \equiv \Delta\phi_A(K) / \phi_0, \quad [S37]$$

where the minimum levels of these sectors ($\phi_{C,0}$ and $\phi_{A,0}$) have been taken out of the regulation functions. Note that ϕ_0 may generally take on complex growth-rate dependences¹⁰, but the regulation functions g_C and g_A are not expected to depend explicitly on the growth-rate.

Let us consider typical regulation functions as described by Hill functions^{39,40}:

$$g_C(K) = \frac{b_C}{1 + (K / K_C)^{h_C}}, \quad [\text{S38}]$$

$$g_A(K) = \frac{b_A \cdot (K / K_A)^{h_A}}{1 + (K / K_A)^{h_A}}. \quad [\text{S39}]$$

Eq. [S38] describes an inhibitory function with a maximal level b_C at low input levels ($K \ll K_C$) ; $h_C \geq 1$ is the Hill coefficient which describes the degree of cooperativity. Similarly, Eq. [S39] describes an activating function which has a maximal level b_A at high input levels ($K \gg K_A$), and $h_A \geq 1$ is the Hill coefficient. In terms of the regulation functions, the solubility condition Eq. [S32] becomes

$$v_C \cdot \phi_0 g_C(K^*) = v_A \cdot \phi_0 g_A(K^*). \quad [\text{S40}]$$

The complex factor ϕ_0 drops out of the equation, and the solution, $K^*(v_C / v_A)$, can be obtained graphically as shown in Fig. S36 for any Hill functions as long as $g_C(K)$ is inhibitory and $g_A(K)$ is activating. Similar solution a^* for Eq. [S35] can be obtained for an activating function $g_C(a) \equiv \Delta\phi_R(a) / \phi_0$ which increases ribosomal synthesis for increasing amino acid levels. Thus, integral feedback with the appropriate signs of feedback is sufficient to guide the cell to a state where the conditions Eqs. [S5]-[S8] and the constraint [S2] are simultaneously satisfied.

Supplementary Tables

Carbon source	Growth rate λ (h ⁻¹)	<i>PlacZ-lacZ</i> activity <i>L</i> (in 10 ³ MU)
60 mM acetate	0.37±0.00	20.8±0.3
20 mM arabinose	0.40±0.01	22.8±0.1
20 mM mannose	0.41±0.00	20.4±1.8
15 mM succinate	0.46±0.01	20.4±0.5
20 mM sorbitol	0.46±0.01	18.4±0.2
20 mM pyruvate	0.61±0.02	15.6±1.7
20 mM fructose	0.61±0.02	17.3±0.1
0.4% (v/v) glycerol	0.63±0.01	16.4±0.2
0.2% (w/v) maltose	0.67±0.00	15.8±0.3
0.4% (w/v) glucose	0.85±0.00	8.23±0.21
20 mM gluconate	0.88±0.04	9.45±0.99
0.2% (w/v) lactose	0.98±0.01	5.80±0.09
10 mM glucose-6P+10 mM gluconate	1.09±0.01	1.87±0.14

Table S1. The native *lacZ* expression for cells grown in various carbon sources. Wild-type *E. coli* NCM3722 strain was grown in N⁻C⁻ medium supplied with 20 mM NH₄Cl, 1 mM IPTG and each of the above carbon sources. 1mM IPTG was used to fully deactivate LacI. The growth rate (λ) and LacZ activity (*L*) were determined at least 3 times for each condition. The average values and errors displayed as \pm standard error among replicates are listed in the table. These data are shown as filled red circles (●) in Fig. 1a. LacZ activity is reported in Miller Unit (MU) as described in Supp. Method.

3MBA (μ M)	Growth rate λ (h ⁻¹)	<i>PlacZ-lacZ</i> activity <i>L</i> (in 10 ³ MU)
0	0.39±0.01	18.8±0.9
12.5	0.48±0.01	17.2±0.8
25	0.57±0.01	14.9±0.7
50	0.63±0.01	13.2±0.6
100	0.70±0.01	11.4±0.5
200	0.78±0.02	12.0±0.6
500	0.84±0.02	9.58±0.44

Table S2. The native *lacZ* expression for cells under C-limitation caused by titrating lactose permease (LacY). *E. coli* NQ381 (Titratable lacY; Fig. S2) strain was grown in N⁻C⁻ medium supplied with 0.2% lactose (w/v), 20 mM NH₄Cl, 1 mM IPTG and each of the above 3MBA levels. 1mM IPTG was used to fully deactivate LacI. 3MBA was used to titrate the expression of LacY. The growth rate (λ) and LacZ activity (*L*) were determined at least 3 times for each condition. The average values and errors displayed as \pm standard error among replicates are listed in the table. These data are shown as solid red triangles (▲) in Fig. 1a. MU: Miller Unit.

3MBA (μM)	Growth rate λ (h^{-1})	<i>PlacZ-lacZ</i> activity <i>L</i> (in 10^3 MU)
30	0.18 \pm 0.00	25.8 \pm 1.2
50	0.31 \pm 0.01	23.4 \pm 1.1
100	0.44 \pm 0.01	19.2 \pm 0.9
500	0.59 \pm 0.01	16.1 \pm 0.7

Table S3. The native *lacZ* expression for cells under C-limitation caused by titrating the glycerol uptake system (GlpFK). *E. coli* NQ399 (Titratable GlpFK; Fig. S3) strain was grown in N⁻C⁻ medium supplied with 0.4% glycerol (v/v), 20 mM NH₄Cl, 1 mM IPTG and each of the above 3MBA levels. 1mM IPTG was used to fully deactivate LacI. The growth rate (λ) and LacZ activity (*L*) were determined at least 3 times for each condition. The average values and errors displayed as \pm standard error among replicates are listed in the table. These data are shown as solid red diamonds (\blacklozenge) in Fig. 1a, MU: Miller Unit.

Strain	Genotype	Description
NCM3722	wild-type <i>E. coli</i> K12 strain ^{1,2}	parent strain for all strains used here.
FG1195	$\Delta gltD$	<i>gltD</i> null
NQ5	$\Delta gltD$, $PgdhA::km-P_{Ltet-O1}-gdhA$	<i>gltD</i> null and $P_{Ltet-O1}$ driving <i>gdhA</i>
NQ34	$\Delta gltD$, $PgdhA::km-P_{Ltet-O1}-gdhA$, $attB::P_{Ltet-O1}-tetR$	titratable GDH, GOGAT-null
NQ93	$\Delta cyaA::km$	<i>cyaA</i> -null
NQ102	$\Delta gltD$, $PgdhA::P_{Ltet-O1}-gdhA$	NQ5 with <i>km</i> gene flipped out
NQ122	$PlacZ::km-P_{Ltet-O1}-lacZ$	$P_{Ltet-O1}-lacZ$ fusion
NQ124	$\Delta gltD$, $PgdhA::P_{Ltet-O1}-gdhA$, $PlacZ::km-P_{Ltet-O1}-lacZ$	$P_{Ltet-O1}-lacZ$ fusion in titratable GDH activity, GOGAT-null background
NQ158	$PlacZ::km-rrnBT-PglnA$, $\Delta lacI$, $\Delta lacY$	<i>PglnA-lacZ</i> fusion
NQ309	$\Delta lacI \Delta lacY \Delta galK$, pKD46	a MG1655 strain with <i>lacI</i> -, <i>lacY</i> - and <i>galK</i> -null ¹⁰ , and with pKD46 plasmid
NQ315	$PlacZ::km-rrnBT-PglnA$, $\Delta lacI$, $\Delta lacY$, <i>glnL302</i>	<i>PglnA-lacZ</i> fusion in a constitutive NtrB (NtrB ^{con}) background
NQ351	pKD46	NCM3722 with pKD46 plasmid
NQ354	$\Delta lacI$	<i>lacI</i> -null
NQ367	$PlacZ::km-rrnBT-Plac-\Delta_{Ctp}-lacZ$, $\Delta lacI$, $\Delta lacY$	$Plac-\Delta_{Ctp}-lacZ$ fusion
NQ372	$\Delta glpR$	<i>glpR</i> -null
NQ373	$PlacZ::km-rrnBT-PglpF$, $\Delta lacI$, $\Delta lacY$, $\Delta glpR$	<i>PglpF-lacZ</i> fusion in $\Delta glpR$ background
NQ381	$attB::P_{Llac-O1}-xylR$, $lacY::km-Pu-lacY$	titratable LacY
NQ385	$\Delta cpdA::km$	<i>cpdA</i> null
NQ386	$attB::P_{Llac-O1}-xylR$	<i>xylR</i> expression strain
NQ399	$attB::P_{Llac-O1}-xylR$, $PglpFK::km-Pu$	titratable GlpFK
NQ474	$\Delta gltD$, $PgdhA::P_{Ltet-O1}-gdhA$, $attB::P_{Ltet-O1}-tetR$	NQ34 with <i>km</i> gene flipped out
NQ475	$\Delta gltD$, $PgdhA::P_{Ltet-O1}-gdhA$, $\Delta lacI$, $\Delta lacY$ $rrnB::P_{Ltet-O1}-tetR$, $PlacZ::km-rrnBT-Plac-\Delta_{Ctp}-lacZ$	$Plac-\Delta_{Ctp}-lacZ$ fusion in titratable GDH, GOGAT-null background
NQ477	$\Delta gltD$, $PgdhA::P_{Ltet-O1}-gdhA$, $\Delta lacI$, $\Delta lacY$ $rrnB::P_{Ltet-O1}-tetR$, $PlacZ::km-rrnBT-PglnA$	<i>PglnA-lacZ</i> fusion in titratable GDH, GOGAT-null background
NQ481	$PlacZ::km-rrnBT-PthrA$	<i>PthrA-lacZ</i> fusion
NQ482	$\Delta gltD$, $PgdhA::P_{Ltet-O1}-gdhA$, $\Delta lacI$, $\Delta lacY$ $rrnB::P_{Ltet-O1}-tetR$, $PlacZ::km-rrnBT-PthrA$	<i>PthrA-lacZ</i> fusion in titratable GDH, GOGAT-null background
NQ489	$\Delta gltD$, $PgdhA::P_{Ltet-O1}-gdhA$, $rrnB::P_{Ltet-O1}-tetR$, $\Delta glpR$	$\Delta glpR$ in NQ474 background
NQ490	$\Delta gltD$, $PgdhA::P_{Ltet-O1}-gdhA$, $rrnB::P_{Ltet-O1}-tetR$, $\Delta glpR$ $PlacZ::km-rrnBT-PglpF$, $\Delta lacI$, $\Delta lacY$,	<i>PglpF-lacZ</i> fusion in $\Delta glpR$, titratable GDH, GOGAT-null background
NQ506	$\Delta ptsHI-crr$, $\Delta fryA$, $\Delta ptsA$, $\Delta ptsP$, $\Delta dhaM$	<i>ptsHI-crr</i> operon null, and other four EI (4EI) analogs null. In short, $\Delta 5EI \Delta pts$
NQ554	$PlacZ::km-rrnBT-PfucP$, $\Delta lacI$, $\Delta lacY$	<i>PfucP-lacZ</i> fusion
NQ567	$\Delta ptsHI-crr$, $\Delta fryA$, $\Delta ptsA$, $\Delta ptsP$, $\Delta dhaM$, $attB::P_{Llac-O1}-xylR$, $lacY::km-Pu-lacY$	titratable LacY in $\Delta 5EI \Delta pts$ background
NQ721	$km::\Delta ptsHI-crr$	<i>ptsHI-crr</i> operon null. In short, Δpts
NQ738	<i>kgtP^{up}</i>	a NCM3722 mutant selected from cells grown in <i>akg</i> as a sole carbon source

NQ739	<i>PlacZ::km-rrnBT-Plac-Δ_{C_{TP}}-lacZ, ΔlacI, ΔlacY, kgtP^{up}</i>	<i>Plac-Δ_{C_{TP}}-lacZ</i> fusion in <i>kgtP^{up}</i> background
NQ741	<i>ΔptsHI-crr, kgtP^{up}</i>	<i>ptsHI-crr</i> operon null in <i>kgtP^{up}</i> background
NQ747	<i>PlacZ::km-rrnBT-PglNA, ΔlacI, ΔlacY, kgtP^{up}</i>	<i>PglNA-lacZ</i> fusion in <i>kgtP^{up}</i> background
NQ748	<i>ΔptsHI-crr</i>	NQ721 with <i>km</i> gene flipped out
NQ773	<i>ΔptsHI-crr, rrnB::P_{Lac-O1}-xylR, lacY::km-Pu-lacY</i>	titratable LacY in <i>Δpts</i> background
NQ780	<i>PlacZ::km-rrnBT-PglNA, ΔlacI, ΔlacY, ΔcyoA</i>	<i>PglNA-lacZ</i> fusion in <i>ΔcyoA</i> background
NQ976	<i>ΔptsHI-crr, cpdA::km</i>	<i>ptsHI-crr</i> operon null and <i>cpdA</i> null
NQ977	<i>ΔptsHI-crr, ΔfryA, ΔptsA, ΔptsP, ΔdhaM, cpdA::km</i>	Δ5EI <i>Δpts</i> and <i>cpdA</i> null
NQ979	<i>PlacZ::km-rrnBT-PcysJ, ΔlacI, ΔlacY</i>	<i>PcysJ-lacZ</i> fusion
NQ980	<i>PlacZ::km-rrnBT-PlysC, ΔlacI, ΔlacY</i>	<i>PlysC-lacZ</i> fusion
NQ982	<i>ΔgltD, PgdhA::P_{Ltet-O1}-gdhA, ΔlacI, ΔlacY rrnB::P_{Ltet-O1}-tetR, PlacZ::km-rrnBT-PcysJ</i>	<i>PcysJ-lacZ</i> fusion in titratable GDH, GOGAT-null background
NQ983	<i>ΔgltD, PgdhA::P_{Ltet-O1}-gdhA, ΔlacI, ΔlacY rrnB::P_{Ltet-O1}-tetR, PlacZ::km-rrnBT-PlysC</i>	<i>PlysC-lacZ</i> fusion in titratable GDH, GOGAT-null background
NQ1053	<i>PlacZ::km-rrnBT-PlacUV5, ΔlacI, ΔlacY</i>	<i>PlacUV5-lacZ</i> fusion
NQ1054	<i>ΔgltD, PgdhA::km-P_{Ltet-O1}-gdhA, PlacZ::km-rrnBT-PlacUV5, ΔlacI, ΔlacY</i>	<i>PlacUV5-lacZ</i> fusion in titratable GDH, GOGAT-null background
NQ1078	<i>PlacZ::km-rrnBT-PlacUV5, ΔlacI, ΔlacY, kgtP^{up}</i>	<i>PlacUV5-lacZ</i> fusion in <i>kgtP^{up}</i> background
NQ1180	<i>ΔgltD, PgdhA::P_{Ltet-O1}-gdhA, ΔlacI, ΔlacY rrnB::P_{Ltet-O1}-tetR, PlacZ::km-rrnBT-PfucP</i>	<i>PfucP-lacZ</i> fusion in titratable GDH, GOGAT-null background
EQ123	<i>ΔmotA, intS::Plac-gfp</i>	<i>Plac-gfp</i> fusion
EQ129	<i>ΔmotA, intS::Plac-gfp, ΔglnK, ΔamtB</i>	<i>Plac-gfp</i> fusion in <i>glnK</i> -null and <i>amtB</i> -null background

Table S4. Strains used in this study. Note: all the strains used are derived from the *E. coli* K12 strain NCM3722^{1,2} provided kindly by Sydney Kustu lab.

<i>PlacZ</i>		C-limited (WT)	NC-limited (glycerol)	NC-limited (lactose)	A-limited (glucose)	C-limited (fixed GDH)	R-limited (glucose)
source of data		Fig. 1a ●▲◆	Fig. 1a ◇◆	Fig. 1a ▲▲	Fig. S19 □	Fig. S20 ▼	Fig. S15b ■
fitted	L_{\max} (MU, $\times 10^3$)	32±1	--	--	--	38±3	--
	λ_C (h ⁻¹)	1.2±0.0	--	--	--	0.80±0.03	--
	L_0 (MU, $\times 10^3$)	--	1.4±0.8	0.77±0.25	0.12±0.52	--	-1.2±0.7
	α_C (MU·h, $\times 10^3$)	--	24±2	3.8±0.4	9.0±0.8	--	9.9±1.2
	linearity (r^2)	0.94	0.93	0.89	0.95	0.75	0.95
$\tilde{\lambda}_C$ (h ⁻¹)	1.2±0.0	--	--	--	0.80±0.03	--	
$\tilde{\alpha}_C$ (h)	--	0.78±0.07	0.12±0.01	0.29±0.03	--	0.30±0.04	
ν_C (h ⁻¹)	--	3.0	20	8.0	--	7.8	

Table S5: Parameters describing the growth-rate dependence of *PlacZ* under various modes of growth limitations. All parameter values shown are the best linear-fit to data indicated in the “source of data” row. Data for C-limited growth are fitted to the form $L = L_{\max} \cdot (1 - \lambda / \lambda_C)$, while data for non-carbon modes of limitations are fit to the form $L = L_0 + \alpha_C \cdot \lambda$; see Table N1 in Supp Note 3. The last two rows provide the values of the scaled parameters, $\tilde{\lambda}_C = \lambda_C \cdot (1 - L_0 / L_{\max})$ and $\tilde{\alpha}_C = \alpha_C / (L_{\max} - L_0)$; see Table N2 of Supp Note 3. In the scaling, we used the fitted L_{\max} value for wild-type cells since it is the most reliably determined. We used the fitted L_0 value for each mode of growth limitations in the scaling of the corresponding $\tilde{\alpha}_C$. For the scaling of $\tilde{\lambda}_C$, we used the average of all the fitted L_0 values for the complementary (non-carbon) modes of growth limitations since L_0 is not defined for C-limitation. The phenomenological parameter ν_C of the proteome partition model (Eq. [S6] in Supp Note 1) is obtained as $\nu_C = 1 / (\tilde{\alpha}_C \cdot \phi_{\max})$ (Eq. [S23] in Supp Note 3), using $\phi_{\max} = 43\%$ from Fig. S18.

Strain	chemostat	Carbon source	Dilution rate (h ⁻¹)	<i>PlacZ-lacZ</i> activity L (in 10^3 MU)
NQ354	ammonium-limited	0.4% (w/v) glucose	0.52	4.65
			0.41	3.84
			0.30	3.37
			0.62	5.07
			0.73	5.73
			0.83	6.26
NCM3722	ammonium-limited	0.2% (w/v) lactose	0.34	2.29
			0.46	2.24
			0.61	3.00
			0.77	3.09
			0.91	3.64
NQ354	sulfate-limited	0.4% (v/v) glycerol	0.16	5.10
			0.26	7.31
			0.36	9.74
			0.47	10.8
			0.16	4.41

Table S6. The native *lacZ* expression under NC-limitation for cells grown in continuous culture with ammonium- or sulfate- limitation. The native *lacZ* expression in wild-type NCM3722 strain grown in an ammonium-limited chemostat with lactose as the sole carbon source, NQ354 ($\Delta lacI$) strain grown in an ammonium-limited chemostat with glucose as the carbon source or NQ354 ($\Delta lacI$) strain grown in a sulfate-limited chemostat with glycerol as the carbon source were characterized. LacZ expression at above each dilution rate was taken at least 8 generations after setting to the desired dilution rate. These data are plotted as yellowed filled symbols in Fig. 1a. The dilution rates were used for the growth rate λ . MU: Miller Unit.

Carbon source	cTc (ng/ml)	Growth rate λ (h ⁻¹)	PlacZ-lacZ activity (in 10 ³ MU)
0.2% (w/v) lactose	10	0.25±0.03	2.03±0.20
	15	0.34±0.03	2.14±0.21
	20	0.43±0.04	2.30±0.12
	40	0.68±0.07	3.52±0.81
0.4% (w/v) glucose	20	0.27±0.01	2.78±0.28
	30	0.37±0.01	3.60±0.18
	40	0.52±0.04	4.56±0.11
0.4% (v/v) glycerol	15	0.32±0.03	9.71±0.10
	20	0.38±0.01	11.1±0.4
	30	0.45±0.01	12.0±0.2
	40	0.52±0.02	13.7±1.8

Table S7. The native *lacZ* expression for cells under NC-limitation caused by titrating nitrogen uptake through GDH. *E. coli* NQ34 (Titratable GDH; Fig S6) strain was grown in N⁻C⁻ medium supplied with 20 mM NH₄Cl, 1 mM IPTG and each of the above carbon sources and 3MBA levels. 1mM IPTG was used to fully deactivate LacI. The growth rate (λ) and LacZ activity (L) were determined at least 3 times for each condition. The average values and errors displayed as \pm standard error among replicates are listed in the table. These data are plotted as open symbols with no filling (Δ for lactose, \square for glucose and \diamond for glycerol) in Fig. 1a. MU: Miller Unit.

Strain	Carbon source	3MBA (μ M)	Growth rate λ (h ⁻¹)	cAMP excretion rate (μ M/OD ₆₀₀ /h)
NCM3722	0.2% (w/v) lactose	0	0.96	0.088
NQ381	0.2% (w/v) lactose	0	0.32	0.43
		25	0.57	0.34
		50	0.65	0.27
		500	0.84	0.15

Table S8. The cAMP excretion rate indicating the internal cAMP level (Fig. S11) for cells grown under C-limitation. C-limitation was achieved by growing NQ381 (Titratable lacY; Fig. S2) in N⁻C⁻ medium supplied with 0.2% (w/v) lactose, 20 mM NH₄Cl, 1 mM IPTG and above various 3MBA level to titrate LacY amount and NCM3722 in N⁻C⁻ medium supplied with 0.2% (w/v) lactose, 20 mM NH₄Cl, 1 mM IPTG. The growth rate λ and cAMP excretion rate at each growth conditions were determined and listed in the table. These data are plotted as solid circles or triangles (\bullet for NCM3722 and \blacktriangle for NQ381) in Fig. 1b.

Strain	Carbon source	cTc (ng/ml)	Growth rate λ (h ⁻¹)	cAMP excretion rate ($\mu\text{M}/\text{OD}_{600}/\text{h}$)
NQ34	0.2% (w/v) lactose	20	0.36	0.018
		25	0.46	0.028
		40	0.73	0.046
		100	0.90	0.075

Table S9. The cAMP excretion rate indicating the internal cAMP level for cells grown under NC- limitation. NC-limitation was achieved by growing NQ34 (Titratable GDH; Fig. S6) cells in N⁻C⁻ medium supplied with 0.2% (w/v) lactose, 20 mM NH₄Cl, 1 mM IPTG and above various cTc levels to titrate GDH amount. The growth rate (λ) and cAMP excretion rate at each growth conditions were determined and listed in the table. These data are plotted as black open triangles (Δ) in Fig. 1b.

Strain	Carbon source	Growth rate λ (h ⁻¹)	R/P ($\mu\text{g RNA}/\mu\text{g total protein}$)
NCM3722 (wt)	60 mM acetate	0.44±0.01	0.17±0.00
	20 mM sorbitol	0.41±0.04	0.17±0.00
	20 mM pyruvate	0.62±0.02	0.23±0.00
	0.4% (v/v) glycerol	0.64±0.01	0.23±0.00
	0.4% (w/v) glucose	0.87±0.01	0.28±0.01
	10 mM G6P + 10 mM gluconate	1.0±0.0	0.31±0.01

Table S10. RNA/protein ratio for cells under C-limitation. NCM3722 cells were grown in N⁻C⁻ medium supplied with 20 mM NH₄Cl and each of above various carbon sources. The growth rate λ and RNA/protein ratio were determined at least 3 times for each condition. The average values and errors displayed as \pm standard error among replicates are listed in the table. These data are plotted as solid green circles (\bullet) in Fig. 1c.

Strain	Carbon source	NH ₄ Cl (mM)	cTc (ng/ml)	Growth rate λ (h ⁻¹)	R/P ($\mu\text{g RNA}/\mu\text{g total protein}$)
NQ5	0.4% (w/v) glucose	3	0	0.24±0.01	0.13±0.00
NQ5		5	0	0.32±0.01	0.15±0.00
NQ34		20	0	0.51±0.01	0.19±0.00
NQ34		20	40	0.60±0.01	0.20±0.02
NQ34		20	100	0.76±0.01	0.24±0.01
NQ5	0.4% (v/v) glycerol	5	0	0.30±0.01	0.15±0.00
NQ5		20	0	0.45±0.01	0.18±0.00
NQ34		20	15	0.46±0.01	0.19±0.01
NQ34		20	40	0.61±0.00	0.23±0.02
NQ34		20	100	0.66±0.01	0.23±0.00
NQ5 (Titratable GDH activity by NH ₄ Cl); NQ34 (Titratable GDH amount by cTc)					

Table S11. RNA/protein ratio for cells under NC- limitation. NQ5 (Fig. S6) cells were grown in N⁻C⁻ medium supplied with 0.4% (w/v) glucose or 0.4% (v/v) glycerol, and each of above various levels of NH₄Cl to titrate GDH activity and the resulted nitrogen uptake. NQ34 (Fig. S6) cells were grown in N⁻C⁻ medium supplied with 0.4% (w/v) glucose or 0.4% (v/v) glycerol, 20 mM NH₄Cl and each of above various levels of cTc to titrate GDH amount and the resulted nitrogen uptake. The growth rate λ and RNA/protein ratio were determined at least 3 times for each condition. The average values and errors displayed as \pm standard error among replicates are listed in the table. These data are plotted as green open symbols (\square for glucose and \diamond for glycerol) in Fig. 1c.

Carbon source	Growth rate λ (h ⁻¹)	<i>PglnA-lacZ</i> activity <i>G</i> (in 10 ³ MU)
maltose	0.73±0.01	0.13±0.01
0.4% (w/v) glucose	0.91±0.00	0.12±0.00
60 mM acetate	0.48±0.01	0.062±0.002
15 mM succinate	0.69±0.01	0.068±0.001
0.4% (v/v) glycerol	0.70±0.01	0.077±0.001
20 mM pyruvate	0.60±0.01	0.087±0.005
20 mM sorbitol	0.47±0.02	0.073±0.001
20 mM fructose	0.64±0.01	0.072±0.000
20 mM gluconate	0.82±0.05	0.10±0.00
20 mM OAA	0.90±0.00	0.13±0.01

Table S12. The *PglnA-lacZ* expression for cells under C-limitation caused by varying carbon sources. *E. coli* NQ158 (*PglnA-lacZ*) strain was grown in N⁻C⁻ medium supplied with 20 mM NH₄Cl and each of the above carbon sources. The growth rate (λ) and LacZ activity (*G*) were determined at least 3 times for each condition. The average values and errors displayed as \pm standard error among replicates are listed in the table. These data are plotted as solid blue circles (\bullet) in Fig. 1d. MU: Miller Unit.

cTc (ng/ml)	Growth rate λ (h ⁻¹)	<i>PglA-lacZ</i> activity <i>G</i> (in 10 ³ MU)
10	0.30±0.01	0.29±0.01
15	0.37±0.03	0.22±0.03
20	0.45±0.01	0.18±0.02
25	0.49±0.01	0.16±0.02
30	0.53±0.02	0.14±0.02
40	0.57±0.02	0.19±0.00

Table S13. The *PglA-lacZ* expression for cells under A-limitation caused by titrating nitrogen uptake through GDH. *E. coli* NQ477 (*PglA-lacZ*, Titratable GDH) strain was grown in N⁻C⁻ medium supplied with 0.4% (w/v) glycerol, 20 mM NH₄Cl and each of the above cTc to titrate GDH. The growth rate (λ) and LacZ activity (*G*) were determined at least 3 times for each condition. The average values and errors displayed as \pm standard error among replicates are listed in the table. These data are plotted as blue open diamonds (\diamond) in Fig. 1d. MU: Miller Unit.

RNA/protein ratio		C- and A- limited	R-limited (glycerol)	R-limited (glucose)
source of data		Fig. 1c $\bullet \diamond \square$	Fig. S15a \diamond	Fig. S15a \square
fitted	r_{\max}	--	0.63±0.01	0.67±0.02
	λ_R (h ⁻¹)	--	1.1±0.0	1.7±0.1
	r_0	0.076±0.005	--	--
	α_R (h)	0.25±0.01	--	--
	linearity (r^2)	0.90	0.98	0.98
	$\tilde{\lambda}_R$ (h ⁻¹)	--	0.93±0.03	1.5±0.1
	$\tilde{\alpha}_R$ (h)	0.44±0.02	--	--
	ν_R (h ⁻¹)	5.3	--	--

Table S14: Parameters describing the growth-rate dependence of RNA/protein ratio under various modes of growth limitations. All parameter values shown are the best linear-fit to data indicated in the “source of data” row. Data for translation-limited growth by sub-inhibitory dose of Chloramphenicol¹⁷ are fitted to the form $r = r_{\max} \cdot (1 - \lambda / \lambda_R)$, while data for C- and A- limited growth are fit to the form $r = r_0 + \alpha_R \cdot \lambda$; see Table N1 in Supp Note 3. The last two rows provide the values of the scaled parameters, $\tilde{\lambda}_R = \lambda_R \cdot (1 - r_0 / r_{\max})$ and $\tilde{\alpha}_R = \alpha_R / (r_{\max} - r_0)$; see Table N2 of Supp Note 3. In the scaling, we used the average value of r_{\max} . The phenomenological parameter ν_R of the proteome partition model (Eq. [S5] in Supp Note 1) is obtained as $\nu_R = 1 / (\tilde{\alpha}_R \cdot \phi_{\max})$ (Eq. [S23] in Supp Note 3), using $\phi_{\max} = 43\%$ from Fig. S18.

PglnA		C-limited (WT)	A-limited (glycerol)	A-limited (glucose)	C-limited (fixed GDH)	R-limited (glucose)
source of data		Fig. 1d ●	Fig. 1d ◇	Fig. S19 □	Fig. S20 ▼	Fig. S15c ■
fitted	G_{\max} (Miller U, $\times 10^3$)	--	0.42±0.02	0.57±0.04	--	--
	λ_A (h^{-1})	--	0.81±0.02	1.0±0.1	--	--
	G_0 (Miller U)	8.1±12	--	--	0.0±0.0	27±7
	α_A (Miller U·h, $\times 10^3$)	0.12±0.02	--	--	0.24±0.01	0.12±0.02
	linearity (r^2)	0.60	0.90	0.82	0.19	0.92
$\tilde{\lambda}_A$ (h^{-1})	--	0.79±0.02	1.0±0.1	--	--	
$\tilde{\alpha}_A$ (h)	0.28±0.04	--	--	0.57±0.04	0.29±0.04	
ν_A (h^{-1})	8.3	--	--	4.1	8.0	

Table S15: Parameters describing the growth-rate dependence of PglnA under various modes of growth limitations. All parameter values shown are the best linear-fit to data indicated in the “source of data” row. Data for A-limited growth are fit to the form

$G = G_{\max} \cdot (1 - \lambda / \lambda_A)$, while data for C- and R- limited growth are fit to the form

$G = G_0 + \alpha_A \cdot \lambda$; see Table N1 in Supp Note 3. [For C-limited with fixed GDH, we used a linear fit with $G_0 = 0$ due to the noisiness of the data (Fig S19A).] The last two rows provide the

values of the scaled parameters, $\tilde{\lambda}_A = \lambda_A \cdot (1 - G_0 / G_{\max})$ and $\tilde{\alpha}_A = \alpha_A / (G_{\max} - G_0)$; see Table N2 of Supp Note 3. In the scaling, we used the fitted G_{\max} value for A-limitation with glycerol since it is more reliably determined. (There is a modest growth defect for the titratable GDH strain at high level of GDH expression in fast carbon sources; this is responsible for the downward bend of the data in Fig. S19 and S20 for the faster growth rates.) We used the fitted G_0 value for the corresponding $\tilde{\alpha}_A$. For the scaling of $\tilde{\lambda}_A$, we used the average of the fitted G_0 values for the complementary C-limited modes of growth since G_0 is not defined for A-limitation. The phenomenological parameter ν_A of the proteome partition model (Eq. [S7] in Supp Note 1) is obtained as $\nu_A = 1 / (\tilde{\alpha}_A \cdot \phi_{\max})$ (Eq. [S23] in Supp Note 3), using $\phi_{\max} = 43\%$ from Fig. S18.

parameters		C-limited (WT)	A-limited (glycerol)	A-limited (glucose)	C-limited (fixed GDH)	R-limited (glucose)
empirical	C-sector (from Table S3)	$\tilde{\lambda}_C$ (h ⁻¹) 1.2±0.0	$\tilde{\alpha}_C$ (h) 0.78±0.07	$\tilde{\alpha}_C$ (h) 0.29±0.03	$\tilde{\lambda}_C$ (h ⁻¹) 0.80±0.03	$\tilde{\alpha}_C$ (h) 0.30±0.04
	A-sector (from Table S5)	$\tilde{\alpha}_A$ (h) 0.28±0.04	$\tilde{\lambda}_A$ (h ⁻¹) 0.80±0.02	$\tilde{\lambda}_A$ (h ⁻¹) 1.0±0.1	$\tilde{\alpha}_A$ (h) 0.57±0.04	$\tilde{\alpha}_A$ (h) 0.29±0.04
	R-sector (from Table S4)	$\tilde{\alpha}_R$ (h) 0.44±0.02				$\tilde{\lambda}_R$ (h ⁻¹) 1.5±0.1
predicted	U-sector	$\tilde{\alpha}_U^{(i)}$ (h) 0.13±0.04				
	$\tilde{\lambda}_C, \tilde{\lambda}_A, \tilde{\lambda}_R$	--	$\tilde{\lambda}_A^{(ii)}$ (h ⁻¹) 0.74±0.05	$\tilde{\lambda}_A^{(ii)}$ (h ⁻¹) 1.2±0.1	$\tilde{\lambda}_C^{(iii)}$ (h ⁻¹) 0.88±0.05	$\tilde{\lambda}_R^{(iv)}$ (h ⁻¹) 1.4±0.1
	$\lambda_C, \lambda_A, \lambda_R$	--	$\lambda_A^{(v)}$ (h ⁻¹) 0.75±0.06	$\lambda_A^{(v)}$ (h ⁻¹) 1.2±0.1	$\lambda_C^{(vi)}$ (h ⁻¹) 0.91±0.06	$\lambda_R^{(vii)}$ (h ⁻¹) 1.6±0.2

Table S16: Predicted parameters based on the proteome partition model. The scaled parameters, $\tilde{\lambda}$ s and $\tilde{\alpha}$ s, which describe the normalized proteome fractions f s as specified in Table N2 of Supp Note 3, are predicted to be related according to Eqs. [S24]-[S26] of Supp Note 3. In this table, the parameters values in the first 3 rows are obtained empirically as indicated parenthetically in the first column. The predicted values appearing in the last 2 rows are obtained as follows:

(i) $\tilde{\alpha}_U$ is obtained from Eq. [S24] using the empirical values of $\tilde{\lambda}_C$, $\tilde{\alpha}_A$, and $\tilde{\alpha}_R$ derived for wild-type cells in C-limited growth, our most complete and reliable dataset. This value is used for all other modes of growth limitations studied here.

(ii) The predicted value of $\tilde{\lambda}_A$ is obtained from Eq. [S25] using the predicted value of $\tilde{\alpha}_U$ as described in (i) above, and the empirical values of $\tilde{\alpha}_C$, and $\tilde{\alpha}_R$ for A-limited growth under the specific carbon source.

(iii) The predicted value of $\tilde{\lambda}_C$ for C-limited growth under a fixed degree of GDH expression is obtained from Eq. [S24] using the predicted value of $\tilde{\alpha}_U$ as described in (i) above, and the empirical values of $\tilde{\alpha}_A$, and $\tilde{\alpha}_R$ for this mode of growth limitation.

(iv) The predicted value of $\tilde{\lambda}_R$ is obtained from Eq. [S26] using the predicted value of $\tilde{\alpha}_U$ as described in (i) above, and the empirical values of $\tilde{\alpha}_C$, and $\tilde{\alpha}_A$ for R-limited growth under glucose as the sole carbon source.

(v) $\lambda_A = \tilde{\lambda}_A / (1 - G_0 / G_{\max})$ to undo the scaling used in Table S15.

(vi) $\lambda_C = \tilde{\lambda}_C / (1 - L_0 / L_{\max})$ to undo the scaling used in Table S5.

(vii) $\lambda_R = \tilde{\lambda}_R / (1 - r_0 / r_{\max})$ to undo the scaling used in Table S14.

	Wild-type					<i>kgtP^{up}</i>
		oaa	pyr	succ	akg	akg
	alone	53	68	91	n.g.	182
glycerol	66	44	50	58	66	54
glucose	49	41	45	47	49	43
lactose	42	39	42	42	42	42

Table S17: Doubling time with combination of carbon sources in steady state culture. Wild-type NCM3722 strain or *kgtP^{up}* strain NQ738 was grown in N⁻C⁻ medium supplied with 20 mM NH₄Cl, 1 mM IPTG and each of the carbon source combinations. These carbon source are: 0.2% (w/v) lactose; 0.4% (w/v) glucose; 0.4% (v/v) glycerol; 20 mM akg; 20 mM oaa; 20 mM pyr; 15 mM succ. The results are reported in minutes. The grey shades are the doubling times for single carbon sources, and the remainders are for combinations given by the row and column headings. Each growth condition was monitored at least three times and the average doubling time is reported. Note: NCM3722 and NQ738 have same doubling time when lactose, glucose or glycerol was used as the sole carbon source.

akg: α -ketoglutarate; oaa: oxaloacetate; pyr: pyruvate; succ: succinate; n.g.:no growth.

Carbon source	3MBA (μM)	Growth rate λ (h^{-1})	<i>PlacZ-lacZ</i> activity <i>L</i> (in 10^3 MU)
NQ721 (Δpts)			
0.2% (w/v) lactose	0	0.61±0.02	3.3±0.1
20 mM pyruvate	0	0.63±0.00	3.8±0.1
0.2% (w/v) lactose + 20 mM OAA	0	0.92±0.18	1.9±0.2
10 mM glucose-6P + 10 mM gluconate	0	1.05±0.04	0.84±0.09
NQ773 (Δpts ; Titratable LacY)			
0.2% (w/v) lactose	0	0.27±0.04	6.7±0.7
	25	0.60±0.06	4.9±0.3
	50	0.67±0.04	4.2±0.2
	100	0.70±0.01	3.9±0.1
NQ506 (Δ5EI , Δpts)			
0.2% (w/v) lactose	0	0.50±0.03	5.7±0.5
20 mM pyruvate	0	0.71±0.00	8.5±0.2
0.4% (w/v) lactose+20 mM OAA	0	0.88±0.01	3.5±0.4
10 mM glucose-6P+10 mM gluconate	0	0.99±0.04	2.2±0.2
NQ567 (Δ5EI , Δpts ; Titratable LacY)			
0.2% (w/v) lactose	0	0.17±0.02	15±1
	10	0.33±0.05	13±1
	25	0.53±0.05	10±1
	50	0.64±0.04	9.2±0.4
	100	0.72±0.01	7.4±0.2

Table S18. Growth rate dependence of the steady state *PlacZ-lacZ* expression in PTS mutants under various modes of C-limitations. C-limitation through changing carbon sources: Strains NQ721 (Δpts) or NQ506 (Δ5EI Δpts) were grown in N^-C^- medium supplied with 20 mM NH_4Cl , 1 mM IPTG and each of above various carbon sources. C-limitation through titrating lactose influx through LacY: NQ773 (Δpts with titratable LacY) or NQ567 (Δ5EI Δpts with titratable LacY) grown in N^-C^- medium supplied with 0.2% (w/v) lactose, 20 mM NH_4Cl , 1 mM IPTG and each of above 3MBA levels to titrate LacY. 1mM IPTG was used to fully deactivate LacI. The growth rate (λ) and LacZ activity (*L*) were determined at least 3 times for each condition. The average values and errors displayed as \pm standard error among replicates are listed in the table. Parameters of the best linear fit were shown in Table S19. These data are plotted as solid circles or triangles (pink circles (●) for NQ721, pink triangles (▲) for NQ773, orange circles (●) for NQ506 and orange triangles (▲) for NQ567 in Fig. 4c. MU: Miller Unit.

Background	Strain	L_{\max} (in 10^3 MU)	λ_C (h^{-1})	linearity (r^2)
Δpts	NQ721; NQ773	8.8 ± 0.6	1.2 ± 0.0	0.92
$\Delta 5EI \Delta pts$	NQ506; NQ567	17 ± 2	1.2 ± 0.0	0.78

Table S19. Parameters of the best linear fit of growth rate dependence of the steady state *PlacZ-lacZ* expression in PTS mutants under various modes of C-limitations. The raw data used for the fits are from Table S18.

Supplementary Figures

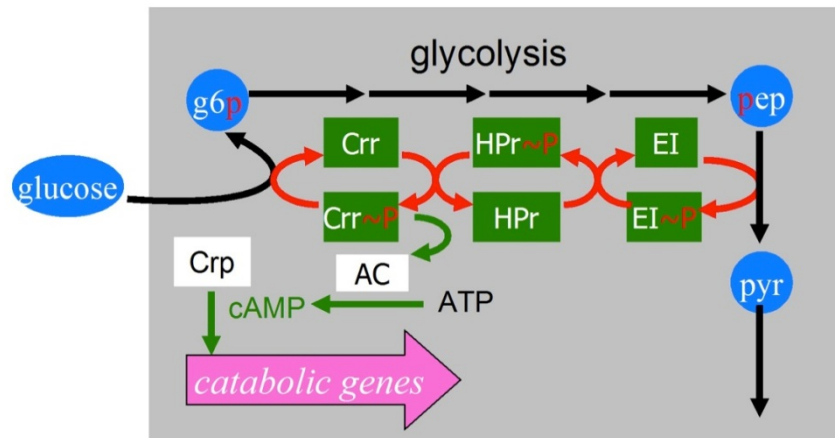


Figure S1: A schematic illustration of the regulatory interactions known to affect catabolic gene expression in *E. coli*; adapted from Ref. 41. It is well established that Crp complexed with cAMP activates catabolic gene expression. cAMP is synthesized by Adenylate Cyclase (AC), whose activity is stimulated by the phosphorylated moiety of EI^{Glc} (encoded by *crr*), denoted as Crr~P in the above illustration. The phosphorylation of Crr is derived from the transformation of phosphoenolpyruvate (pep) to pyruvate (pyr), via proteins of the phosphotransferase system (PTS), HPr and EI, encoded by *ptsH* and *ptsI* respectively. Crr~P in turn transfers its phosphate group to glucose as it is transported by EIIBC^{Glc} (encoded by *ptsG*, not shown), hence capturing it in the form of glucose-6-phosphate (g6p). It is thought that the import of glucose shifts the equilibrium of Crr from the phosphorylated to the unphosphorylated moiety, thereby reducing the stimulation of AC activity, resulting ultimately in reduced expression of catabolic genes. However, the degree of Crr phosphorylation was found to correlate negatively with the growth rate (for different degrees of carbon limitation) even for non-PTS sugars^{42,43}. Very recently, it has also been shown that EI phosphorylation is inhibited by alpha ketoglutarate⁴⁴.

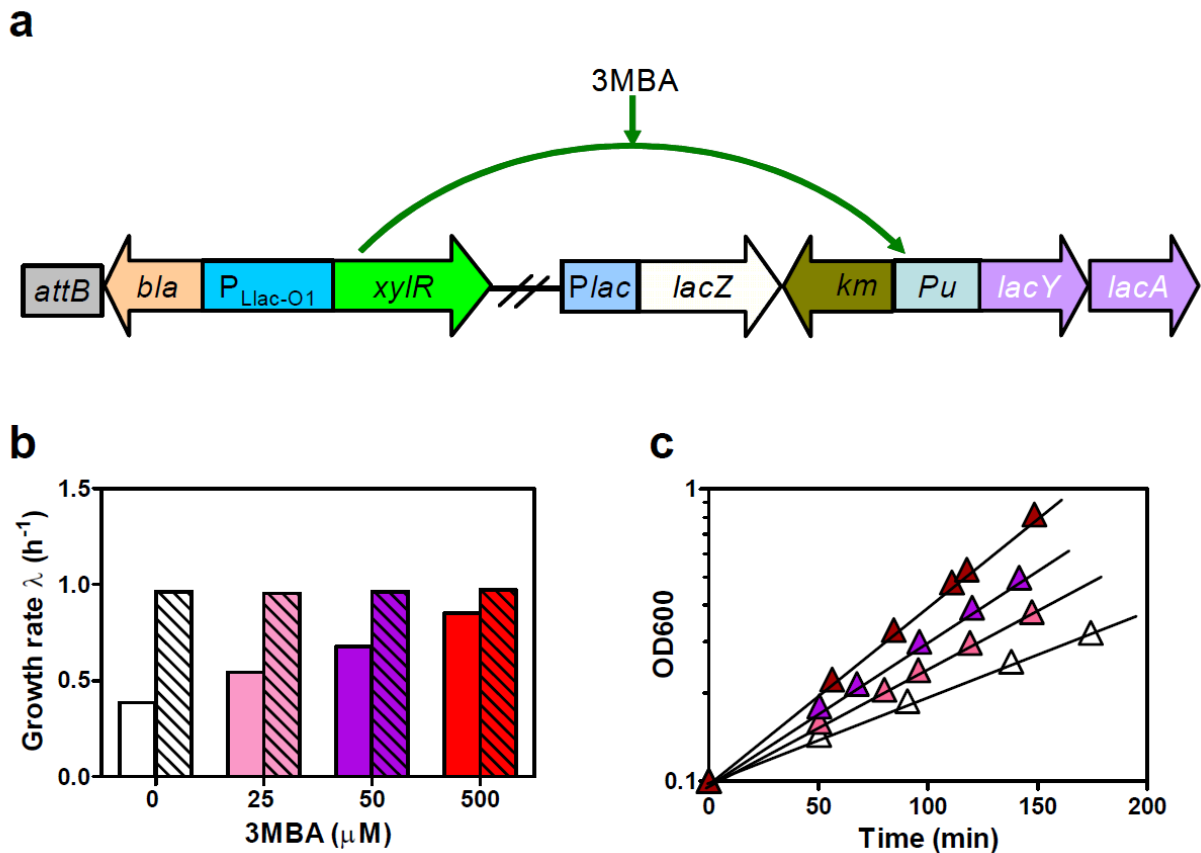


Figure S2: Titratable control of lactose uptake. LacY is the only transporter that allows *E. coli* to grow on lactose as the sole carbon source. We therefore attempted to control lactose uptake by titrating the expression of LacY. (a) We constructed a strain (NQ381) by inserting a titratable *Pu* promoter from *Pseudomonas putida*^{10,14} between the *lacZ* stop codon and *lacY* start codon. No terminator was placed upstream of the *Pu* promoter since this promoter has been reported to be able to block transcription from its upstream DNA region⁴⁵. The expression of the *Pu* promoter is activated by the regulator XylR upon induction by 3-methylbenzyl alcohol (3MBA). Located at the chromosomal *attB* site, *xyIR* expression is in turn driven by a synthetic P_{Lac-O1} promoter that does not need Crp-cAMP for activation¹⁵; see Supp Methods for details of strain construction. Strain NQ381 was grown in N⁻C⁻ medium with 0.2% (w/v) lactose, 20mM NH₄Cl, and 1 mM IPTG, with various 3MBA levels (0-0.5 mM) to stimulate XylR and titrate the expression of LacY. A range of growth rates were obtained as shown by the bars of different colors in panel (b), with their corresponding growth curves (triangles of same colors) shown in panel (c). Straight lines show fit to exponential growth. The growth rates obtained for a controlled strain (NQ386) containing the same P_{Lac-O1} promoter-driven *xyIR* expression at *attB* site but with native *lacY* expression grown in the same medium were shown as the striped bars in panel (b).

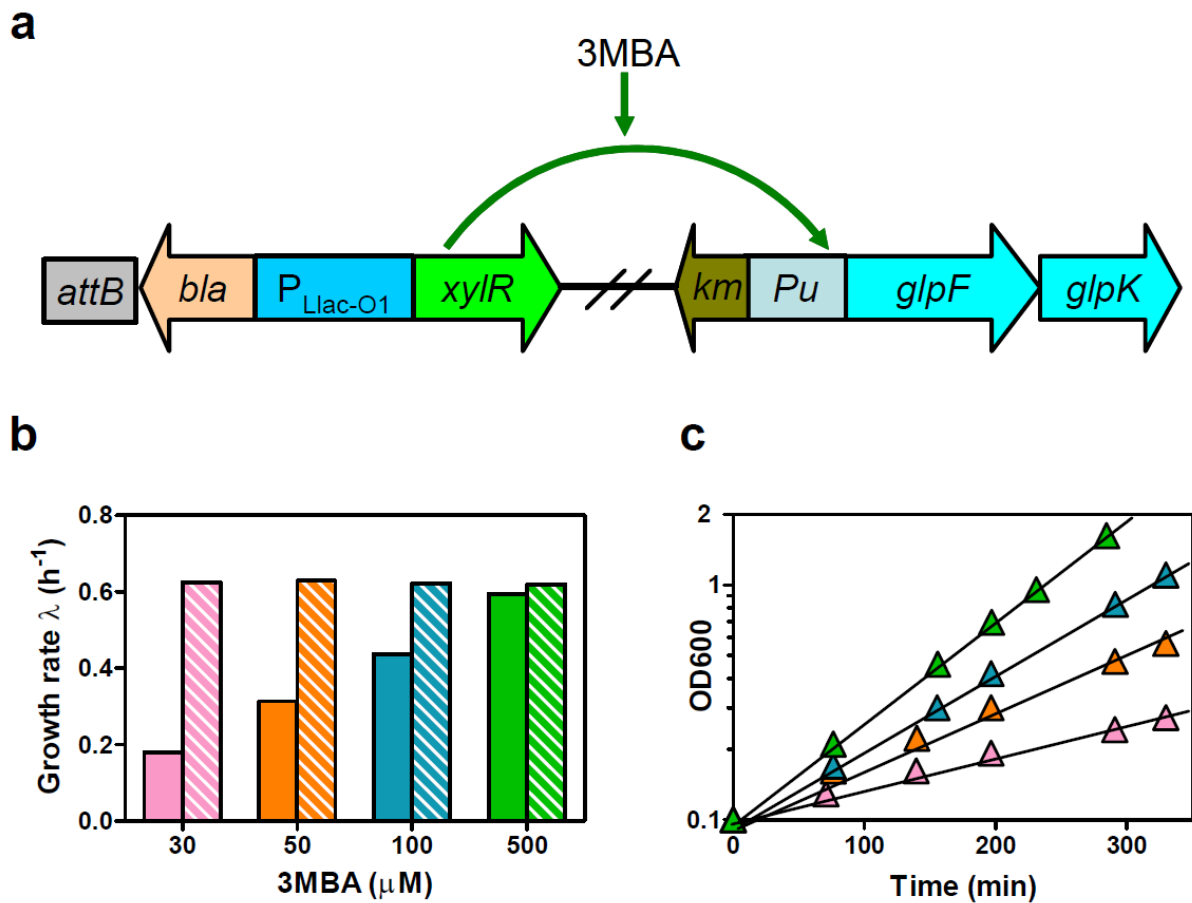
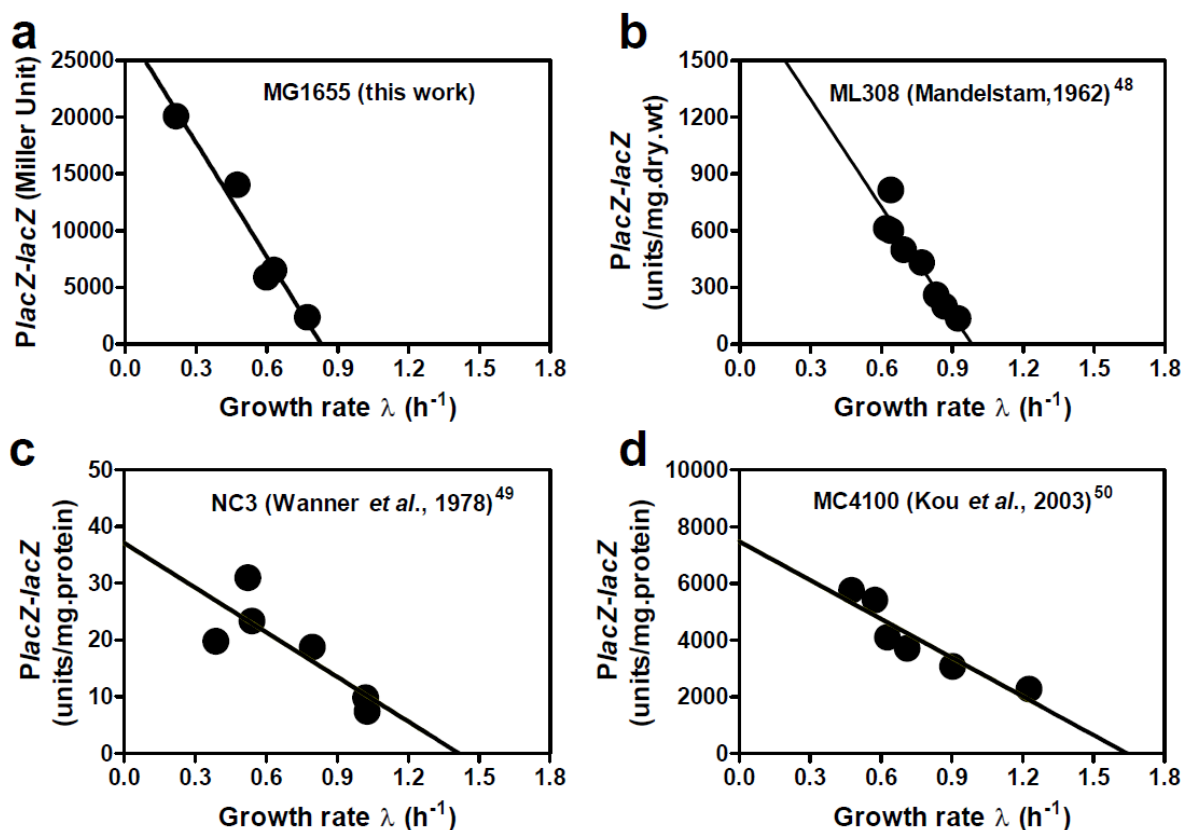
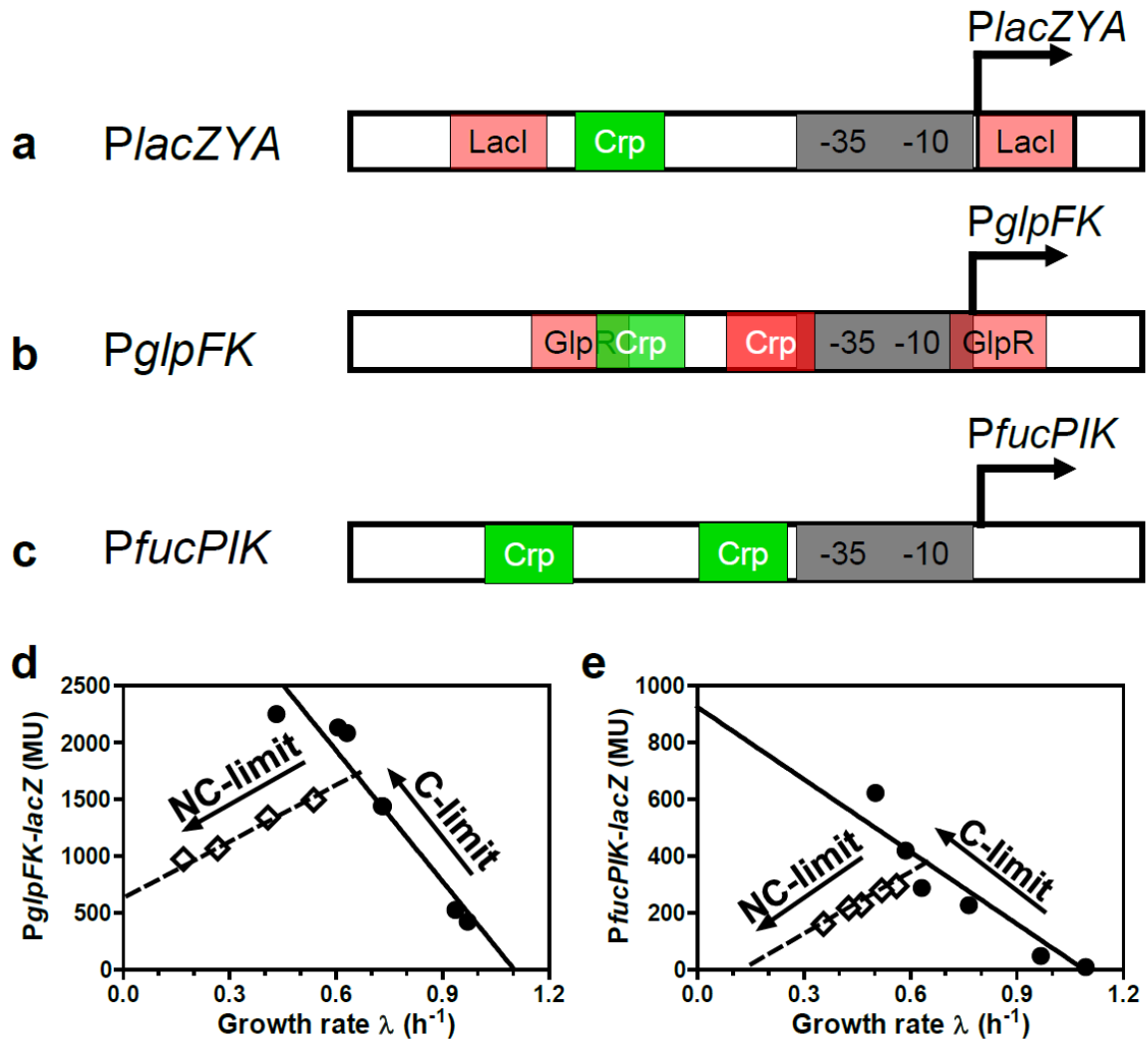


Figure S3: Titratable control of glycerol uptake. Glycerol enters *E. coli* by facilitated diffusion via the glycerol facilitator (encoded by *glpF*), and is subsequently phosphorylated by glycerol kinase (encoded by *glpK*)⁴⁶. (a) We constructed a strain (NQ399) with the promoter of the *glpFK* operon⁴⁷ (from -1 to -252 bp) replaced by the *Pu* promoter^{10,14}. As shown in Fig. S2, the activator XylR is driven by the $P_{Llac-O1}$ promoter at the *attB* site. NQ399 was grown in N⁺C⁻ medium with 0.4% (v/v) glycerol, 20mM NH₄Cl, 1 mM IPTG, and various 3MBA levels (0.02-0.5 mM). The growth rates obtained at various 3MBA levels are shown as the colored bars in panel (b), with their corresponding growth curves (triangles of like colors) shown in panel C. Straight lines show fit to exponential growth. The growth rates obtained for a controlled strain (NQ386) containing the same $P_{Llac-O1}$ promoter-driven *xylR* expression at *attB* site but with native *glpFK* expression grown in the same medium were shown as the striped bars with like colors in panel (b)



Strain	$L_{\max} (\times 10^3)$	$\lambda_C (\text{h}^{-1})$	linearity (r^2)
MG1655	28 ± 1 (Miller Unit)	0.81 ± 0.01	0.96
ML308	1.9 (units/mg dr wt)	0.98	0.89
NC3	0.037 (units/mg protein)	1.42	0.67
MC4100	7.8 (units/mg protein)	1.64	0.86

Figure S4: C-line for various strains of *E. coli*. Various *E. coli* strains were grown in minimal medium with various carbon sources and supplied with 1 mM IPTG to deactivate LacI when necessary. a: MG1655 (this work); b: ML308 Ref. (48); c: NC3 Ref. (49); d: MC4100 Ref. (50). The linear regression in each panel shows the strain-specific C-line and the table shows all fitted values as defined in Supp. Note 3.



C-limitation		NC-limitation (glycerol)	
Strain and Description	Fitted values	Strain and Description	Fitted values
NQ373 <i>glpR PglpFK-lacZ</i>	● $L_{max} = 4.2 \pm 0.4$ (10^3 MU)	NQ490 $\Delta glpR, PglpFK-lacZ$ $\Delta GOGAT P_{LtetO1}:GDH$	◇ $L_0 = 0.70 \pm 0.03$ (10^3 MU)
	● $\lambda_C = 1.1 \pm 0.0$ (h^{-1})		◇ $\alpha_C = 1.5 \pm 0.08$ (10^3 MU·h)
	● Linearity (r^2) = 0.93		◇ Linearity (r^2) = 0.99
NQ554 <i>PfucPIK-lacZ</i>	● $L_{max} = 0.99 \pm 0.13$ (10^3 MU)	NQ1180 <i>PfucPIK-lacZ</i> $\Delta GOGAT P_{LtetO1}:GDH$	◇ $L_0 = -0.07 \pm 0.02$ (10^3 MU)
	● $\lambda_C = 1.1 \pm 0.0$ (h^{-1})		◇ $\alpha_C = 0.66 \pm 0.05$ (MU·h)
	● Linearity (r^2) = 0.90		◇ Linearity (r^2) = 0.99

Figure S5: The C- and NC- lines for several Crp-regulated promoters. Panels A-C depict the architecture of the promoter regions of 3 catabolic operons, *lacZYA*, *glpFK*, and *fucPIK*. The regulator binding sites are marked by the colored boxes (green for activation, red for repression), and RNA polymerase binding sites (-35,-10) are marked by the grey boxes. The transcriptional start sites are marked by the black arrows. (a) *PlacZYA* is repressed by LacI and activated by Crp-cAMP⁵¹. There is one Crp-cAMP binding site in the *PlacZYA* promoter (centered at position -61.5) and two LacI binding sites (centered at positions -82 and +11). A third LacI binding site centered at position +412 is not shown. (b) *PglpFK* is repressed by GlpR and activated by Crp-

cAMP⁴⁷. The *glpFK* promoter has four GlpR and two Crp-cAMP binding sites. The two Crp-cAMP binding sites are located at positions -37.5 and -60.5. The site at -37.5 is at a position that would normally occlude the binding of the RNA polymerase to its site. The four GlpR binding sites are located at positions -17.5, -37.5, -58.5, -79.5. (c) *PfucPIK* is activated by both Crp-cAMP⁵² and fucose-1-phosphate induced FucR^{53,54}. The *PfucPIK* has two Crp-cAMP binding sites (centered at positions -40.5 and -80.5)^{52,55}. The fucose-1-phosphate induced FucR binding site on *PfucPIK* has not been identified till now. (d) Strain NQ373 carrying *PglpF-lacZ* in a Δ *glpR* background grown with various carbons (C-limitation; circles); strain NQ490 carrying *PglpF-lacZ* in a Δ *glpR* and a GOGAT-null background with GDH expression titration grown in glycerol as a sole carbon source (NC-limitation; open diamonds). (e) Strain NQ554 carrying *PfucP-lacZ* grown with various carbons (C-limitation; circles); strain NQ1180 carrying *PfucP-lacZ* in a GOGAT-null background with GDH expression titration grown in glycerol as a sole carbon source (NC-limitation; open diamonds). The linear regression in each panel shows the C- (solid) and NC- (dashed) lines and the table shows all fitted values as defined in Supplementary Note 3. MU: Miller Unit.

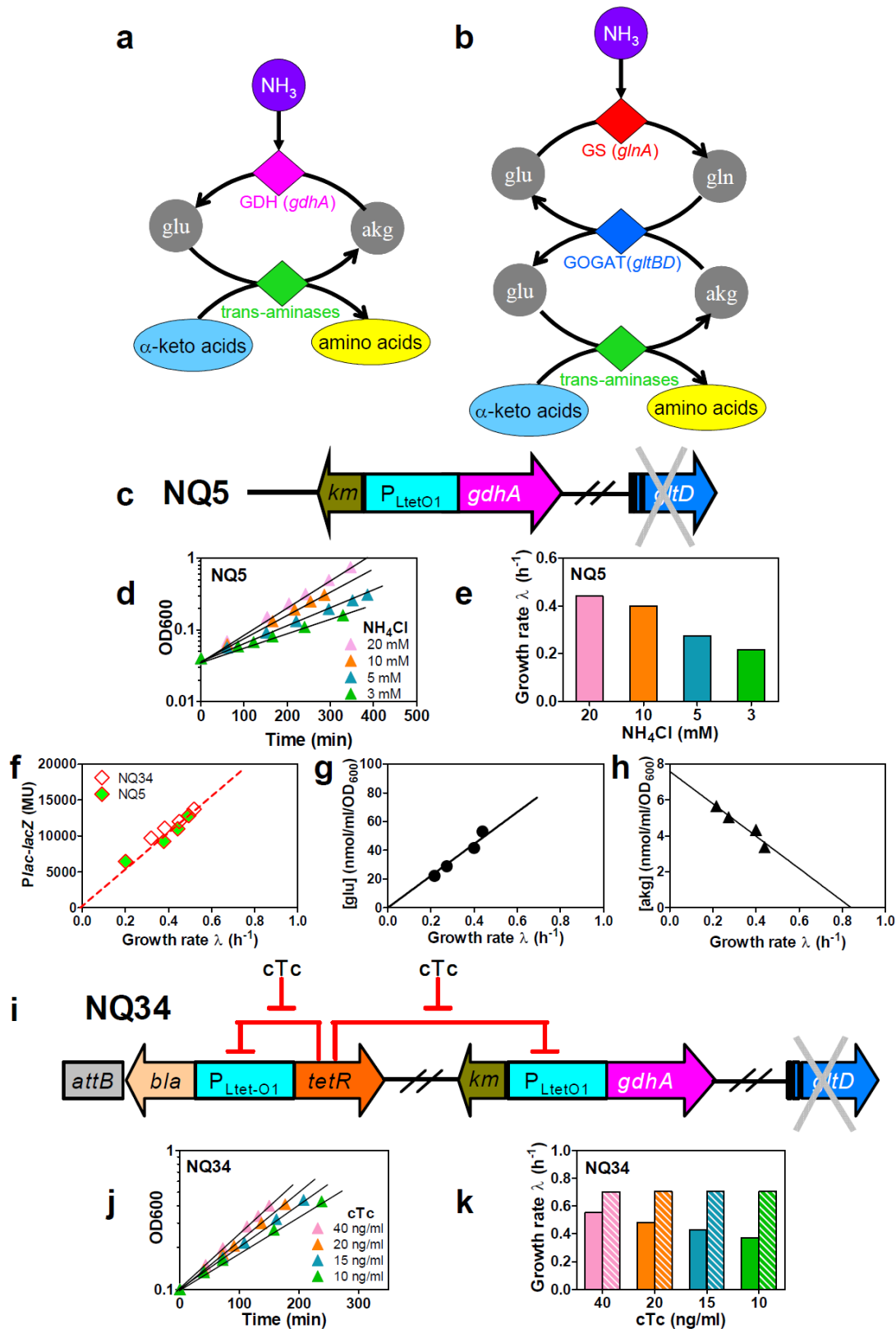


Figure S6: Titration of ammonia assimilation. To impose non-carbon modes of growth limitation, we avoided using organic nitrogen or sulfur sources as their carbon content may introduce unintended complications. In this study, we used ammonium- and sulfate- limited chemostats (Tables S6). Additionally, we constructed strains whose abilities to assimilate

ammonium as the sole nitrogen source can be varied in graded manners (Table S7). These constructs allowed us to impose C- and N- limitations in different combinations and are described in detail below.

Panels (a) and (b) illustrate the two known pathways for the assimilation of ammonium in *E. coli*⁵⁶. In the simpler pathway (a), ammonium is fixed onto alpha-ketoglutarate (akg) via the enzyme glutamate dehydrogenase (GDH, purple diamond, encoded by *gdhA*) to form glutamate (glu), which subsequently trans-aminates (green diamond) one of many alpha-ketoacids (light blue oval) to form amino acids (yellow oval), regenerating akg in the process. In the pathway depicted in b, the overall process is the same except that GDH is replaced by two enzymes, glutamine synthetase (GS, red diamond, encoded by *glnA*) and glutamate synthase (GOGAT, blue diamond, encoded by the *gltBD* operon). In this pathway, ammonium is first assimilated into glutamine (gln) and then passed on to glu. Pathway b is the major ammonium assimilation pathway⁵⁷. It has a much higher affinity for ammonium: The K_m of GS for ammonium is $\sim 0.1\text{mM}$ ^{58,59} while the K_m of GDH for ammonium exceeds 1mM; see Ref. 60 and references therein. This pathway requires ATP consumption and is highly regulated at multiple levels⁵⁶: Upon severe ammonium limitation (sensed by gln^{56,61}), it is known that *E. coli* upregulates ammonium transport (by GlnK-AmtB) and ammonium assimilation (by GS-GOGAT), both via the well-characterized nitrogen-response (Ntr) regulatory system⁵⁶ to maintain the internal ammonium concentration¹³.

Our strategy is to bypass the Ntr system so that nitrogen shortage is imposed directly on cellular metabolism. Panel (c) depicts our basic strain construct (NQ5), which is deleted of *gltD* and has the promoter of *gdhA* replaced by the $P_{\text{Ltet-O1}}$ promoter¹⁵ which is constitutive in the absence of TetR repressor. In this strain, pathway b is broken and ammonium assimilation must proceed by pathway a, the flux through which can be controlled in a graded manner by either controlling the external ammonium concentration (due to the lower affinity of GDH for ammonium) or by dialing the expression level of GDH. [The conversion of gln to glu by other pathways (e.g., glutaminases⁶² and amido-transferases⁶³) can support only a small fraction of the cellular nitrogen need⁶⁴, as *gltD gdhA* double deletion cells cannot grow in medium with ammonium as the sole nitrogen source.] Panels (d) and (e) show that the cells indeed grew exponentially but at different rates in glycerol minimal medium with different ammonium concentrations (3-20 mM). Panel (f) shows the IPTG-induced *PlacZ-lacZ* expression level of this strain NQ5 (in Miller Unit or MU) vs its growth rate (open diamonds with green filling) for different ammonium concentrations in the medium. The dashed red line shows the best linear fit of the data. Coincidentally with the linear decrease of *PlacZ* with the reducing growth rate, the intracellular glu pool, [glu], also decreased linearly with the growth rate (g) while the intracellular akg pool, [akg], increased linearly with the growth rate (h). These results suggest the growth reduction of this strain is due to limitation in glu, which presumably affects amino acid synthesis and other anabolic reactions via trans-amination (a). Note that this type of growth limitation is distinct from the type of ammonium limitation heavily studied in the literature^{56,61}, e.g., based on the ammonium-limited chemostat and associated with a limited gln pool and a constant glu pool⁶¹. It is remarkable that despite the very different responses exhibited by these key metabolites, both type of growth limitations led to similar responses by the catabolic systems (open symbols, Fig. 1a).

In our study, we actually adopted a variant of NQ5, NQ34. As shown in panel (i), NQ34 has an additional module incorporated into NQ5; it consists of a *tetR* gene driven by the $P_{Ltet-O1}$ promoter and integrated at the *attB* site. The $P_{Ltet-O1}$ promoter¹⁵ is repressed by TetR and the repression is relieved by an inducer chloro-tetracycline (cTc). Hence TetR represses both its own expression and also the expression of GDH. The autorepression of TetR allows one to control the output of the $P_{Ltet-O1}$ promoter, particularly GDH expression level and hence cell growth, in a graded manner by varying the concentration of cTc¹⁰. Another advantage of this auto-repressed control system is that for a fixed concentration of cTc, the output is only weakly affected by changes in the cell's growth status due to changes in other nutrient conditions¹⁰. Panels (j) and (k) show the growth of strain NQ34 in glycerol minimal medium with 20 mM NH₄Cl, for cTc concentrations ranging between 10–40 ng/ml. The growth rates of the control strain (NQ387), with $P_{Ltet-O1}$ -*tetR* at the *attB* site but with the native *ghdA* and *gltBD*, are shown as the striped bars in (k). The IPTG-induced *PlacZ-lacZ* expression levels of NQ34 vs its growth rate are shown in panel (f) (open diamonds without filling). It is seen to follow the same trend as that of the NQ5 strain under A-limited growth. Similarly, the glu and akg pools of NQ34 varied with its growth rate in the same manner as those of NQ5 (data not shown).

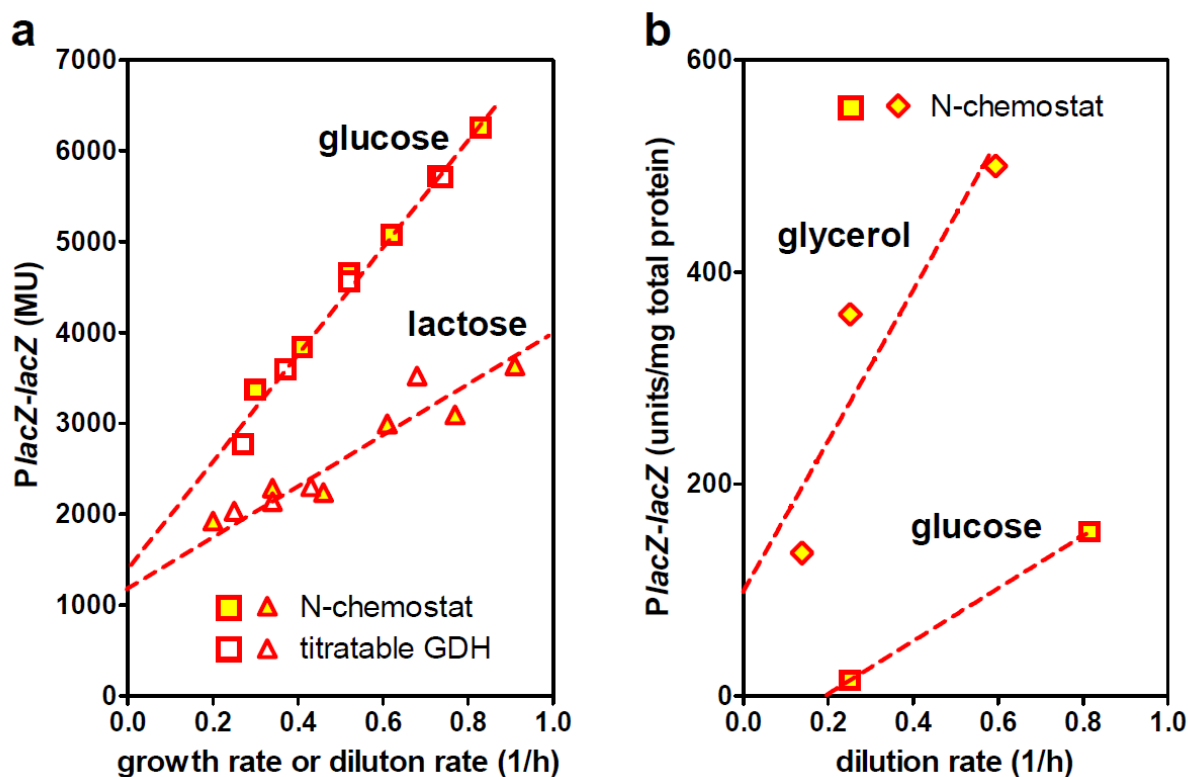


Figure S7: *Plac-lacZ* expression for growth under NC-limitations. (a) The NC-lines of *Plac-lacZ* obtained with lactose or glucose as the sole carbon source shown in Fig. 1A were re-plotted here with an enlarged y-axis. The yellow-filled symbols are data from ammonium-limited chemostat, with triangles for wild type (NCM3722) cells grown on lactose, and squares for NQ354 (*lacI*-null) cells grown on glucose. The open symbols with no filling are data from batch culture with titrating GDH expression in a GOGAT-null background (NQ34), grown on lactose (triangles) and glucose (squares). MU: Miller Unit. (b) The NC-lines of *Plac-lacZ* obtained from Ref. 48. The reported expression of *Plac-lacZ* obtained from ML308 strain grown in ammonium-limited chemostat with glycerol or glucose as the sole carbon source was plotted against its corresponding dilution rate. Note: We also tried characterizing our strain (NQ354) in glycerol-fed ammonium-limited chemostat, but did not find any significant changes in *Plac-lacZ* expression down to a dilution rate of 0.14/hr (corresponding to 300-min doubling time). The harvested cells exhibited heterogeneity in sizes and even some filamentation, suggesting unknown physiological problems and possibly mutation.

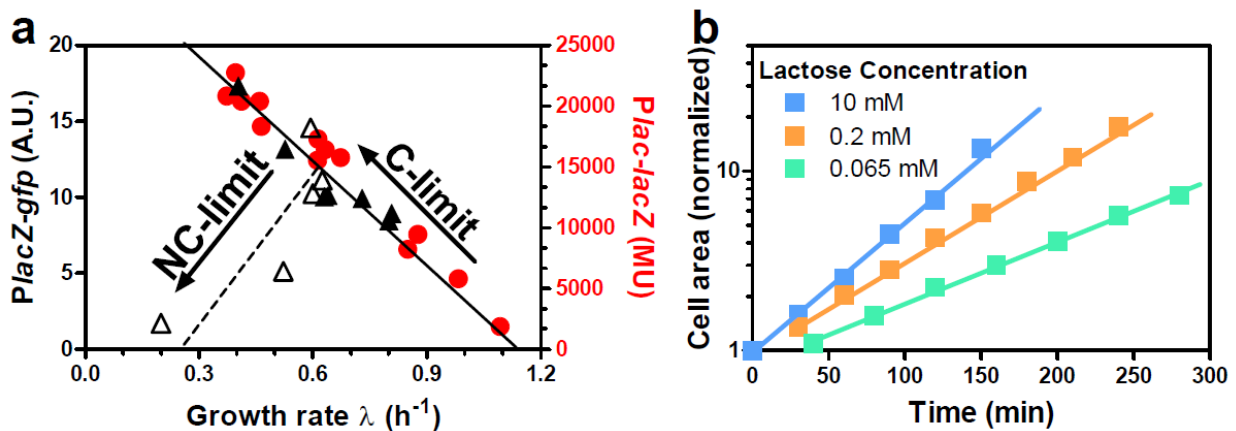


Figure S8: *PlacZ* expression in microfluidic chemostat. In the main text, we showed the linear relationship between the activity of *PlacZ* promoter and growth rate (the C-line) for wild-type cells grown in medium with various carbon sources and IPTG, replotted as red solid circles in panel a. Here, we checked this relationship as we varied the growth rate by reducing the concentrations of lactose in the medium with saturating amount (20mM) of ammonium (solid triangles in panel a); the results are seen to be consistent with the batch culture results with *PlacZ* induction by IPTG. To maintain steady state growth at reduced lactose concentrations, we employed a microfluidic chemostat in which the growth medium is continuously replenished by the fresh medium and nutrients in growth medium are always maintained at desired concentrations¹³. The exponentiality of cell growth at low lactose concentrations is demonstrated by the linearity of the growth curves on semi-log plot (panel b), with the vertical axis being the total cell area obtained from time-lapse brightfield images; see Supp. Methods. We used immotile $\Delta\textit{motA}$ cells for the ease of cell tracking by time-lapse microscopy¹³. *PlacZ* activity is characterized by monitoring the fluorescence intensity of strain EQ123 which harbors a chromosomal *PlacZ-gfp* transcriptional fusion reporter in $\Delta\textit{motA}$ background. We also attempted to impose NC limitation using the same device, by applying medium with various concentrations of ammonium, with the lactose concentration fixed at 65 μM . Since it is difficult to bring the ammonium concentration to a low enough level to affect cell growth, due to the active transport of ammonium by wild-type cells¹³, we further deleted from strain EQ123 the *glnK-amtB* operon which encodes the ammonium transporter AmtB and its regulator GlnK. The resulting strain, EQ129, exhibited growth reduction upon reduction in the concentration of ammonium (open triangles). The corresponding *PlacZ-gfp* reporter expression decreased with decreasing growth rates (open triangles), and the behavior is adequately described by the NC-line (dashed black line in panel a). MU: Miller Unit.

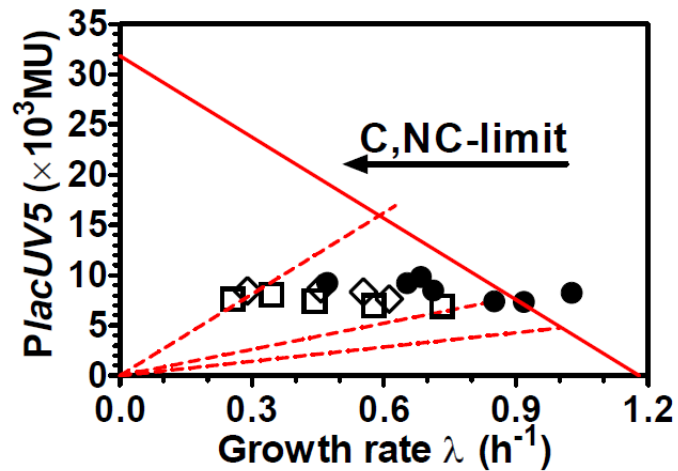
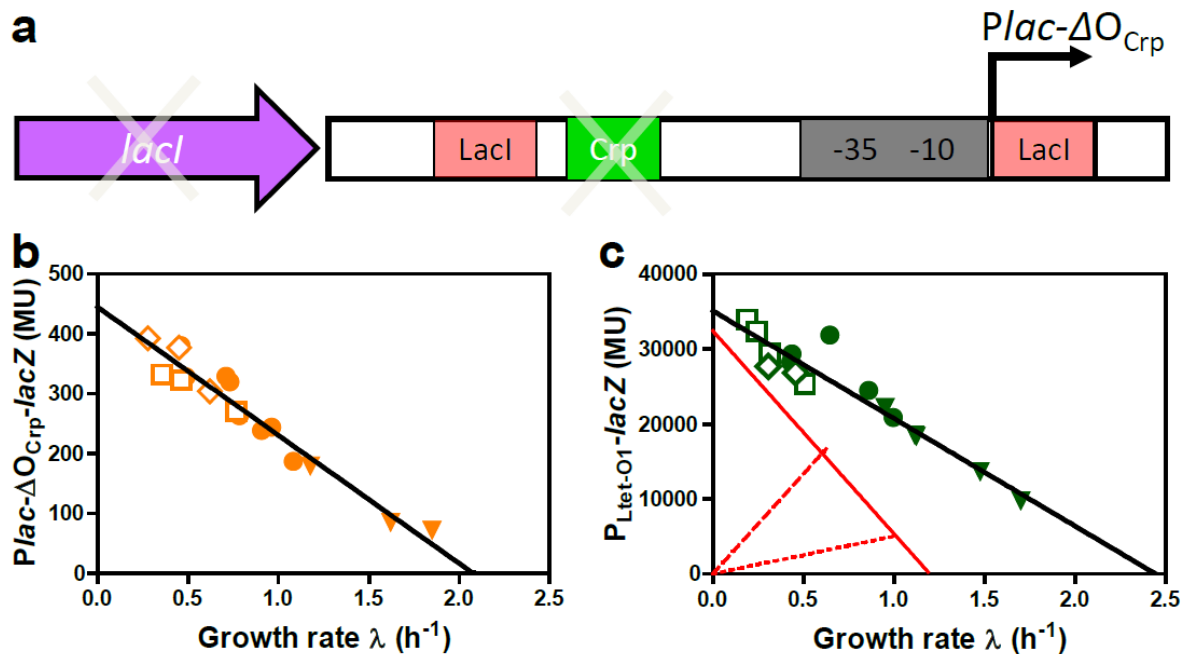


Figure S9: The growth-rate dependences of *PlacUV5* under C- and NC- limitation.

Expression of *PlacUV5-lacZ* by NQ1053 (*PlacUV5-lacZ*) cells under C-limitation with various carbon sources (●) and NQ1054 (*PlacUV5-lacZ*; titratable GDH) cells under NC-limitation via GDH titration with either glycerol (◇) or glucose (□) as the sole carbon source were determined. No apparent growth-rate dependence is seen. The red lines are those from Fig. 1a. MU: Miller Unit.



C-limitation				NC-limitation			
Strain	Description	Carbon	LacZ	Strain	Description	Carbon	LacZ
NQ367	<i>Plac-ΔO_{Crp}-lacZ</i>	various	●	NQ475	<i>Plac-ΔO_{Crp}-lacZ ΔGOGAT</i> cTc titrated GDH amount	glucose	□
		rich medium	▼			glycerol	◇
NQ122	<i>P_{Ltet-O1}-lacZ</i>	various	●	NQ124	<i>P_{Ltet-O1}-lacZ ΔGOGAT</i> NH ₄ Cl titrated GDH activity	glucose	□
		rich medium	▼			glycerol	◇

Figure S10: The growth-rate dependences of promoters not regulated by Crp-cAMP. (a) The genetic structure of the synthetic *Plac-ΔO_{Crp}* promoter. This promoter was constructed by replacing the Crp-cAMP binding site in the native *Plac* promoter with a random DNA sequence of the same length; see Supp Methods for details. (b) Expression of LacZ (in Miller Unit or MU) in NQ367 cells which harbors *Plac-ΔO_{Crp}-lacZ* in $\Delta lacI$ background or in NQ475 cells which additionally harbors the titratable GDH construct in $\Delta gldD$ background (Fig. S6). NQ367 cells were grown with various carbon sources (red filled circles) and NQ475 cells were grown in 20 mM NH₄Cl and varying amounts of cTc, with either glycerol (red open diamonds) or glucose (red open squares) as the sole carbon source. They are seen to all fall on the same line, with an x-intercept at $2.1 \pm 0.2 \text{ h}^{-1}$. (To better define the behavior at high growth rates, data were also taken for cells grown in rich defined medium (see Supp Method for their composition), shown as the filled inverted triangles.) This behavior is substantially different from Crp-regulated promoters (Fig. 1a and S5de): Not only is the x-intercept of the black line nearly twice that of λ_c for the C-line (solid lines in Fig. 1a and S5de) under C-limitation, the actual expression level of *Plac-ΔO_{Crp}-lacZ* over the range of growth rate between 0.5 h^{-1} and 1 h^{-1} varied by less than 2-fold while that of the native *Plac-lacZ* varied by nearly 10-fold. Moreover, the response of *Plac-ΔO_{Crp}-lacZ* to NC-limitation is completely the opposite of that of *Plac-lacZ* (dashed lines in

Fig. 1a and Fig. S5de). The responses of *Plac-ΔO_{C_{rp}}-lacZ* to C- and NC- limitations shown here are very similar to those exhibited by the constitutive LacZ expression driven by the synthetic *P_{Ltet-O1}* promoter under both C- and NC- limitations as shown in panel c: C-limitation is accomplished by growing NQ122 cells (harboring *P_{Ltet-O1}-lacZ*) with various carbon sources and 20mM NH₄Cl (green filled circles), and NC-limitation is accomplished by growing NQ124 cells (harboring *P_{Ltet-O1}-lacZ*, in *ΔgltD* background with constitutive GDH expression, see Fig. S6c) in varying amounts of NH₄Cl, with either glycerol (green open diamonds) or glucose (green open squares) as the sole carbon source. Data in various rich defined medium are shown in green filled inverted triangles. The black solid line shows the best linear fit, with an x-intercept of $2.4 \pm 0.3 \text{ h}^{-1}$. The C- and NC- lines for *PlacZ* (Fig. 1a) are drawn here in red for comparison. The response of *P_{Ltet-O1}-lacZ* falls on the same line as that determined previously¹⁷ for constitutive gene expression in various rich medium, shown here for NQ122 cells (filled inverted triangles in panel c). Note that both *Plac-ΔO_{C_{rp}}* and *P_{Ltet-O1}* promoters behave differently from *PlacUV5* (Fig. S9) which is nearly growth-rate independent in the growth rate range 0.25/h ~ 1/h tested. This suggests that perhaps *PlacUV5* has some residual regulation, but such details are well beyond the scope of this study.

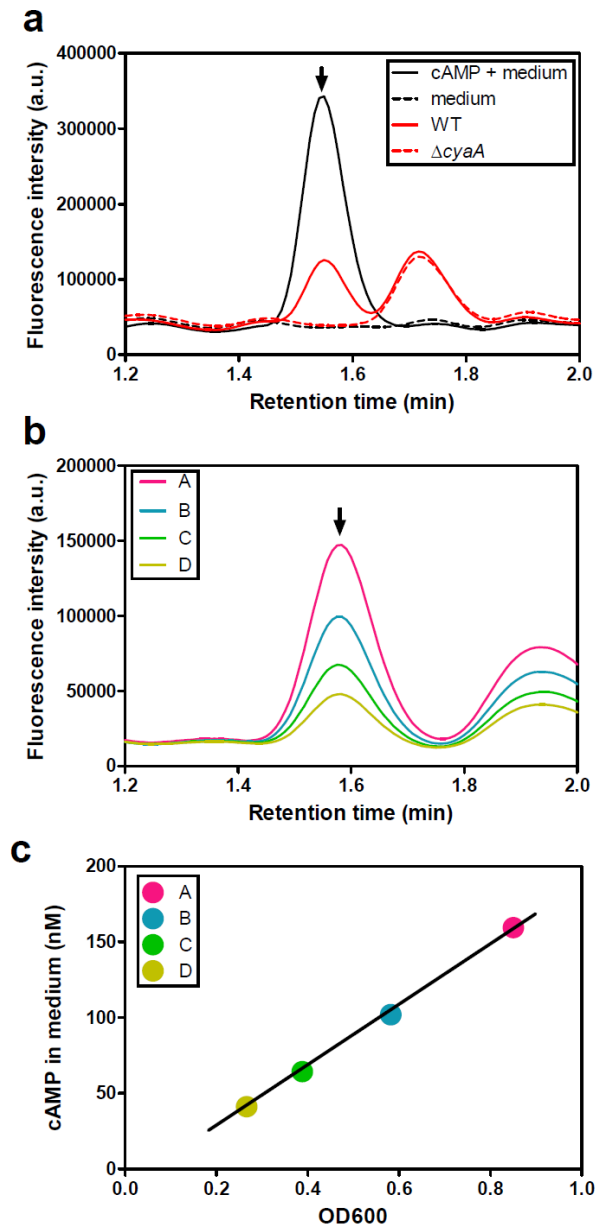
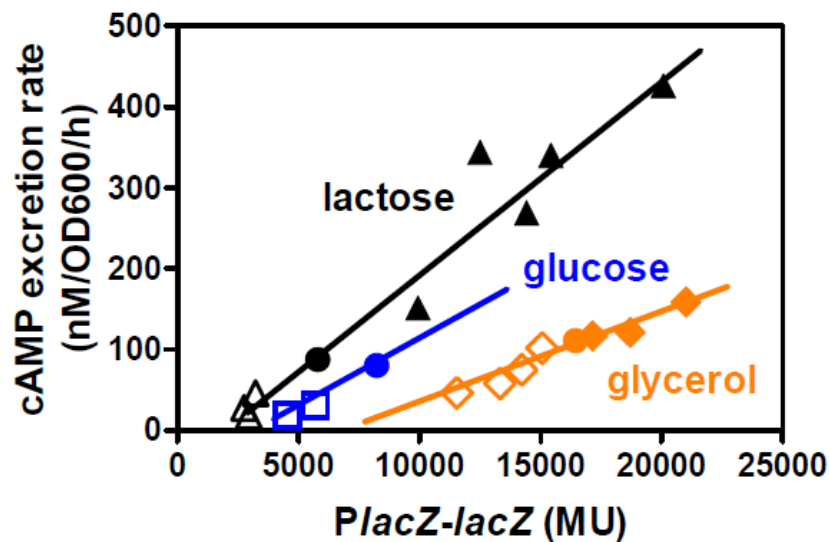


Figure S11: cAMP assay by HPLC. (a) Chromatograms of cAMP assay in wild-type strain NCM3722 and $\Delta cyaA$ strain NQ93. Strains were grown in N^+C^- medium supplemented with 20 mM NH_4Cl , 0.4% (w/v) glucose, and 1 mM IPTG. *Black solid line*, 40 pmol cAMP standard in the medium; *black broken line*, the medium only; *red solid line*, the filtrate of the NCM3722 strain culture taken at $OD_{600} = 0.4$; *red broken line*, the filtrate of the $\Delta cyaA$ strain NQ93 culture taken at $OD_{600} = 0.4$. The arrow in each panel shows the position of the cAMP peak. (b) and (c) show an example of cAMP excretion rate measurement, derived from the culture of NQ381 grown in N^+C^- medium supplemented with 20 mM NH_4Cl , 0.2% (w/v) lactose, 1 mM IPTG, and 500 μM 3MBA. (c) Chromatograms of the samples taken at four different OD_{600} (A, B, C, D). The plot of cAMP amounts at four different (A, B, C, D) points against OD_{600} . The slope of the linear relation (in nM/ OD_{600}) is further multiplied by the growth rate of the culture (1/hour) to obtain the cAMP excretion rate (in nM/ OD_{600} /hour).



Strain	Description	Carbon	Limitation	cAMP
NCM3722	wild-type	lactose	C-limit	●
NQ381	Titrate LacY			▲
NQ34	Δ GOGAT titratable GDH		NC-limit	△
NCM3722	wild-type	glucose	C-limit	●
NQ34	Δ GOGAT titratable GDH		NC-limit	□
NCM3722	wild-type	glycerol	C-limit	●
NQ399	Titrate GlpFK			◆
NQ34	Δ GOGAT titratable GDH		NC-limit	◇

Figure S12: Correlation of cAMP level and LacZ activity. The cAMP excretion rate (y-coordinate), used here as a proxy for the internal cAMP concentration²¹, is plotted against the native *PlacZ* expression (x-coordinate) for various modes of C- and NC- limited growth. C-limited growth was achieved by titrating LacY expression in NQ381 cells grown on 0.2% (w/v) lactose (filled triangles), titrating GlpFK expression in NQ399 cells grown on 0.4% (v/v) glycerol (filled diamonds), and growing NCM3722 cells in 0.2% (w/v) lactose, 0.4% (w/v) glucose and 0.4% (v/v) glycerol (filled circles). NC limited growth was achieved by titrating GDH expression in NQ34 cells grown on 0.2% (w/v) lactose, 0.4% glucose (w/v), and 0.4% (v/v) glycerol (open triangles, squares, diamonds, respectively). NC⁻ medium supplemented by 1mM IPTG and 20 mM NH₄Cl was used in all these cases. The strong correlation between the cAMP excretion rate and *Plac-lacZ* expression is clearly seen for each fixed carbon source. However, there is a systematic modulation of this relation for different carbon sources. The source of this shift is not known; it does not appear to be related to the PTS system as the response of glucose, a PTS sugar, is in between those of lactose and glycerol, both being non-PTS sugars.

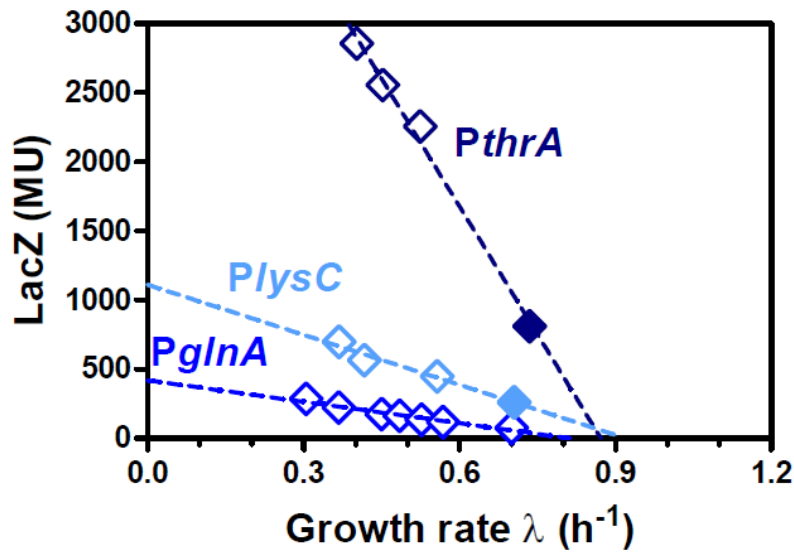


Figure S13: Biosynthetic genes expression under A-limited conditions. Strains NQ482 and NQ983 carrying *PthrA-lacZ* and *PlysC-lacZ* respectively in the genetic background of NQ34 (Δ *gltD* and titratable GDH) were grown in N^+C^- medium with 0.4% (v/v) glycerol and 20 mM NH_4Cl , each with various degrees of GDH expression induced by cTc (20-40 ng/ml). Open diamonds show the plot of LacZ activity against the growth rate for each of these conditions for each strain. Also shown (solid diamonds) are the results for strain NQ481 and NQ980 carrying *PthrA-lacZ* and *PlysC-lacZ* respectively in wild-type background, grown in N^+C^- medium with 0.4% (v/v) glycerol and 20 mM NH_4Cl . The A-line of *PlysC* is a least square fit ($r^2 = 0.97$) with $\lambda_A = 0.92 \pm 0.13$ (h^{-1}). The A-line of *PthrA* is a least square fit ($r^2 = 0.99$) with $\lambda_A = 0.87 \pm 0.06$ (h^{-1}). The results for A-line of *PglNA* in glycerol (deep blue diamonds and line shown in Fig. 1d), are reproduced here for comparison. MU: Miller Unit.

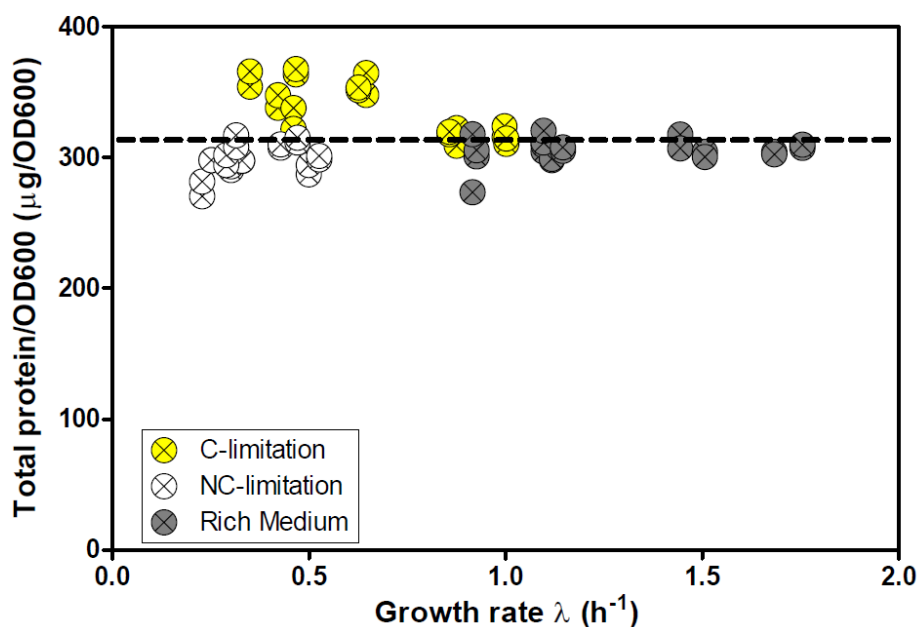


Figure S14: Weak growth-rate dependence of cellular protein mass per OD₆₀₀. *E. coli* strains were grown in rich medium, and in various C and NC- limited conditions. Total protein per OD₆₀₀ was measured four times under each condition (see Supp. Methods) and was found to have weak growth rate dependences. The dash line indicated the average value, $\sim 314 \mu\text{g}/\text{OD}_{600}$.

Rich medium (grey cycles with cross): NCM3722 grown in N⁻C⁻ medium with 20 mM NH₄Cl, 0.4% (w/v) glucose and supplemented by (i) 7 amino acids (glycine, histine, isoleucine, leucine, lysine, methionine, phenylalanine), each of which cannot be utilized as the sole carbon source; (ii) 9 amino acids (proline, serine, tryptophan, glutamate, glutamine, aspartate, asparagine, alanine, arginine), each of which can be utilized as the sole carbon source; (iii) all 16 amino acids (the remaining 4 amino acids were not used because of either low solubility or stability) in (i) and (ii); (iv) 0.2% (w/v) casamino acids; (v) rich defined media¹⁷ (see Supp. Methods for details).

C-limited (yellow circles with cross.): NCM3722 grown in N⁻C⁻ medium with 20 mM NH₄Cl and one of the following as the sole carbon source: glucose, glycerol, acetate, sorbitol, G6P+gluconate.

NC-limited (white circle with cross): NQ34 with titratable GDH grown in N⁻C⁻ medium with 20 mM NH₄Cl and with glycerol or glucose as the sole carbon source and induced with different cTc levels.

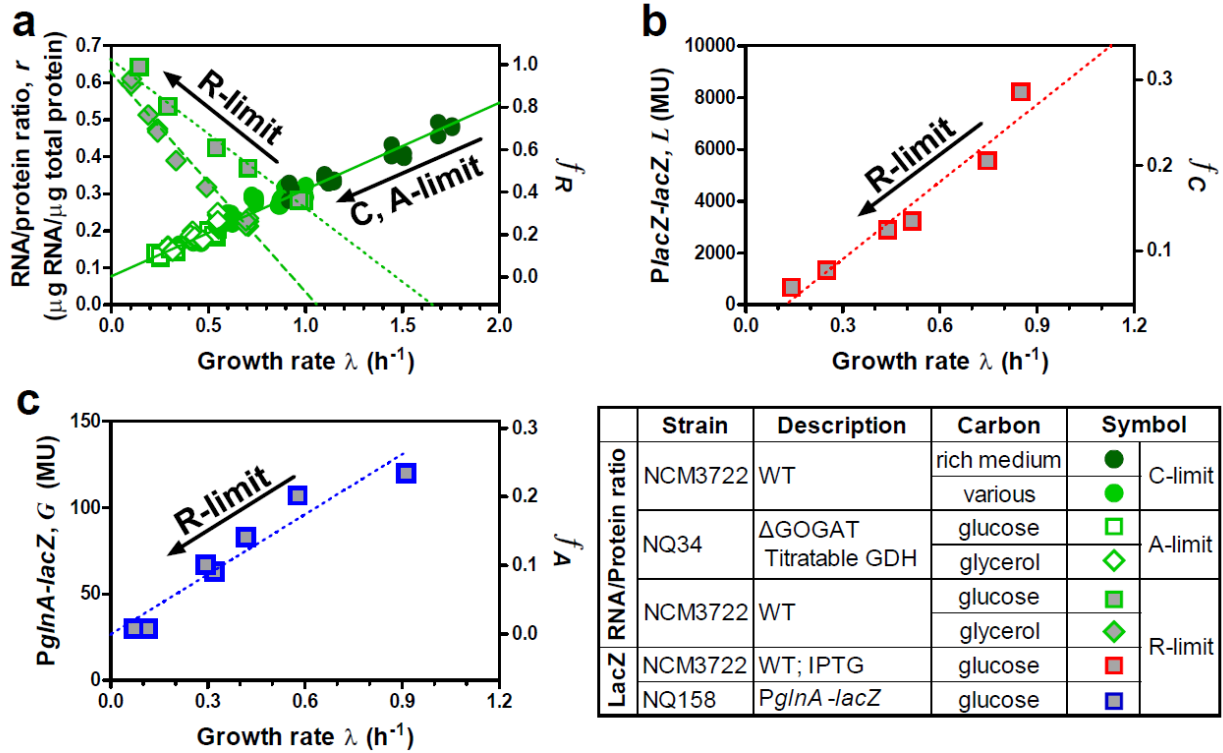


Figure S15: The effect of translational limitations. For translational limitation (or R-limitation), strains were grown in minimal medium with various chloramphenicol (Cm) levels (0-12 μ M). (a) RNA/protein ratio for NCM3722 strain grown in either glucose (grey filled squares) or glycerol (grey filled diamond) with various Cm levels. RNA/protein ratio for strains grown in C- and NC- limited conditions in Fig. 1d was shown as a comparison. RNA/protein ratios for NCM3722 strain grown in various defined rich medium (see Supp Methods) were also shown as dark green circles. The straight lines are the best linear fits; best-fit parameters are provided in Table S14. The right vertical axis shows the normalized R-fraction, f_R , computed according to Supp Note 3. (b) *Plac-lacZ* expression in NCM3722 strain grown in glucose (grey filled squares) with 1 mM IPTG and various Cm levels. The straight line is the best linear fit with parameters given in Table S5. The right vertical axis gives the normalized C-fraction, f_C , computed according to Supp Note 3. (c) NQ158, harboring *PglA-lacZ* expression in wild-type background, is grown in glucose (grey filled squares) and various Cm levels. The straight line is the best linear fit with parameters given in Table S15. The right vertical axis gives the normalized A-fraction, f_A , computed according to Supp Note 3. MU: Miller Unit.

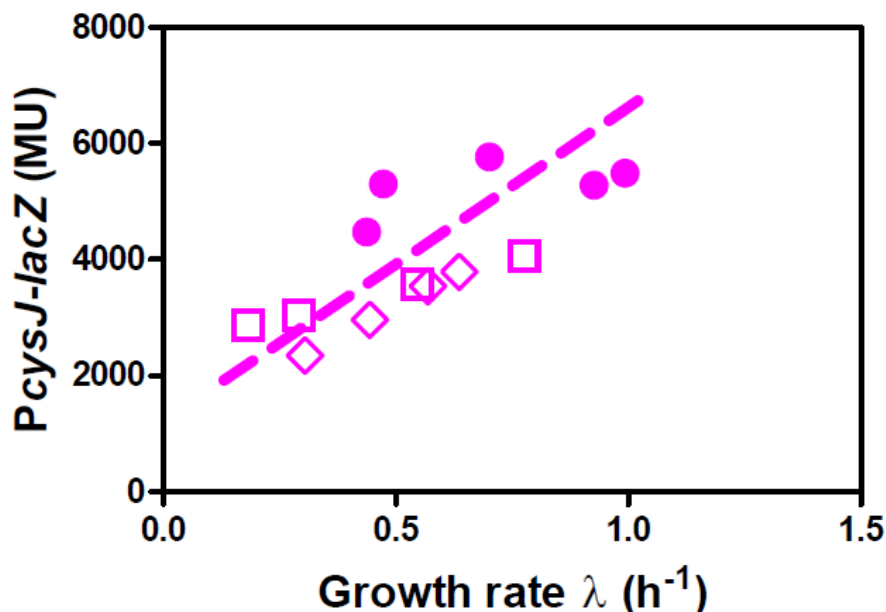


Figure S16: Other responses under C- and A- limitations. Not all non-ribosomal genes respond to C- and A- limitations in opposing manners as exemplified by *PlacZ* (Fig. 1a) and *PglnA* (Fig. 1d). We show one such exception here, *PcysJ-lacZ*, which reports the expression of the sulfate assimilation pathway. For C-limitation, strain NQ979 carrying *PcysJ-lacZ* in wild-type background was grown in minimal medium with various carbons (filled circles). For A-limitation, strain NQ982 carrying *PcysJ-lacZ* in the genetic background of NQ34 ($\Delta glnD$ and titratable GDH) was grown in N⁻C⁻ medium with 0.4% (v/v) glycerol (open diamonds) or 0.4% (w/v) glucose (open squares) as the sole carbon source, with 10-40 ng/ml cTc which provides the desired GDH titration. The dashed line shows the best fit. The reduction in sulfate assimilation upon C- or A- limitation is very reasonable physiologically, as the *need* for sulfate is reduced when cells grow more slowly due to C- or A- limitation. We expect this response to be generic to genes not directly involved in catabolism (for C-limitation) or amino acid synthesis (for A-limitation). For example, we expect the cell to reduce nucleotide synthesis if growth slows down due to limitations in carbon uptake or amino acid synthesis. MU: Miller Unit.

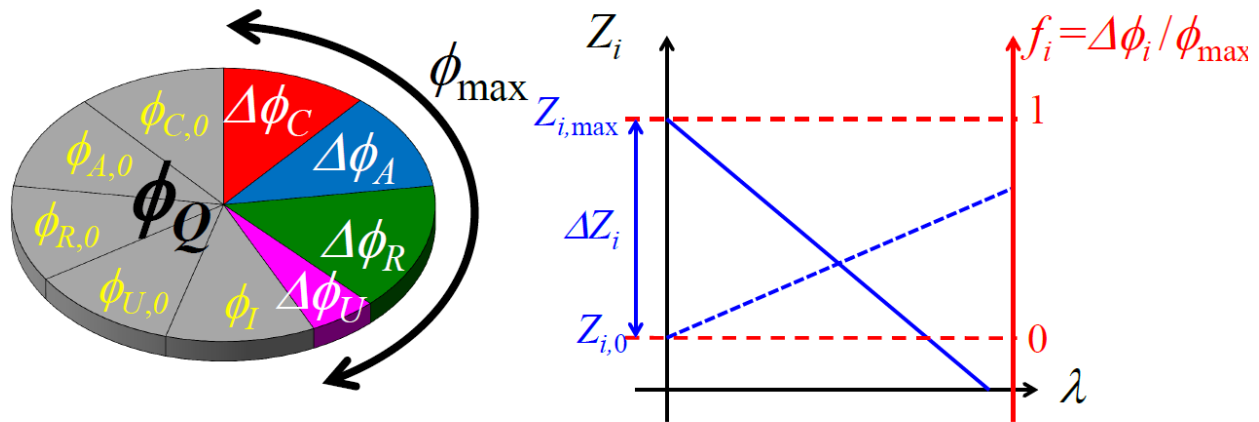


Figure S17: Proteome sectors and model of proteome partition. We describe here an extension of a coarse-grained model of the proteome first introduced in Ref. 17. Proteins whose expression levels would change similarly upon various modes of growth limitation (e.g., the catabolic operons described in Figs. 1a and S5) are summed together in mass and referred to as a “proteome sector”. The sectors, hypothesized to respond specifically to (i.e., up-regulated only upon) the C-, A-, and translational limitations, are referred to as the C-, A- and R- sectors respectively; see Supp. Note 1. Additionally, we propose a sector (U) for proteins which do not respond specifically to any of the three limitations (see e.g., Fig. S16), and another sector (I) for proteins whose expression levels remain constant under different conditions³³. The abundance of each sector j , defined as its fraction of the total cellular protein mass, is referred to as the “proteome fraction” and denoted by ϕ_j . We decompose each proteome fraction into a growth-rate independent component $\phi_{j,0}$ and a growth-rate dependent component $\Delta\phi_j(\lambda)$ such that the minimal proteome fraction under “general response” (where the proteome fraction goes down with decreased growth rate, as illustrated in Fig. 2a) is $\phi_{j,0}$; see detailed explanation in Supp Note 1. The growth-rate dependent components are the quantities of focus; they are shown as slices of a pie with different colors on the left panel and in Fig. 2a. The growth-rate independent components comprise an effective core section referred to as Q, with mass fraction ϕ_Q (the grey slice in the left panel). It does not participate in the proteome dynamics, except for providing a cap, $\phi_{\max} = 1 - \phi_Q$, constraining the maximum allowed changes of the growth-rate dependent components, i.e., $\phi_{\max} = \Delta\phi_C(\lambda) + \Delta\phi_A(\lambda) + \Delta\phi_R(\lambda) + \Delta\phi_U(\lambda)$.

As explained in detail in Supp Note 3 (Eq. [S22]), within our model the proteome fraction for each sector j can be estimated from the expression level of a reporter (Z) for that sector, e.g., *PlacZ* for the C-sector. The panel on the right shows graphically how the reporter expression levels (in blue, e.g., those plotted in Figs. 1 and S15a) can be converted to the normalized proteome fraction, $f_j(\lambda) \equiv \Delta\phi_j(\lambda) / \phi_{\max}$, shown in red. The solid blue line shows the specific response, dashed blue line the general response.

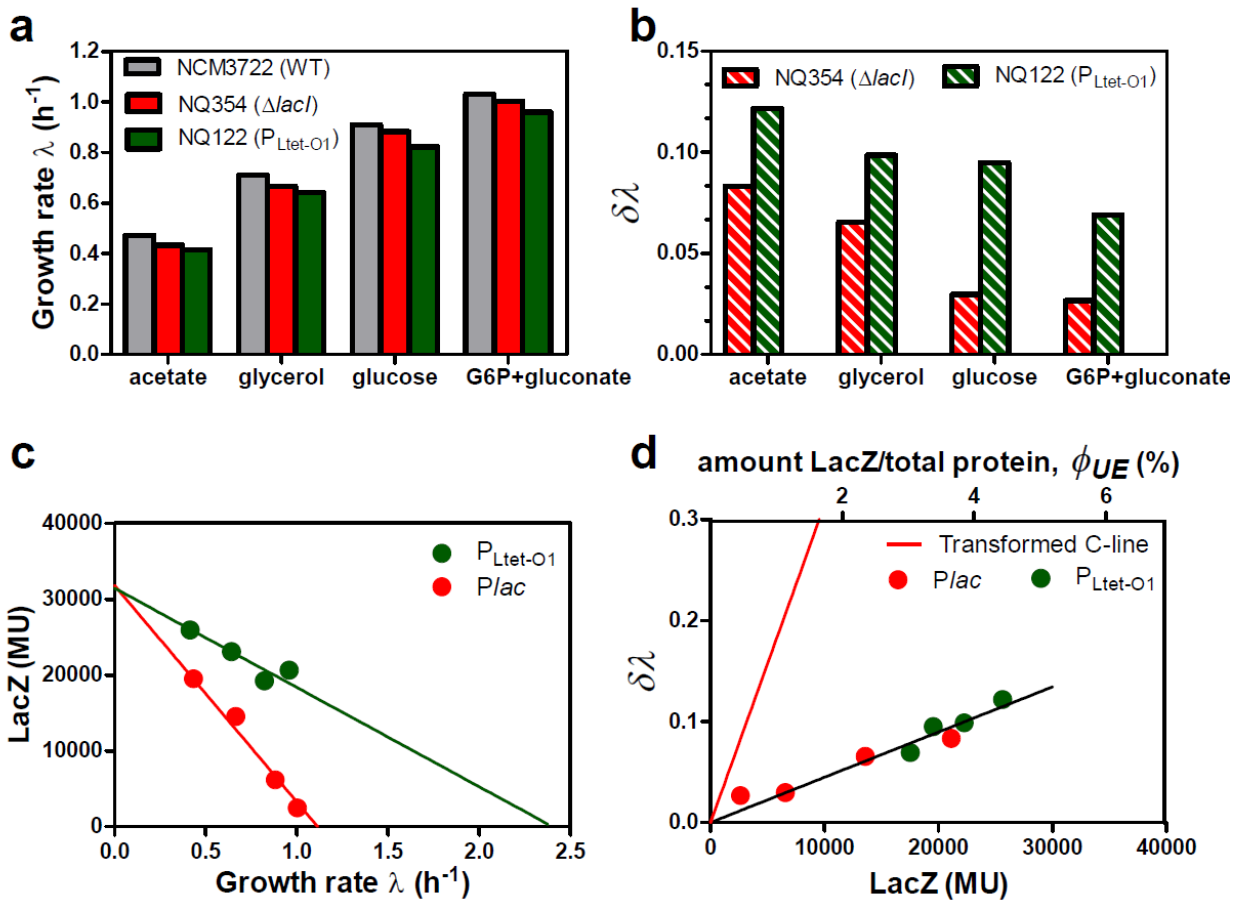


Figure S18: ϕ_{\max} and the fitness cost of protein overexpression. A strong prediction of the proteome partition model of bacterial growth is that the fitness cost of the expression of useless proteins is linear in the level of the protein expressed, independent of *how* the protein is regulated; see Supp Note 2. In particular, if the useless protein expressed comprises a mass fraction ϕ_{UE} of the proteome, then the relative fitness cost, $\delta\lambda \equiv 1 - \lambda(\phi_{UE}) / \lambda(\phi_{UE} = 0)$, which measures the relative difference between the growth rate of cells expressing the useless protein, $\lambda(\phi_{UE})$, and the growth rate not expressing useless proteins, $\lambda(\phi_{UE} = 0)$, is simply given by

$$\delta\lambda = \frac{\phi_{UE}}{\phi_{\max}},$$

where ϕ_{\max} is the maximum increase a proteome fraction can acquire when it is the bottleneck (Supp Note 1). We tested this prediction by varying the unnecessary expression of LacZ in two ways: In the first approach, we compared the growth rate of wild-type NCM3722 cells with *PlacZ-lacZ* repressed ($\lambda(\phi_{UE} = 0)$) grown in N^C medium with various carbons (not including lactose) to the growth rate of the $\Delta lacI$ strain (NQ354) with *PlacZ-lacZ* expressed ($\lambda(\phi_{UE})$) grown in the same medium. Grey and red bars in panel a show the absolute growth rates for both NCM3722 and NQ354 in each of the conditions, respectively. The striped red bars in panel b show $\delta\lambda$ as defined above due to *PlacZ-lacZ* overexpression in NQ354 as compared to NCM3722. Here LacZ expression changes due to Crp-cAMP mediated catabolite repression, as a

plot of LacZ expression vs the growth rate for the $\Delta lacI$ strain yields the C-line, shown as the filled red circles in panel c. If this fitness difference between NCM3722 and NQ354 is due primarily to the expression of the unrepressed *lac* operon, whose primary product is LacZ, then we expect the relative fitness cost to be linearly proportional to the LacZ expression level as prescribed by the display formula above. This is indeed seen in panel d, red filled circles.

In the second approach, we used the unnecessary expression of LacZ driven by the constitutive $P_{Ltet-O1}$ promoter (strain NQ122). LacZ expression also varies in NQ122 grown in various carbon sources; see filled dark green circles in Fig. S10c, reproduced in panel c. Changes in growth rates between the wild-type NCM3722 and NQ122 (absolute growth rates for NQ122 in each of the growth conditions were shown in green bars in panel a and $\delta\lambda$ as defined above due to $P_{Ltet-O1}$ -*lacZ* overexpression in NQ122 as compared to NCM3722 were shown as striped green bars in panel b) are plotted against LacZ expression in panel d (dark green circles). Strikingly, we see that despite the very different growth rate dependences of LacZ expression in the two strains NQ354 and NQ122, due to the different promoters driving *lacZ* (red and green circles in panel c), the data converges to a single line as predicted above when plotted against the relative growth rate changes (black line in panel d). Quantitatively, we can convert LacZ expression from activity/OD (MU, bottom horizontal axis), to LacZ protein as a percentage of total cellular proteins (ϕ_{UE} , top horizontal axis). The slope of the line then provides an estimate for ϕ_{max} , which is $\sim 43\%$, comparable to the value of ϕ_{max} obtained previously by a very different method¹⁷. Based on the C-line of *Plac* expression (Fig. 1a), we also show in panel d the growth rate change (defined as $\delta\lambda \equiv 1 - \lambda / \lambda_c$) as a function of LacZ expression (the “transformed C-line”; the red line). The much steeper slope of the red line as compared to the black line indicates that most of the growth rate change of the C-line is not due to the cost of LacZ synthesis.

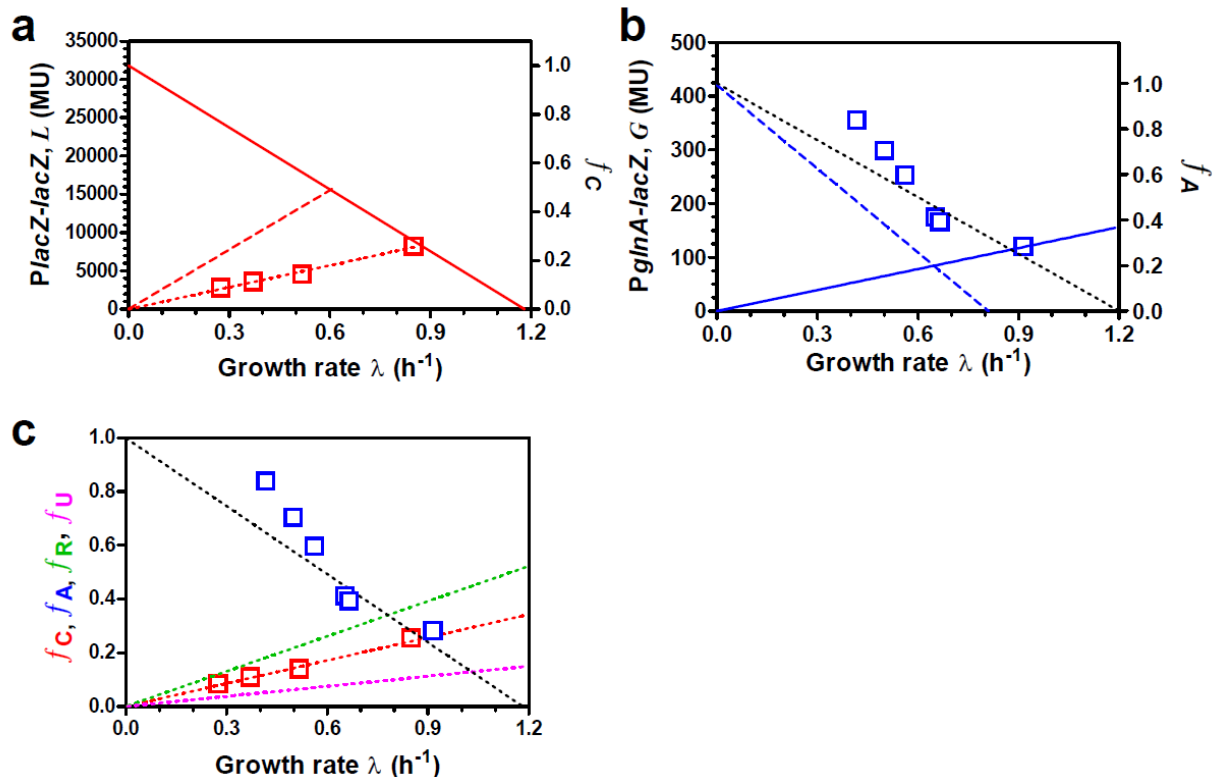


Figure S19: Responses of C- and A- sectors under A-limitations with glucose as a carbon source. (a) The red squares show the expression of *Plac-lacZ* expression under A-limitation with glucose as the sole carbon source. A-limitation was achieved by titrating GDH expression in a GOGAT-null strain (NQ34, Fig. S6) grown in batch culture with 1 mM IPTG. *Plac-lacZ* expression level is converted to the normalized fraction f_C (the right y-axis) using Eq. [S22] in Supplementary Note 3. The dotted red line gives the best linear fit with parameters given in Table S5. For the ease of comparison, we show also the response to A-limitation for growth in glycerol as the dashed red line (same as the dashed red line of Fig. 1a), and the response to C-limitation (C-line in Fig. 1a) as the solid red line. (b) NQ477 carrying *PglnA-lacZ* in the titratable GDH background was grown in glucose with various degrees of GDH expression (blue squares). *PglnA-lacZ* expression level is converted to the normalized fraction f_A (the right y-axis) using Eq. [S22] in Supplementary Note 3. The dashed blue line shows the response to A-limitation for growth in glycerol (same as the dashed blue line of Fig. 1d), and the solid blue line shows the response to C-limitation (same as the solid blue line of Fig. 1d). The dotted black line is the predicted response; see panel c. Note the shift of the x-intercept from glycerol (dashed blue line) to glucose (dotted black line). (c) This plot summarizes how each proteome fraction (the normalized fractions f_j s) depends on the growth rate as the degree of A-limitation is varied. The data points (red and blue squares) are the same as those shown in panels a and b. The dotted green and purple lines, which indicate the R- and X- fractions respectively, are the same as those in Figs. 2b and 2c. The predicted response of the A-sector, $f_A = 1 - \lambda / \tilde{\lambda}_A$ (the dotted black line), is obtained as the difference between 1 and the sum of the colored lines (Eq. [3] of the main text.) The predicted value of $\tilde{\lambda}_A$ is given in Table S16.

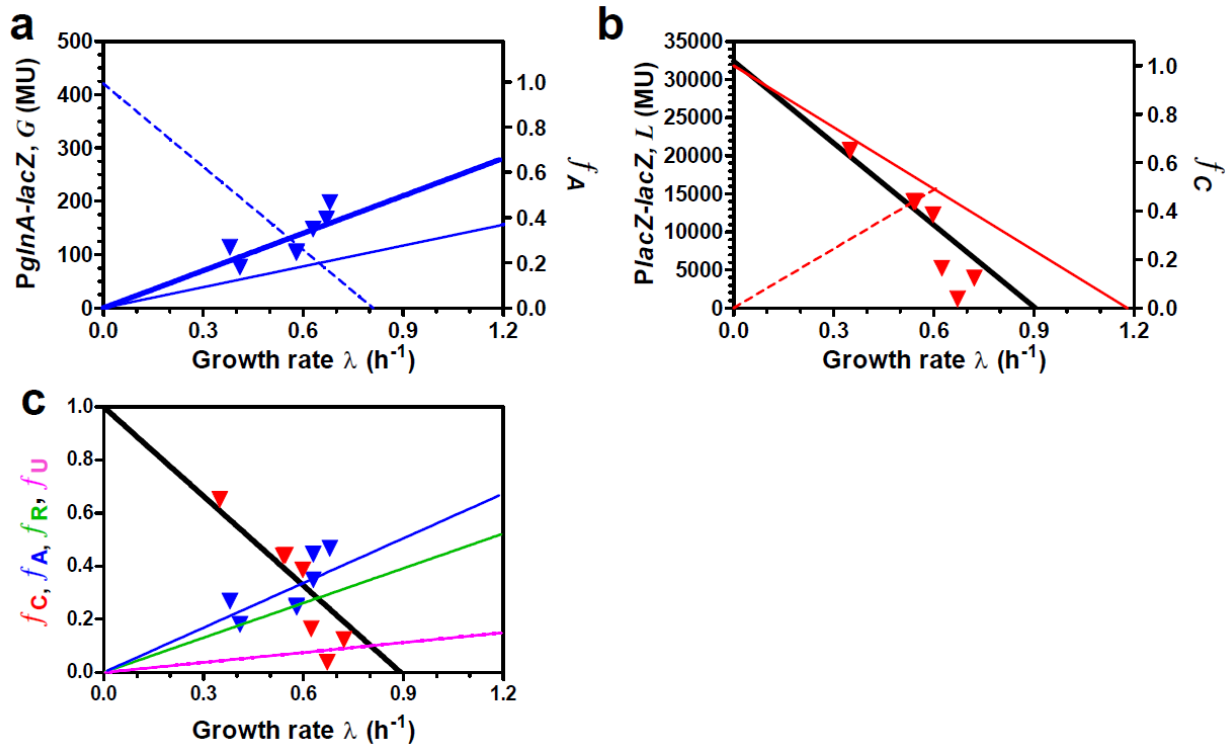


Figure S20: Response of the A-, C- sectors under C-limitation and fixed GDH titration. (a) NQ477 carrying *PglNA-lacZ* in the NQ34 background was grown in various carbon sources with GDH expression set by 40 ng/ml cTc (blue inverted triangles). *PglNA-lacZ* expression level is converted to the normalized fraction f_A (the right y-axis) using Eq. [S22] in Supplementary Note 3. The thick blue line is the best linear fit, with parameters listed in Table S15. For comparison, we show also *PglNA* expression under C-limitation in wild-type background (thin solid blue line, same as the solid blue line in Fig. 1d), and under A-limitation with glycerol as the sole carbon source (dashed blue line, same as the dashed blue line in Fig. 1d). (b) The red inverted triangles show the result of *PlacZ-lacZ* expression of NQ34, grown in various carbon sources with GDH expression set by 40 ng/ml cTc, with 1mM IPTG to induce *PlacZ*. *PlacZ-lacZ* expression level is converted to the normalized fraction f_C (the right y-axis) using Eq. [S22] in Supplementary Note 3. For comparison, we show also *PlacZ* expression under C-limitation (the C-line) in wild-type background (solid red line, same as the solid red line in Fig. 1a), and under A-limitation with glycerol as the sole carbon source (dashed red line, same as the dashed red line in Fig. 1a). The solid black line is the predicted response; see panel c. Note the shift in the x-intercept of the red and black C-lines, at two different degrees of A-limitation. (c) This plot summarizes how each proteome fraction (the normalized fractions f_s) depends on the growth rate for different carbon sources under a fixed degree of GDH expression (set by 40 ng/ml cTc) in NQ34 background. The data points (red and blue inverted triangles) are the same as those shown in panels a and b. The green and purple lines, which indicate the R- and X- fractions respectively, are the same as those in Figs. 2b and 2c. The predicted response of the C-sector, $f_C = 1 - \lambda / \tilde{\lambda}_C$ (the black line), is obtained as the difference between 1 and the sum of the colored lines (Eq. [3] of the main text.) The predicted value of $\tilde{\lambda}_C$ is given in Table S16.

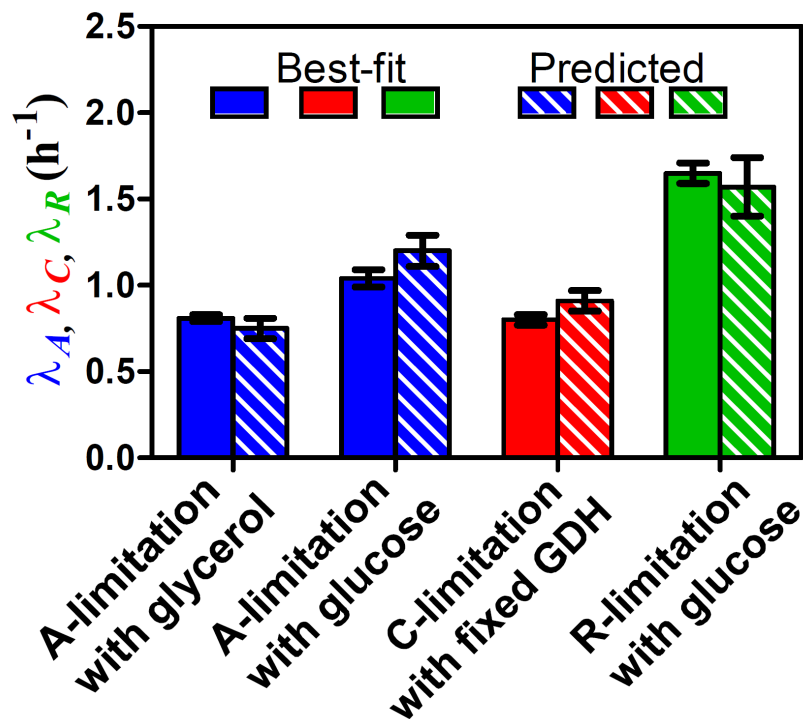


Figure S21: Predictions of the proteome partition model. The proteome partition model (Supp Note 1) predicts that the specific response to a mode of growth limitation is given by (i) the general response, that all sectors non-specific to the applied mode of growth limitation *decreases* linearly with the growth rate (Eqs. [S5]-[S8] in Supp Note 1), and (ii) the constraint that the sum of all sectors is 100% (Eq. [S1] or [S2]). In the main text, we used the responses of wild-type cells to C-limitation (Fig. 2b) to deduce the magnitude of the general response of the uncharacterized U-sector. We then used this result, $f_u(\lambda)$, together with the other general response characterized, $f_c(\lambda)$, $f_A(\lambda)$, and $f_R(\lambda)$ (see Supp Note 3), to deduce the specific responses to other modes of growth limitations. Each specific response, an inverse linear relation with the growth rate such as Eq. [1] and [2] of the main text, is characterized by an x-intercept value, e.g., λ_c for C-limited growth and λ_A for A-limited growth. The observed and predicted values are shown in this figure for the other 4 modes of growth limitation performed in this study (in addition to the one for wild-type cells on C-limited growth). For A-limited growth with glycerol and glucose as the carbon source (blue bars), the values of λ_A are obtained from the data in Fig. 1d and Fig. S19 respectively, and recorded in Table S15. For C-limited growth with fixed degree of GDH titration (red bar), the value of λ_c is obtained from the data in Fig. S20 and recorded in Table S5. For R-limited growth with glucose as the carbon source (green bar), the value of λ_R is obtained from the data in Fig. S15 and recorded in Table S14. All the predicted values are given in the last row of Table S16 as explained in the table caption and Supp Note 3.

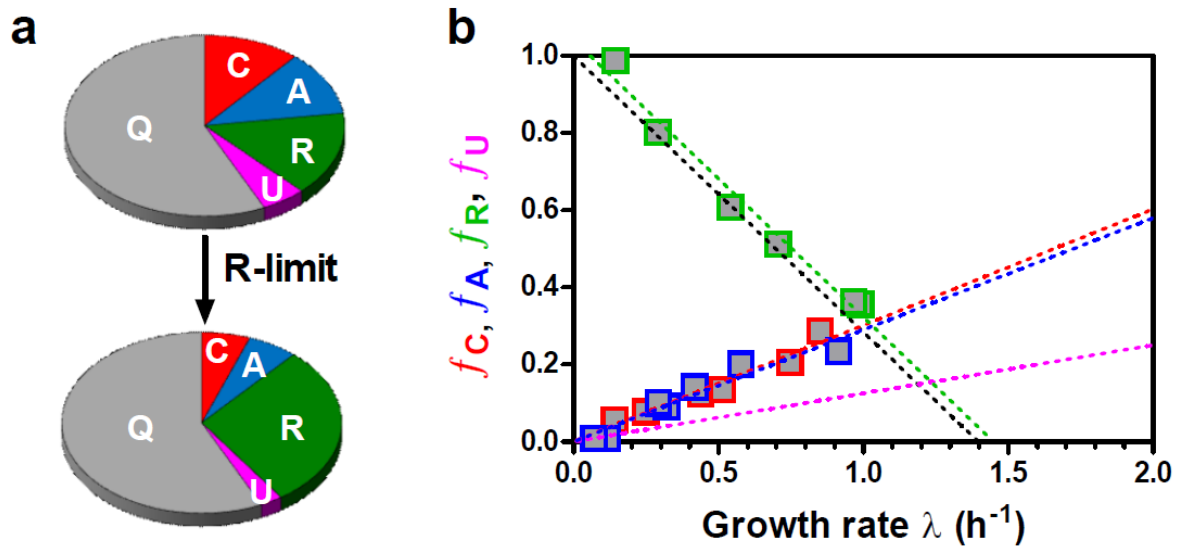


Figure S22: Responses of the proteome sectors under translational limitations. (a) The proteome partition model expects the R-sector to increase, and the C-, A- U- sectors to decrease, upon translational (or R-) limitation; see Supp Note 1. (b) The responses of the R-, C-, A- sector reporters in wild-type (NCM3722) background, grown in glucose with various Cm levels to inhibit translation. 1mM IPTG was used to induce *PlacZ* for the C-sector reporter (red squares); strain NQ158 harboring *PglnA-lacZ* was used as the A-sector reporter (blue squares); RNA/protein ratio was used as the R-sector reporter (green squares). All data were taken from Fig. S15, plotted as the normalized fractions (the right axis in each panel of Fig. S15). The green, red, and blue dotted lines indicate the best-fit lines to the data sets, with the parameters listed in Table S14. The dotted purple line is the expected U-sector from Figs. 2b and 2c. The dotted black line indicates the predicted response of the R-sector, $f_R = 1 - \lambda / \tilde{\lambda}_R$ according to Eq. [3] of the main text. The predicted value of $\tilde{\lambda}_R$ is given in Table S16.

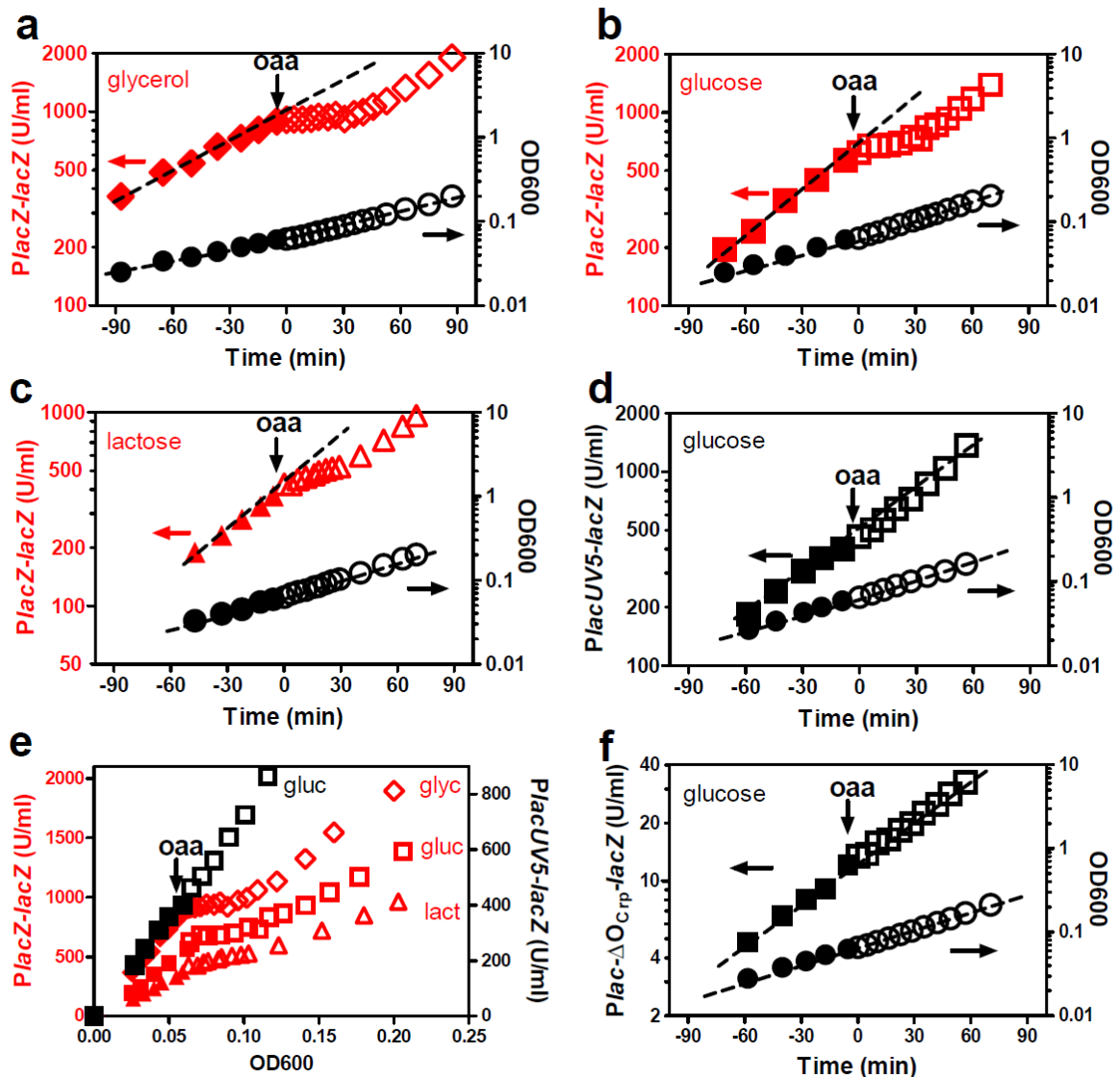


Figure S23: Transient repression of *PlacZ-lacZ* expression by oxaloacetate (oaa) addition. 20 mM oaa (final concentration) was added at time zero to *E. coli* strains grown exponentially in N⁺C⁻ medium with 20 mM NH₄Cl, and one of the following as the sole carbon source: 0.4% (v/v) glycerol, 0.4% (w/v) glucose, or 0.2% (w/v) lactose. 1mM IPTG was added to deactivate LacI when strain NCM3722 was grown. LacZ activity and OD₆₀₀ were monitored before (filled symbols) and after (open symbols) oaa addition. (a) The wild-type strain (NCM3722) grown first on glycerol; (b) NCM3722 grown first on glucose; (c) NCM3722 grown first on lactose. (d) Strain NQ1053 harboring *PlacUV5-lacZ* grown first on glucose. (e) Scatter plot of LacZ activity vs OD₆₀₀ for the data shown in panels a-d. The local slopes of these data were used to compute the average fold-repression shown in Fig. 3c; see Supp Methods for details. (f) Strain NQ367 carrying *Plac-ΔO_{C_{rip}}-lacZ* grown first on glucose. LacZ activity vs time is plotted on the left axis, as red symbols for NCM3722 in panels (a)-(c) and as black squares for NQ1053 (panel d) and NQ367 (panel f). The corresponding OD₆₀₀ vs time are shown as black circles on the right y-axis. The black dashed lines indicate exponential dependences to guide the eye. Horizontal arrows indicate corresponding y-axes.

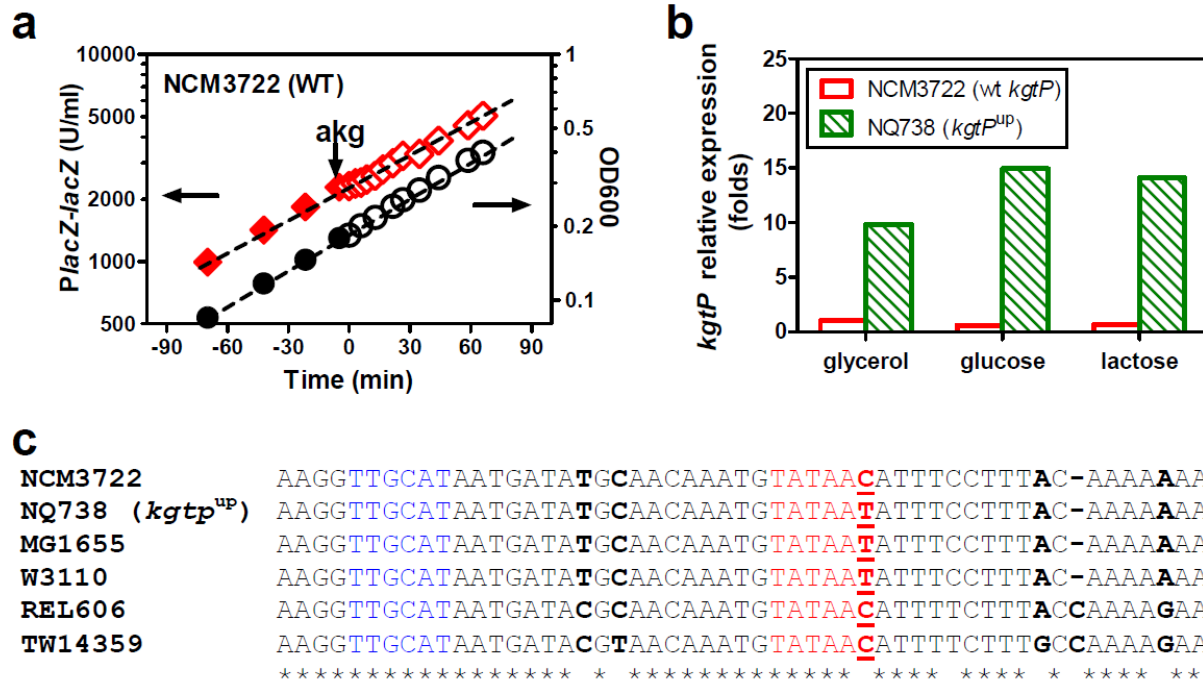


Figure S24: Lack of transient repression on *PlacZ-lacZ* expression in wild-type strain

NCM3722 by α -ketoglutarate (akg) addition due to low expression of the akg transporter

protein *KgtP*. (a) Wild-type strain NCM3722 was grown exponentially in N^C medium with 0.4% (v/v) glycerol, 20 mM NH₄Cl, and 1 mM IPTG. 20 mM akg (final concentration) was added at time zero. LacZ activity and OD₆₀₀ were monitored before (solid symbols) and after (open symbols) akg addition. LacZ activity vs time (diamonds) is plotted on the left y-axis and OD₆₀₀ vs time (circles) is plotted on the right y-axis. The black dashed lines indicate simple exponential dependences to guide the eye. Horizontal arrows indicate corresponding y-axes. In contrast to *oaa* (Fig. S23), the addition of akg did not increase the growth rate. In fact, NCM3722 cannot grow on akg as the sole carbon source; see also Table S17. (b) A spontaneous mutant of NCM3722, named NQ738, was selected by incubating cells on agar plates with akg as the sole carbon source (see Supp. Methods). Real-time PCR showed substantially increased *kgpP* expression in strain NQ738 compared to NCM3722; hence NQ738 was also named the *kgpP*^{up} strain. The mRNA level of *kgpP* of NCM3722 strain grown in glycerol was normalized to 1 and all other *kgpP* mRNA levels were determined relative to this value. (c) Alignment of *kgpP* gene promoter sequence in various *E. coli* strains. Only the DNA region that showed difference was listed. Mismatched nucleotides are shown in bold. The -35 and -10 motifs of each promoter are labeled in blue and red, respectively. MG1655, W3110, NCM3722 are all K-12 strains. REL606 is an *E. coli* B strain and TW14359 is a sub-strain of *E. coli* O157:H7. NQ738 is a NCM3722 spontaneous mutant selected in this study. Sequencing analyses of the *kgpP* regulatory region showed a single base substitution at position -6 (underlined), changing the -10 element of this σ^{70} -dependent promoter from TATAAC in NCM3722 to the consensus sequence TATAAT in NQ738. Interestingly, while both MG1655 and W3110 have the same consensus promoter TATAAT, NCM3722 shares its core promoter sequence with those of the B strain (REL606) and the virulent strain (O157:H7).

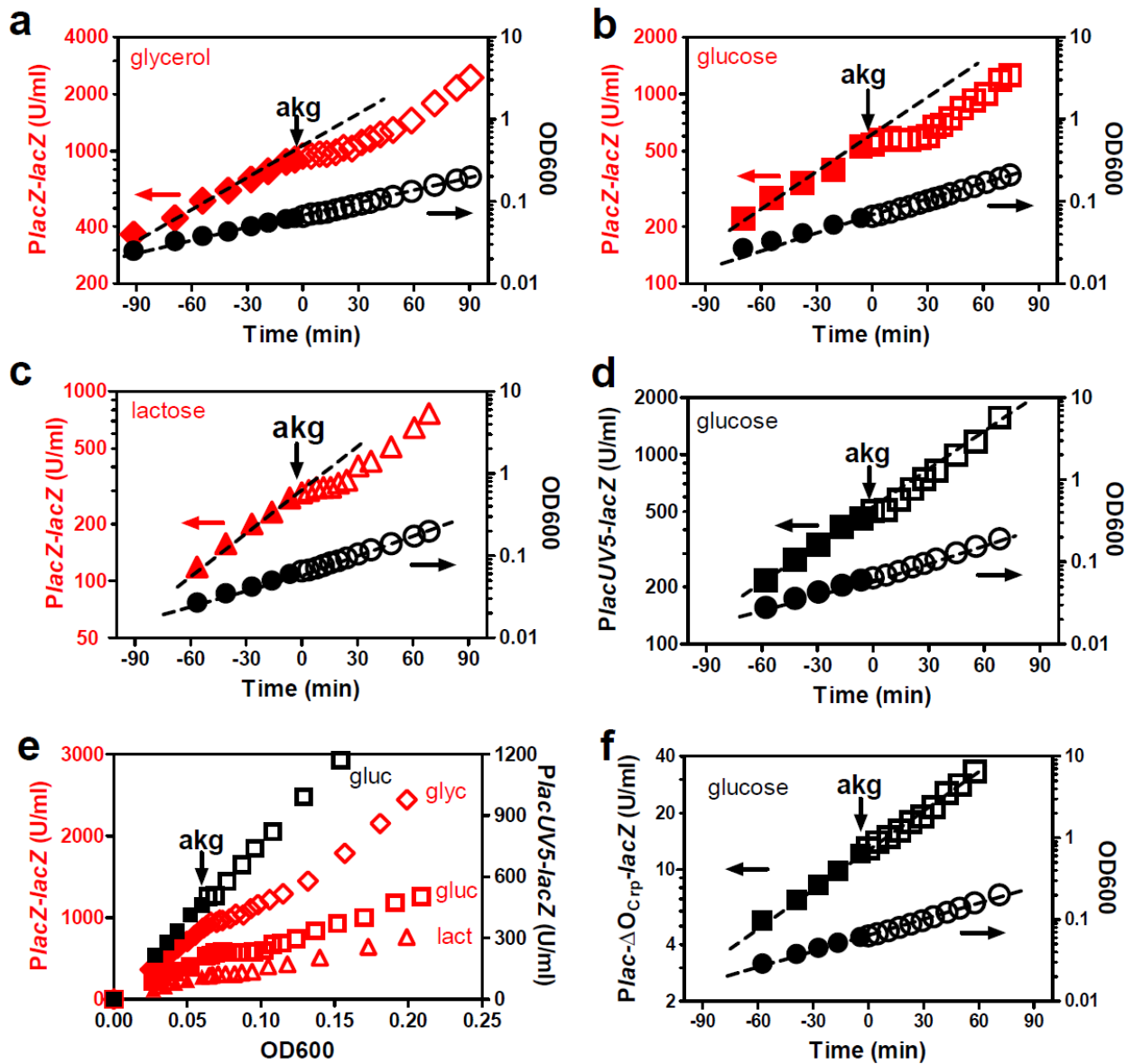


Figure S25: Transient repression of *PlacZ-lacZ* expression by *aqg* addition in *kgtP^{up}* strains. 20 mM *aqg* (final concentration) was added at time “zero” to *kgtP^{up}* strains NQ738 (see Fig. S24) and its two isogenic controls, NQ1078, harboring the *PlacUV5-lacZ*, and NQ739, harboring the *Plac-ΔO_{Crp}-lacZ*. These strains were grown exponentially in N⁺C⁻ medium with 20 mM NH₄Cl and one of the followings as the sole carbon source: 0.4% (v/v) glycerol, 0.4 (w/v) glucose, or 0.2% (w/v) lactose. 1mM IPTG was added to deactivate LacI when NQ738 was grown. LacZ activity and OD₆₀₀ were monitored before (solid symbols) and after (open symbols) *aqg* addition. (a) The *kgtP^{up}* strains NQ738 grown first on glycerol; (b) NQ738 grown first on glucose; (c) NQ738 grown first on lactose. (d) Strain NQ1078 harboring *PlacUV5-lacZ* in *kgtP^{up}* background grown first on glucose. (e) Scatter plot of LacZ activity vs OD₆₀₀ for the data shown in panels a-d. (f) Strain NQ739 carrying *Plac-ΔO_{Crp}-lacZ* in *kgtP^{up}* background grown first on glucose. LacZ activity vs time is plotted on the left y-axis, as red symbols for NQ738 in panels (a)-(c), and as black squares for NQ1078 (panel d) and NQ739 (panel f). The corresponding OD₆₀₀ vs time are shown as black circles on the right y-axis. The black dashed lines indicate

simple exponential dependences to guide the eye. Horizontal arrows indicate corresponding y-axes.

Note: The transient repression of *PlacZ* by *akg* was in fact reported long ago⁶⁵. However, this result was found not so reproducible by others (A. Danchin, personal communication) and this line of pursuit was terminated. In retrospect, different findings on the effectiveness of *akg* on transient repression may well have been due to the strain-to-strain difference in the *kgtP* promoters (Fig. S24c), which accidentally masked the very significant findings in Ref. 65.

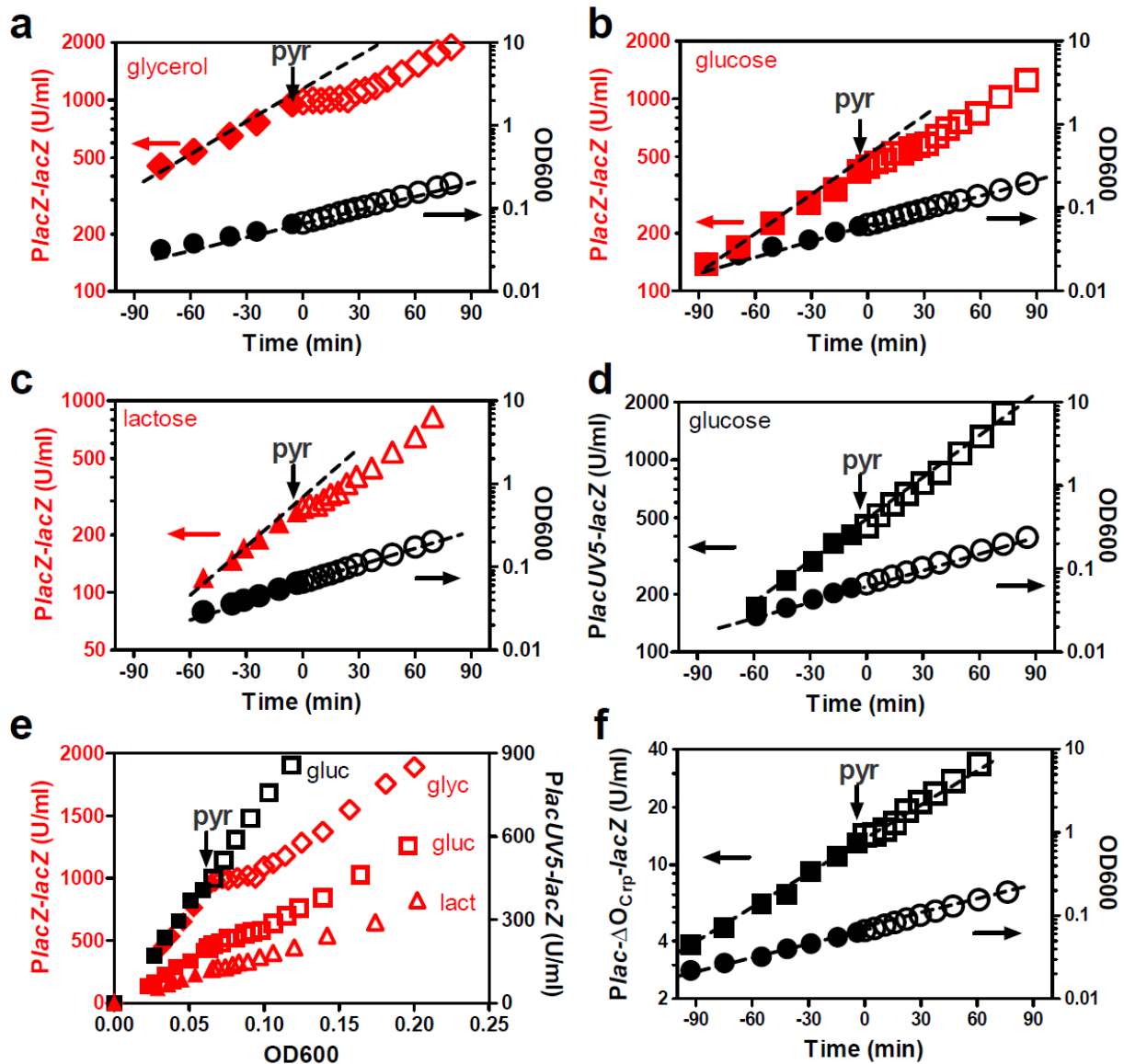


Figure S26: Transient repression of *PlacZ-lacZ* expression by pyruvate (pyr) addition.

20 mM pyr (final concentration) was added at time “zero” to *E. coli* strains grown exponentially in N^-C^- medium with 20 mM NH_4Cl , and one of the following as the sole carbon source: 0.4% (v/v) glycerol, 0.4% (w/v) glucose, or 0.2% (w/v) lactose. 1mM IPTG was added to deactivate LacI when NCM3722 was grown. LacZ activity and OD_{600} were monitored before (solid symbols) and after (open symbols) pyr addition. (a) The wild-type strain (NCM3722) grown first on glycerol; (b) NCM3722 grown first on glucose; (c) NCM3722 grown first on lactose. (d) Strain NQ1053 harboring *PlacUV5-lacZ* grown first on glucose. (e) Scatter plot of LacZ activity vs OD_{600} for the data shown in panels a-d. (f) Strain NQ367 carrying *Plac- $\Delta\text{O}_{\text{C}_{\text{rp}}}$ -lacZ* grown first on glucose. LacZ activity vs time is plotted on the left y-axis, as red symbols for NCM3722 in panel (a)-(c) and as black squares for NQ1053 (panel d) and NQ367 (panel f). The corresponding OD_{600} vs time are shown as black circles on the right y-axis. The black dashed lines indicate simple exponential dependences to guide the eye. Horizontal arrows indicate corresponding y-axes.

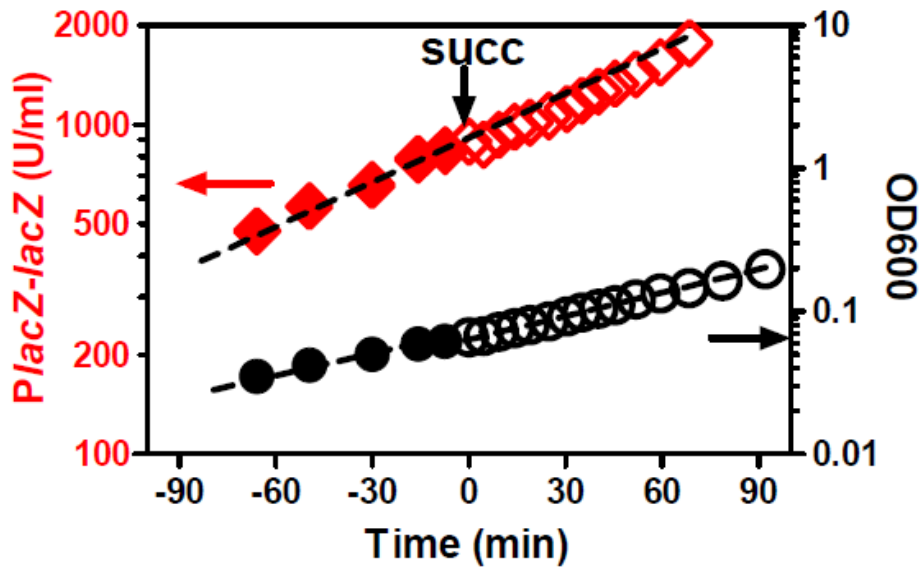


Figure S27: Transient repression on *PlacZ-lacZ* expression in wild-type strain NCM3722 by succinate (succ) addition. Wild-type strain NCM3722 was grown exponentially in N⁻C⁻ medium with 0.4% (v/v) glycerol, 20 mM NH₄Cl, 1 mM IPTG and 20 mM succ (final concentration) were added at time zero. *PlacZ-LacZ* expression and OD₆₀₀ were monitored before (solid symbols) and after (open symbols) succ addition. *LacZ* activity vs time (red diamonds) is plotted on the left y-axis and OD₆₀₀ vs time (black circles) is plotted on the right y-axis. The black dashed lines indicate a simple exponential dependence to guide the eye. Horizontal arrows indicate corresponding y-axes.

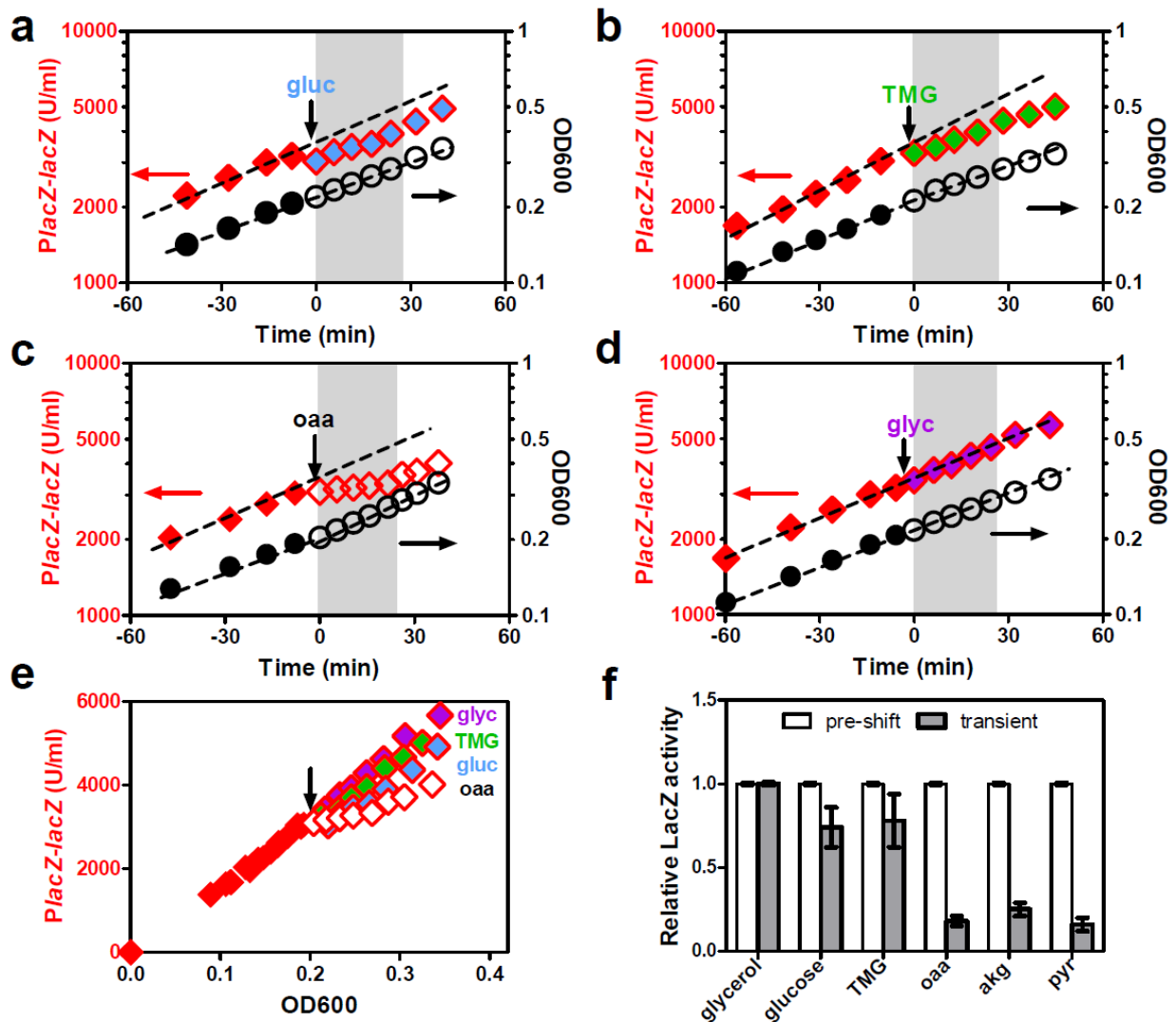


Figure S28: Comparing transient repression of *PlacZ-lacZ* by TMG (methyl- β -D-thiogalactoside), glucose, oaa, akg and pyr. Wild-type strain NCM3722 was grown exponentially in N⁻C⁻ medium with 0.4% (v/v) glycerol, 20 mM NH₄Cl, and 1 mM IPTG. 20 mM glucose, 20 mM TMG, 20 mM oaa or 20 mM glycerol (final concentration) was added at time zero. *PlacZ-LacZ* expression and OD_{600} were monitored before and after these chemicals addition. In panels (a)-(d), *LacZ* activity vs time (diamonds) is plotted on the left y-axis and OD_{600} vs time (circles) is plotted on the right y-axis. The dashed lines indicate simple exponential dependences to guide the eye. The transient period ~30 min after chemicals addition was shaded in grey. Horizontal arrows indicate corresponding y-axes. (a) glucose addition; (b) TMG addition; (c) oaa addition; (d) glycerol addition. Glycerol addition in panel d is used as a control. In panel b, it should be noted that TMG addition slowed down growth (comparing solid and open circles): steady state growth rate in glycerol is 0.63 ± 0.01 (1/hr) and in glycerol with TMG is 0.51 ± 0.01 (1/hr). (e) Scatter plot of *LacZ* activity vs OD_{600} for the data shown in panels (a) through (d). (f) Relative *LacZ* activities before and during the transient period in panels b-d were quantified as described in Supp. Method. The results of akg and pyr transient repression effect on *PlacZ-lacZ* of NCM3722 grown in glycerol shown in Fig. 3c is included here as a comparison.

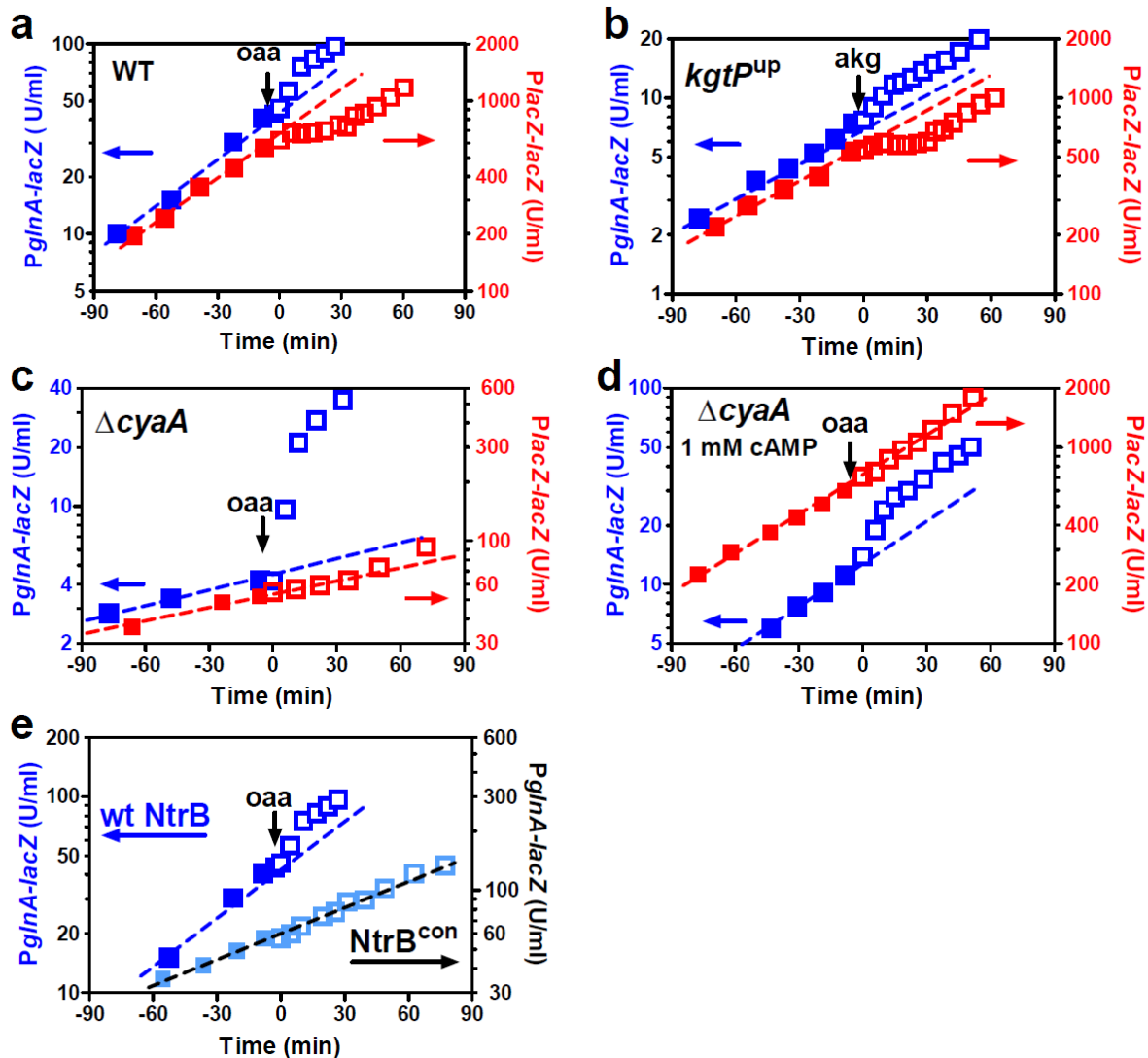


Figure S29: Transient activation of *PglNA-lacZ* expression by *akg* or *oaa* addition. Various *E. coli* strains were grown exponentially in N^{C} medium with 0.2% (w/v) glucose, 20 mM NH_4Cl and 1 mM cAMP (panel d only). 1 mM IPTG was supplied when native *PlacZlacZ* activity was studied. 20 mM *oaa* or *akg* (final concentration) was added at time zero. The dashed lines indicate simple exponential dependences to guide the eye. Horizontal arrows indicate corresponding y-axes. In panels (a)-(d), *PglNA-lacZ* activity (blue squares, left y-axis) and *PlacZ-lacZ* activity (red squares, right y-axis) were monitored before and after *oaa* and *akg* addition respectively: (a) *oaa* addition to wild-type NCM3722 cells (red) and to NQ158 cells harboring *PglNA-lacZ* in wild-type background (blue); (b) *akg* addition to the *kgtP^{up}* strain NQ738 (red) and to NQ747 cells harboring *PglNA-lacZ* in *kgtP^{up}* background (blue); (c) *oaa* addition to the ΔcyaA strain NQ93 (red) and to NQ780 cells harboring *PglNA-lacZ* in ΔcyaA background (blue). The two ΔcyaA strains are incapable of synthesizing cAMP. (d) Same as panel c, except with the addition of 1 mM cAMP to activate CRP-cAMP. (e) Comparison between the transient response of *PglNA-lacZ* to *oaa* addition in wild-type background (NQ158, blue squares, left y-axis) and in a *NtrB^{con}* background (NQ315, light blue squares, right y-axis) in which the Ntr response is constitutively on.

Note: *NtrB^{con}* is encoded by *glnL302* which was originally obtained from an isolate when a GOGAT-mutant was selected for fast growth in medium with both arginine and proline as N-sources^{11,12}. *glnL302* encodes the mutant protein *NtrB^{A219T}* which has a reduced phosphatase activity on *NtrC~P*⁶⁶, resulting in a high level of GS expression even in NH_4^+ medium.

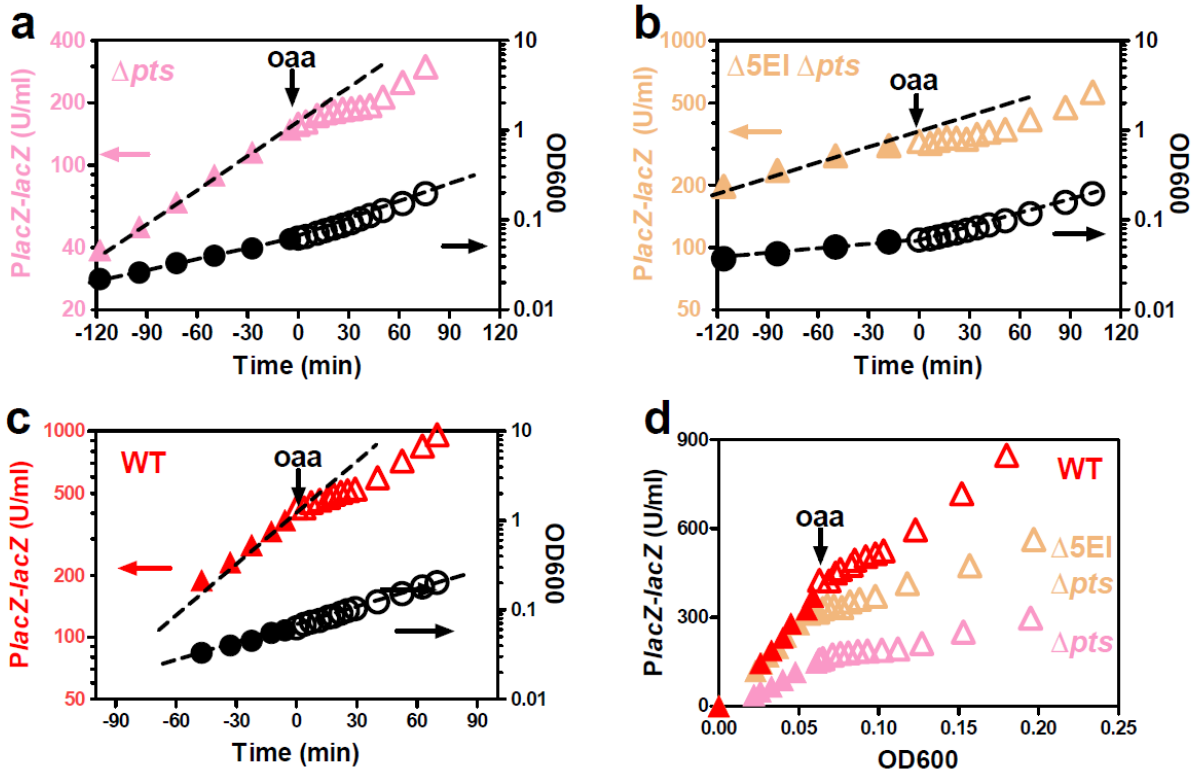


Figure S30: Transient repression of *PlacZ-lacZ* expression by *oaa* addition in PTS mutants.

The PTS mutant strains NQ721 (Δpts) and NQ506 ($\Delta 5EI \Delta pts$) were grown exponentially in N⁺C⁻ medium with 0.2% (w/v) lactose, 20 mM NH₄Cl and 1 mM IPTG. 20 mM *oaa* (final concentration) was added at time zero. LacZ activity and OD₆₀₀ were monitored before and after *oaa* addition (filled and open symbols, respectively). Horizontal arrows indicate corresponding y-axes. In panels (a)–(c), LacZ activity vs time (triangles) is plotted on the left y-axis and OD₆₀₀ vs time (circles) is plotted on the right y-axis. The dashed lines indicate simple exponential dependences to guide the eye. (a) NQ721 grown first in lactose; (b) NQ506 grown first in lactose; (c) Transient effect of *oaa* on *Plac-lacZ* expression in NCM3722, shown in Fig. S23c, is replotted here for comparison. (d) Scatter plot of LacZ activity vs OD₆₀₀ for the data shown in panels (a) through (c): The local slopes of these data were used to compute the average fold-repression shown in Fig. 4b; see Supp Methods for details.

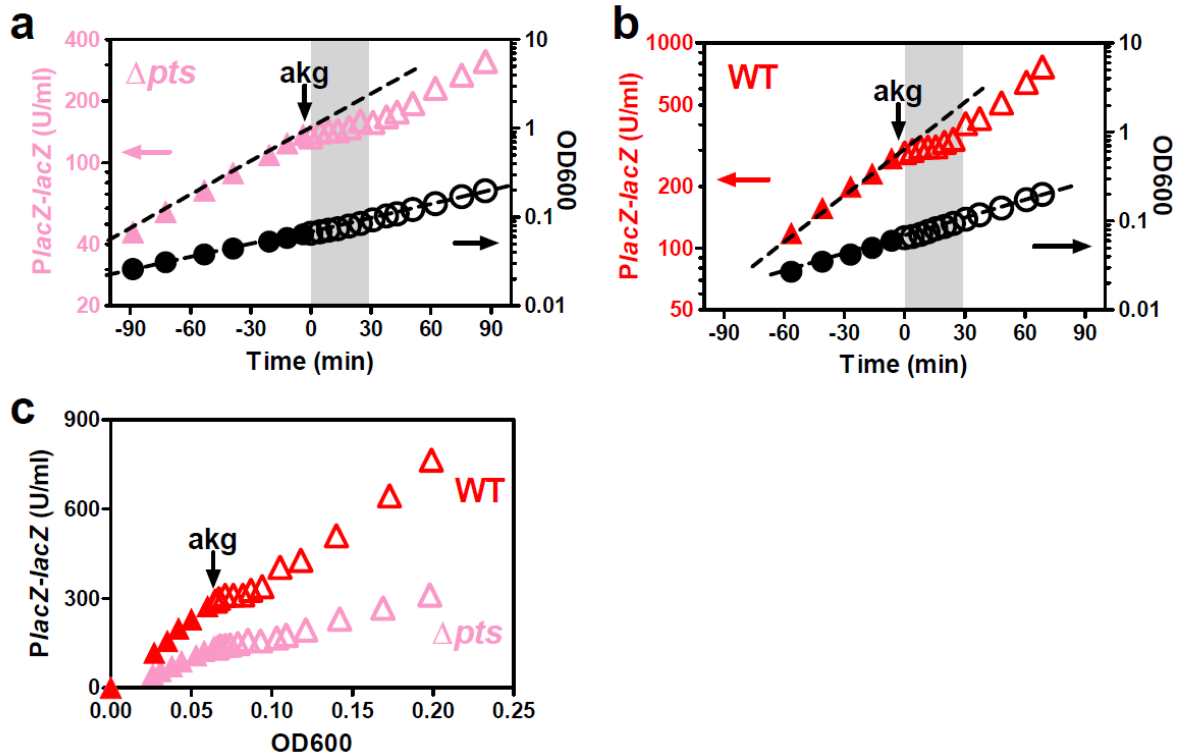


Figure S31: Transient repression of *PlacZ-lacZ* expression by *akg* addition in PTS mutant.

The PTS mutant strain NQ741 (Δpts *kgtP^{up}*) was grown exponentially in N^+C^- medium with 0.2% (w/v) lactose, 20 mM NH_4Cl and 1 mM IPTG. 20 mM *akg* (final concentration) was added at time zero. LacZ activity and OD_{600} were monitored before and after *akg* addition (filled and open symbols, respectively). Horizontal arrows indicate corresponding y-axes. In panels (a-b), LacZ activity vs time (triangles) is plotted on the left y-axis and OD_{600} vs time (circles) is plotted on the right y-axis. The dashed lines indicate simple exponential dependences to guide the eye. (a) NQ741 grown first in lactose; (b) Transient effect of *akg* on *Plac-lacZ* expression in NQ738 (*pts* wild-type), shown in Fig. S25c, is replotted here for comparison. (c) Scatter plot of LacZ activity vs OD_{600} for the data shown in panels (a) through (b): The local slopes of these data were used to compute the average fold-repression shown in Fig. 4b; see Supp Methods for details.

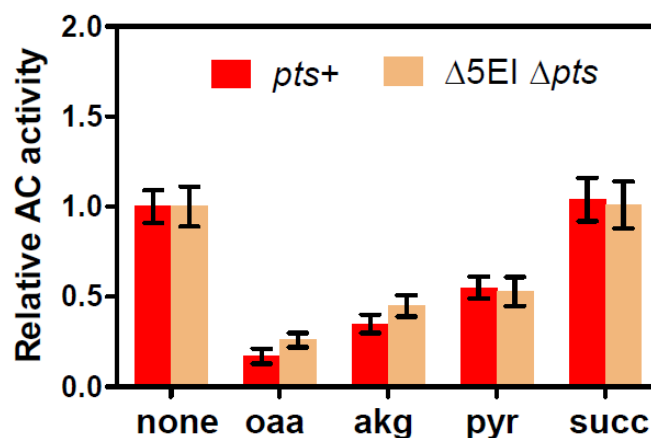


Figure S32: α -ketoacid repression effect on AC activity using a modified rapid-quench assay. *In vitro* AC activities in strains NQ385 (*pts*⁺) and NQ977 ($\Delta 5EI \Delta pts$) were assayed also in a condition modified from that used in Ref. 26 and Supp. Method for obtaining data in Fig. 4d. When the growth of *E. coli* strains reached mid-exponential phase, 4% (v/v) toluene was added to the growth medium and the cells were permeabilized by being shaken at 70 rpm at RT for 10 min. Comparing to the method of Ref. 26, using higher concentration of toluene to permeabilize cells before the cell collection stage gives a more thorough and rapid quench, thereby reducing the cells' exposure to what may be effectively a starvation condition during the sample collection stage. But the harsher treatment may damage proteins and the results are meant to provide an alternative perspective. Toluene permeabilized cells were then collected, washed and concentrated, and the repression effect of 0 or 10 mM various metabolites on AC activities were evaluated as described in Supp. Method. Relative AC activities in both strains exhibited similar responses as the results shown in Fig. 4d, either with and without the PTS proteins. Thus, the repression effect of α -ketoacids on AC activity is robust even in this harsh assay condition.

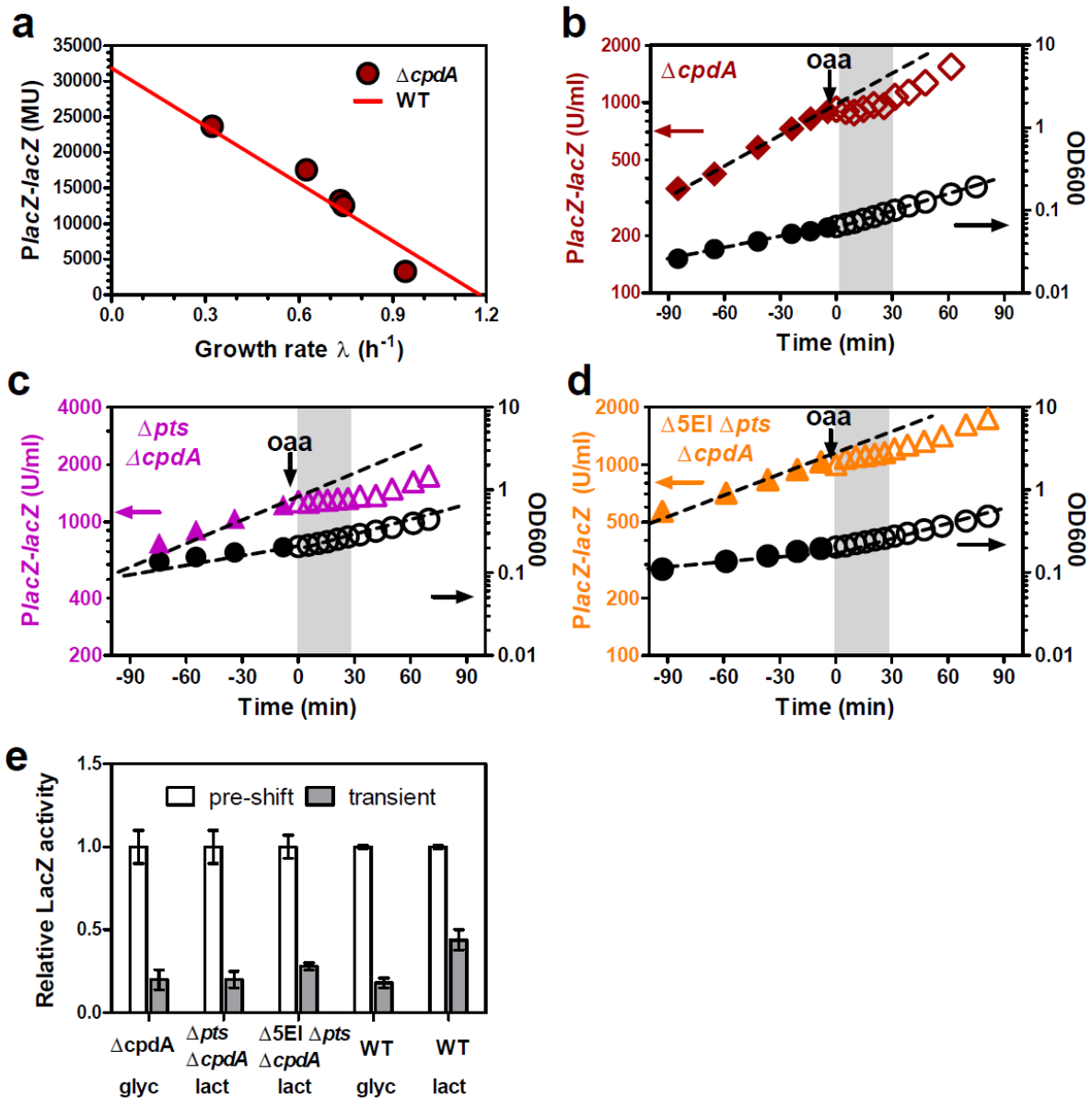


Figure S33: C-line and transient repression in $\Delta cpdA$ strains. The cAMP phosphodiesterase encoded by *cpdA* is known to affect the cAMP-dependent response of the *Plac* promoter⁷. In this figure, we establish that despite this dependence, the existence of the C-line for *PlacZ* and the occurrence of transient repression of *PlacZ* activity by oaa addition are not affected. The results indicate that *cpdA* is not an essential determinant of catabolite repression nor transient repression. (a) $\Delta cpdA$ strain NQ385 was grown in minimal medium with various carbon sources and supplied with 1 mM IPTG to deactivate *lacI*. *Plac-lacZ* activity obtained for various carbon sources was plotted against its corresponding growth rate (circles). [In the order of decreasing growth rates, the carbon sources used were: 10 mM glucose-6P + 10 mM gluconate, 0.4% (w/v) glucose, 0.2% (w/v) lactose, 0.4% (v/v) glycerol, and 60 mM acetate.] These data points fall on the C-line of *Plac-lacZ* obtained in wild-type NCM3722 strain (Fig 1a), which is drawn as the red line here. Comparing to the growth and the *PlacZ* expression data in Table S1, we note that

for the same carbon source, the $\Delta cpdA$ strain exhibits an increased *PlacZ* expression and reduced growth rate. However, these changes are coordinated so that the results remain on the C-line. This fulfills the expectation derived in Supp Note 5 that the occurrence of the C-line does not depend on the details of the cAMP-dependent activation of the *PlacZ* promoter. (b) $\Delta cpdA$ strain NQ385 was grown exponentially in N^+C^- medium with 0.4% (v/v) glycerol, 20 mM NH_4Cl and 1 mM IPTG. 20 mM oaa (final concentration) was added at time zero. LacZ activity and OD_{600} were monitored before and after oaa addition (filled and open symbols, respectively). LacZ activity vs time (diamonds) is plotted on the left y-axis and OD_{600} vs time (circles) is plotted on the right y-axis. The dashed lines indicate simple exponential dependences to guide the eye. Transient repression period ~ 30 min was shaded in grey. (c) Same as panel b, but for $\Delta cpdA \Delta pts$ strain (NQ976) grown first in 0.2% (w/v) lactose (triangles). (d) Same as panel b, but for $\Delta cpdA \Delta 5EI \Delta pts$ strain NQ977 grown first in 0.2% (w/v) lactose (triangles). (e) Relative LacZ activities before and during the transient repression period shown in panels b-d were quantified as described in Supp. Method. The results of wild-type strain shown in Fig. 3c is included here as a comparison. MU: Miller Unit.

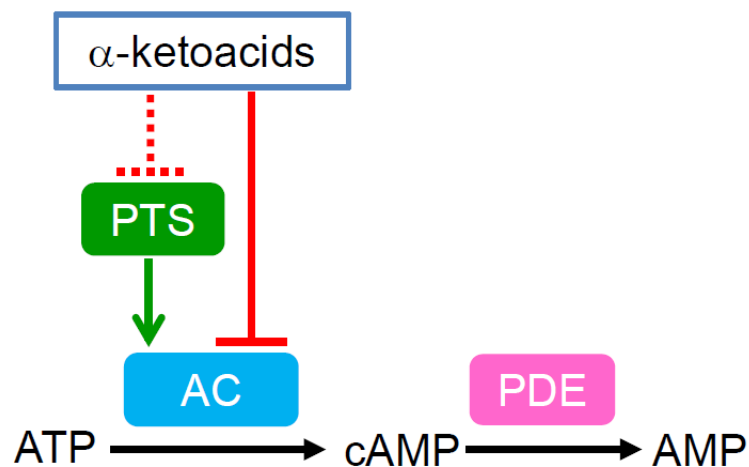


Figure S34: Possible elements affecting cAMP signalling. cAMP is synthesized by Adenylate Cyclase (AC) and is degraded by cAMP phosphodiesterase (PDE) (black arrows). PDE is not primary to cAMP-dependent signaling of CCR (Fig. S32). AC activity is known to be activated by phosphotransferase system (PTS)⁴¹ (green arrow). One α -ketoacid (akg) was reported to interact directly with EI of PTS to inhibit AC activity⁴⁴ (dotted red line). Additionally, the repression of AC activity by several α -ketoacids in PTS-independent manner is proposed in this study (solid red line).

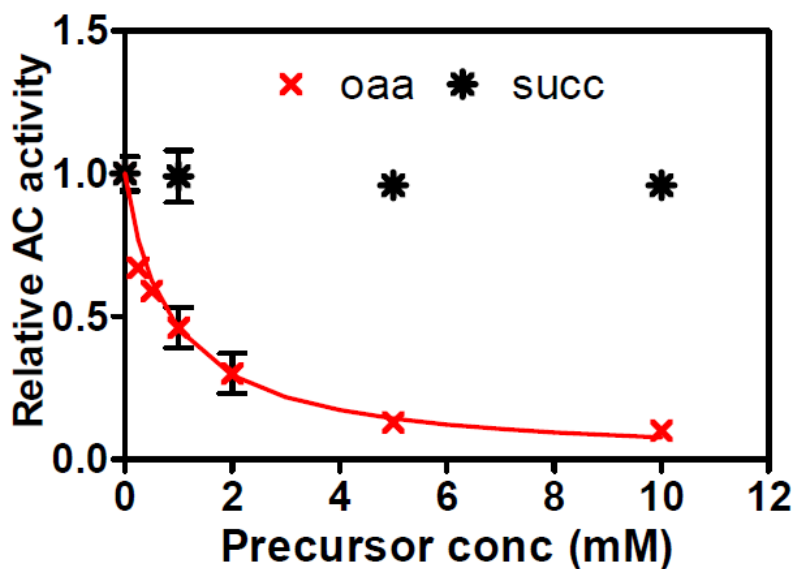


Figure S35: Inhibition kinetics of oaa on AC activities. *in vitro* AC activities of permeabilized NQ385 cells were assayed with 0-10 mM of oaa or succ. See Supp. Method for detailed assay method. The line shows the best-fit to simple inhibition kinetics $1/(1+[oaa]/K_I)$, with the half-inhibition concentration $K_I = 0.84 \pm 0.04$ mM.

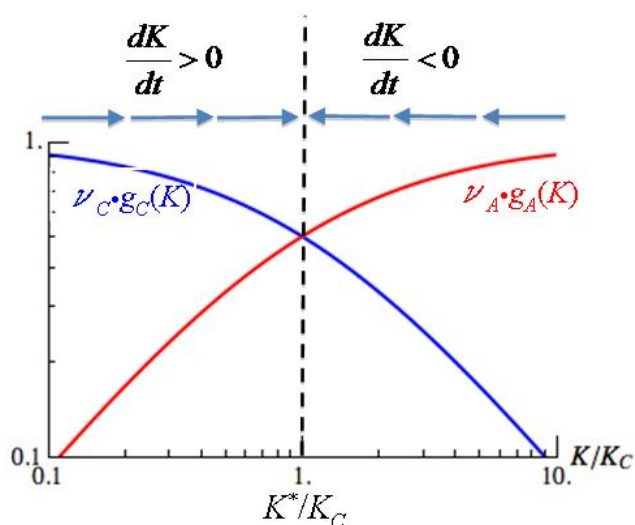


Figure S36: Stability of the precursor feedback model. The dynamics of the precursor feedback model is governed by Eq. [S31], which can be rewritten in the form

$$\frac{dK}{dt} \propto \nu_C g_C(K) - \nu_A g_A(K)$$

with the help of Eqs. [S27], [S28], [S36], [S37]. The first term in the above equation is shown in blue and the second term in red, using the Hill functions defined in Eqs. [S38] and [S39], respectively. For simplicity, we used $K_C = K_A$ and $h_C = h_A = 1$ for illustration. The intersection of the blue and red curves gives the steady-state value K^* (dashed black line). This is a globally stable solution since for $K < K^*$, $\nu_C g_C(K) > \nu_A g_A(K)$ and $dK/dt > 0$, while for $K > K^*$, $dK/dt < 0$, as indicated by the arrows. For different degrees of C- and A- limitations, represented by different values of ν_C and ν_A , the blue and red curves would slide up and down, resulting in different values of the intersection point (K^*). However, the forms of the blue and red curves guarantee that there is always an intersection point and it is always the global stable solution of this feedback system. This result is independent of the detailed shapes of the regulation functions $g_C(K)$ and $g_A(K)$, and particularly independent of the parameters of these regulation functions.

Supplementary References

- 1 Lyons, E., Freeling, M., Kustu, S. & Inwood, W. Using genomic sequencing for classical genetics in *E. coli* K12. *PLoS One* **6**, e16717 (2011).
- 2 Soupene, E. *et al.* Physiological studies of *Escherichia coli* strain MG1655: growth defects and apparent cross-regulation of gene expression. *J Bacteriol* **185**, 5611-5626 (2003).
- 3 Datsenko, K. A. & Wanner, B. L. One-step inactivation of chromosomal genes in *Escherichia coli* K-12 using PCR products. *Proc Natl Acad Sci U S A* **97**, 6640-6645 (2000).
- 4 Cherepanov, P. P. & Wackernagel, W. Gene disruption in *Escherichia coli*: TcR and KmR cassettes with the option of Flp-catalyzed excision of the antibiotic-resistance determinant. *Gene* **158**, 9-14 (1995).
- 5 Barabote, R. D. & Saier, M. H., Jr. Comparative genomic analyses of the bacterial phosphotransferase system. *Microbiol Mol Biol Rev* **69**, 608-634 (2005).
- 6 Baba, T. *et al.* Construction of *Escherichia coli* K-12 in-frame, single-gene knockout mutants: the Keio collection. *Mol Syst Biol* **2**, 2006 0008 (2006).
- 7 Kuhlman, T., Zhang, Z., Saier, M. H., Jr. & Hwa, T. Combinatorial transcriptional control of the lactose operon of *Escherichia coli*. *Proc Natl Acad Sci U S A* **104**, 6043-6048 (2007).
- 8 Zhang, Z. & Saier, M. H., Jr. A mechanism of transposon-mediated directed mutation. *Mol Microbiol* **74**, 29-43 (2009).
- 9 Silverstone, A. E., Arditti, R. R. & Magasanik, B. Catabolite-insensitive revertants of lac promoter mutants. *Proc Natl Acad Sci U S A* **66**, 773-779 (1970).
- 10 Klumpp, S., Zhang, Z. & Hwa, T. Growth rate-dependent global effects on gene expression in bacteria. *Cell* **139**, 1366-1375 (2009).
- 11 Chen, Y. M., Backman, K. & Magasanik, B. Characterization of a gene, *glnL*, the product of which is involved in the regulation of nitrogen utilization in *Escherichia coli*. *J Bacteriol* **150**, 214-220 (1982).
- 12 Pahel, G., Zelenetz, A. D. & Tyler, B. M. *gltB* gene and regulation of nitrogen metabolism by glutamine synthetase in *Escherichia coli*. *J Bacteriol* **133**, 139-148 (1978).
- 13 Kim, M. *et al.* Need-based activation of ammonium uptake in *Escherichia coli*. *Mol Syst Biol* **8**, 616 (2012).
- 14 de Lorenzo, V., Herrero, M., Metzke, M. & Timmis, K. N. An upstream XylR- and IHF-induced nucleoprotein complex regulates the sigma 54-dependent Pu promoter of TOL plasmid. *Embo J* **10**, 1159-1167 (1991).
- 15 Lutz, R. & Bujard, H. Independent and tight regulation of transcriptional units in *Escherichia coli* via the LacR/O, the TetR/O and AraC/I1-I2 regulatory elements. *Nucleic Acids Res* **25**, 1203-1210 (1997).
- 16 Csonka, L. N., Ikeda, T. P., Fletcher, S. A. & Kustu, S. The accumulation of glutamate is necessary for optimal growth of *Salmonella typhimurium* in media of high osmolality but not induction of the proU operon. *J Bacteriol* **176**, 6324-6333 (1994).
- 17 Scott, M., Gunderson, C. W., Mateescu, E. M., Zhang, Z. & Hwa, T. Interdependence of cell growth and gene expression: origins and consequences. *Science* **330**, 1099-1102 (2010).
- 18 Miller, J. H. *Experiments in Molecular Genetics*. (Cold Spring Harbor Laboratory Press, 1972).
- 19 Benthin, S., Nielsen, J. & Jørgensen, V. A simple and reliable method for the determination of cellular RNA content. *Biotechnology Techniques* **5**, 39-41, doi:10.1007/BF00152753 (1991).

- 20 Herbert, D., Phipps, P. J. & Strange, R. E. in *Methods in Microbiology* (eds J.R. Norris & D.W. Ribbons) (Academic Press, 1971).
- 21 Epstein, W., Rothman-Denes, L. B. & Hesse, J. Adenosine 3':5'-cyclic monophosphate as mediator of catabolite repression in *Escherichia coli*. *Proceedings of the National Academy of Sciences of the United States of America* **72**, 2300-2304 (1975).
- 22 Lazarowski, E. R. *et al.* Nucleotide release provides a mechanism for airway surface liquid homeostasis. *J Biol Chem* **279**, 36855-36864 (2004).
- 23 Haink, G. & Deussen, A. Liquid chromatography method for the analysis of adenosine compounds. *J Chromatogr B Analyt Technol Biomed Life Sci* **784**, 189-193, doi:S1570023202007523 [pii] (2003).
- 24 Yan, D. Protection of the glutamate pool concentration in enteric bacteria. *Proc Natl Acad Sci U S A* **104**, 9475-9480 (2007).
- 25 Yan, D., Lenz, P. & Hwa, T. Overcoming fluctuation and leakage problems in the quantification of intracellular 2-oxoglutarate levels in *Escherichia coli*. *Appl Environ Microbiol* **77**, 6763-6771 (2011).
- 26 Harwood, J. P. & Peterkofsky, A. Glucose-sensitive adenylate cyclase in toluene-treated cells of *Escherichia coli* B. *J Biol Chem* **250**, 4656-4662 (1975).
- 27 Gosset, G., Zhang, Z., Nayyar, S., Cuevas, W. A. & Saier, M. H., Jr. Transcriptome analysis of Crp-dependent catabolite control of gene expression in *Escherichia coli*. *J Bacteriol* **186**, 3516-3524 (2004).
- 28 Lemuth, K. *et al.* Global transcription and metabolic flux analysis of *Escherichia coli* in glucose-limited fed-batch cultivations. *Appl Environ Microbiol* **74**, 7002-7015 (2008).
- 29 Pedersen, S., Bloch, P. L., Reeh, S. & Neidhardt, F. C. Patterns of protein synthesis in *E. coli*: a catalog of the amount of 140 individual proteins at different growth rates. *Cell* **14**, 179-190 (1978).
- 30 Shimada, T., Fujita, N., Yamamoto, K. & Ishihama, A. Novel roles of cAMP receptor protein (CRP) in regulation of transport and metabolism of carbon sources. *PLoS One* **6**, e20081 (2011).
- 31 Valgepea, K. *et al.* Systems biology approach reveals that overflow metabolism of acetate in *Escherichia coli* is triggered by carbon catabolite repression of acetyl-CoA synthetase. *BMC Syst Biol* **4**, 166 (2010).
- 32 Barker, M. M., Gaal, T., Josaitis, C. A. & Gourse, R. L. Mechanism of regulation of transcription initiation by ppGpp. I. Effects of ppGpp on transcription initiation in vivo and in vitro. *J Mol Biol* **305**, 673-688 (2001).
- 33 Maaloe, O. in *Biological regulation and development*. Vol. 1979 (Plenum, 1979).
- 34 Dreisigmeyer, D. W., Stajic, J., Nemenman, I., Hlavacek, W. S. & Wall, M. E. Determinants of bistability in induction of the *Escherichia coli* lac operon. *IET Syst Biol* **2**, 293-303 (2008).
- 35 Martinez-Bilbao, M., Holdsworth, R. E., Edwards, L. A. & Huber, R. E. A highly reactive beta-galactosidase (*Escherichia coli*) resulting from a substitution of an aspartic acid for Gly-794. *J Biol Chem* **266**, 4979-4986 (1991).
- 36 Neidhardt, F. C., Curtiss, R., Ingraham, J. L., Lin, E. C. C., Low, K. B., Magasanik, B., Riley, M., Schaechter, M., and Umberger, H. E., eds. *Escherichia coli and Salmonella: Cellular and Molecular Biology*. (American Society for Microbiology (ASM), 1996).
- 37 Yuan, J. *et al.* Metabolomics-driven quantitative analysis of ammonia assimilation in *E. coli*. *Mol Syst Biol* **5**, 302 (2009).

- 38 Paul, B. J., Ross, W., Gaal, T. & Gourse, R. L. rRNA transcription in *Escherichia coli*. *Annu Rev Genet* **38**, 749-770 (2004).
- 39 Bintu, L. *et al.* Transcriptional regulation by the numbers: models. *Curr Opin Genet Dev* **15**, 116-124 (2005).
- 40 Bintu, L. *et al.* Transcriptional regulation by the numbers: applications. *Curr Opin Genet Dev* **15**, 125-135 (2005).
- 41 Deutscher, J., Francke, C. & Postma, P. W. How phosphotransferase system-related protein phosphorylation regulates carbohydrate metabolism in bacteria. *Microbiol Mol Biol Rev* **70**, 939-1031 (2006).
- 42 Bettenbrock, K. *et al.* Correlation between growth rates, EIICrr phosphorylation, and intracellular cyclic AMP levels in *Escherichia coli* K-12. *J Bacteriol* **189**, 6891-6900, doi:10.1128/JB.00819-07 (2007).
- 43 Hogema, B. M. *et al.* Inducer exclusion in *Escherichia coli* by non-PTS substrates: the role of the PEP to pyruvate ratio in determining the phosphorylation state of enzyme IIAGlc. *Mol Microbiol* **30**, 487-498 (1998).
- 44 Doucette, C. D., Schwab, D. J., Wingreen, N. S. & Rabinowitz, J. D. alpha-Ketoglutarate coordinates carbon and nitrogen utilization via enzyme I inhibition. *Nat Chem Biol* **7**, 894-901 (2011).
- 45 Velazquez, F., Fernandez, S. & de Lorenzo, V. The upstream-activating sequences of the sigma54 promoter Pu of *Pseudomonas putida* filter transcription readthrough from upstream genes. *J Biol Chem* **281**, 11940-11948 (2006).
- 46 Lin, E. C. Glycerol dissimilation and its regulation in bacteria. *Annu Rev Microbiol* **30**, 535-578 (1976).
- 47 Weissenborn, D. L., Wittekindt, N. & Larson, T. J. Structure and regulation of the glpFK operon encoding glycerol diffusion facilitator and glycerol kinase of *Escherichia coli* K-12. *J Biol Chem* **267**, 6122-6131 (1992).
- 48 Mandelstam, J. The repression of constitutive beta-galactosidase in *Escherichia coli* by glucose and other carbon sources. *Biochem J* **82**, 489-493 (1962).
- 49 Wanner, B. L., Kodaira, R. & Neidhardt, F. C. Regulation of lac operon expression: reappraisal of the theory of catabolite repression. *J Bacteriol* **136**, 947-954 (1978).
- 50 Kuo, J. T., Chang, Y. J. & Tseng, C. P. Growth rate regulation of lac operon expression in *Escherichia coli* is cyclic AMP dependent. *FEBS Lett* **553**, 397-402 (2003).
- 51 Müller-Hill, B. *The lac Operon : a short history of a genetic paradigm.*, (Walter de Gruyter, 1996).
- 52 Podolny, V., Lin, E. C. & Hochschild, A. A cyclic AMP receptor protein mutant that constitutively activates an *Escherichia coli* promoter disrupted by an IS5 insertion. *J Bacteriol* **181**, 7457-7463 (1999).
- 53 Bartkus, J. M. & Mortlock, R. P. Isolation of a mutation resulting in constitutive synthesis of L-fucose catabolic enzymes. *J Bacteriol* **165**, 710-714 (1986).
- 54 Chen, Y. M., Lu, Z. & Lin, E. C. Constitutive activation of the fucAO operon and silencing of the divergently transcribed fucPIK operon by an IS5 element in *Escherichia coli* mutants selected for growth on L-1,2-propanediol. *J Bacteriol* **171**, 6097-6105 (1989).
- 55 Zhang, Z., Yen, M. R. & Saier, M. H., Jr. Precise excision of IS5 from the intergenic region between the fucPIK and the fucAO operons and mutational control of fucPIK operon expression in *Escherichia coli*. *J Bacteriol* **192**, 2013-2019 (2010).

- 56 Reitzer, L. Nitrogen assimilation and global regulation in *Escherichia coli*. *Annu Rev Microbiol* **57**, 155-176 (2003).
- 57 Yuan, J., Fowler, W. U., Kimball, E., Lu, W. & Rabinowitz, J. D. Kinetic flux profiling of nitrogen assimilation in *Escherichia coli*. *Nat Chem Biol* **2**, 529-530 (2006).
- 58 Meek, T. D. & Villafranca, J. J. Kinetic mechanism of *Escherichia coli* glutamine synthetase. *Biochemistry* **19**, 5513-5519 (1980).
- 59 Alibhai, M. & Villafranca, J. J. Kinetic and mutagenic studies of the role of the active site residues Asp-50 and Glu-327 of *Escherichia coli* glutamine synthetase. *Biochemistry* **33**, 682-686 (1994).
- 60 Sharkey, M. A. & Engel, P. C. Apparent negative co-operativity and substrate inhibition in overexpressed glutamate dehydrogenase from *Escherichia coli*. *FEMS Microbiol Lett* **281**, 132-139 (2008).
- 61 Ikeda, T. P., Shauger, A. E. & Kustu, S. *Salmonella typhimurium* apparently perceives external nitrogen limitation as internal glutamine limitation. *J Mol Biol* **259**, 589-607 (1996).
- 62 Brown, G. *et al.* Functional and structural characterization of four glutaminases from *Escherichia coli* and *Bacillus subtilis*. *Biochemistry* **47**, 5724-5735 (2008).
- 63 Massiere, F. & Badet-Denisot, M. A. The mechanism of glutamine-dependent amidotransferases. *Cell Mol Life Sci* **54**, 205-222 (1998).
- 64 Reitzer, L. J. *Ammonia assimilation and the biosynthesis of glutamine, glutamate, aspartate, asparagine, l-alanine and d-alanine, in Escherichia coli and Salmonella: Cellular and Molecular Biology. American Society for Microbiology (ASM), 2nd edn* (1996).
- 65 Daniel, J. & Danchin, A. 2-Ketoglutarate as a possible regulatory metabolite involved in cyclic AMP-dependent catabolite repression in *Escherichia coli* K12. *Biochimie* **68**, 303-310 (1986).
- 66 Pioszak, A. A. & Ninfa, A. J. Genetic and biochemical analysis of phosphatase activity of *Escherichia coli* NRII (NtrB) and its regulation by the PII signal transduction protein. *J Bacteriol* **185**, 1299-1315 (2003).